Fluorescence photophysics, characterisation and application of labelled glucose/galactose binding protein

Jonathan Coulter

PhD Thesis

2013

Photophysics group

University of Strathclyde

Declaration

This thesis is the result of the author's original research. It has been composed by the author and has not been previously submitted for examination which has led to the award of a degree.

Signed:

Date:

Publications and Conferences

John C. Pickup, Faaizah Khan, Zheng-Liang Zhi, Jonathan Coulter, and David J. S. Birch; "Fluorescence Intensity- and Lifetime-Based Glucose Sensing Using Glucose/Galactose-Binding Protein." *Journal of Diabetes Science and Technology Volume 7, Issue 1, January 2013*

Jonathan Coulter, Faaizah Khan, Dalibor Panek, Tania Saxl, John Pickup, and David Birch; "Characterisation and optimisation of fluorescent labelled bacterial glucose-binding protein in glucose sensing." *Poster presentation: MAF 12 Strasbourg 11-14th September 2011*

Glossary of acronyms

GBP	Glucose/galactose Binding Protein
mGBP	Triple mutant H152C/A213R/L238S glucose/galactose binding protein
BADAN	6-Bromoacetyl-2-Dimethylaminonaphthalene
IANR	Iodoacetamide Nile Red
I-ANS	2-(4-iodoacetamidoanilino)naphthalene-6-sulfonic acid
TMOS	Tetramethyl ortholosilicate
TEOS	Tetraethyl orthosilicate
FMOC-YL	9-Fluorenyl methoxycarbonyl-tyrosine-leucine
PBS	Phosphate buffered saline
BBS	Borate buffered saline
DMF	Dimethyl formamide
TCSPC	Time correlated single photon counting
FRET	Förster Resonance Energy Transfer

Abstract

There is currently a pressing need for reliable, minimally-invasive, continuous glucose monitoring for the treatment of diabetes mellitus. One promising glucose sensor is bacterially-derived glucose binding protein (GBP). In this project, the modified triple mutant H152C/A213R/L238S-GBP (mGBP) was investigated for viability as a functioning glucose sensor. Labelling the protein with the environmentally-sensitive dye BADAN produced repeatable, nearly linear, changes in both fluorescence intensity and fluorescent lifetime measurements. The robustness of the GBP-BADAN sensor response was tested and the results showed no interference from the sugars fructose and lactose- while it was also shown that alterations in temperature and pH level had deleterious effects on the sensor function.

The dyes Texas Red and iodoacetamide nile red (IANR) were attached to the GBP binding site to investigate the possibility of producing an alternative, longer-wavelength sensor system than when using BADAN. The ostensibly environment-insensitive Texas Red dye produced a protein-dye complex with no discernible response to glucose, but a significant response was observed for the GBP labelled with IANR: a 2-exponential lifetime decay relative amplitude change of 18% was recorded. These data provided further evidence for the proposed mechanisms of labelled GBP, while showing proof-of-concept for a long-wavelength fluorescence lifetime based glucose sensor.

Finally, methods of protein encapsulation were examined. Silica sol gels derived from both tetramethyl orthosilicate (TMOS) and tetraethyl orthosilicate (TEOS) precursors were found to be ineffective environments for the GBP-BADAN sensor, as the fluorescence response was significantly impaired. Encapsulation in a hydrogel produced using 9-fluorenylmethoxycarbonyl (FMOC-YL) was also examined, and this arrangement was found to provide an environment where both mGBP-BADAN and mGBP-IANR could function. mGBP-IANR in the FMOC-YL hydrogel was found to have a binding constant of 41.99 (±3.78)mM. It was concluded that mGBP-IANR in an FMOC-YL hydrogel could potentially provide a route to a functioning glucose biosensor.

Table of Contents

Contents

1. Introduction

Diabetes mellitus is an increasingly common medical condition, and a growing burden on the health of the global population. A recent report from the Baker IDI Heart and Diabetes Institute, Australia, calculated the incidence of diabetes worldwide to be around 285 million adults in 2010, with projected figures rising to 439 million adults by 2030[1], with commensurately accelerating healthcare costs to governments and individuals alike. Indeed, 12% of the global health care costs per person are estimated to be diabetes related in 2010, a figure that can only increase as do the number of patients[2].

Diabetes is a metabolic condition that impairs or destroys the patient's ability to process glucose. Glucose control must be externally managed, and controlled through use of the correct, potentially variable dose of medication. Long term complications of the condition include potentially-blinding retinopathy, increased risk of cardiovascular disease, and capillary damage leading to sexual dysfunction, foot ulcers and amputation[3]. These complications can be greatly mitigated with an effective glucose control regimen[4]. Accurate and timely monitoring of the patient's blood glucose level is therefore a necessary component of diabetes care.

Current glucose monitoring procedures require a diabetic individual to self-extract blood samples on a regular basis for ex vivo electrochemical analysis: a procedure which procures the relevant information, but at the cost of causing pain to the patient[3,5]. The main drawback of this type of regimen is that it provides only sporadic information- results are obtained only at the rate at which the patient is prepared to endure the pain of testing. The ideal technology for collection of blood metabolite information would therefore be continuous and non-invasive, and any steps along that route are positive ones for diabetic patients[6,7].

Glucose sensors for continuous monitoring are currently available, but are non-ideal[8]. The existing technologies mainly consist of amperometric enzyme electrodes and microdialysis probes, both of which are prone to sensor drift and require frequent calibration[8,9]. Alternative therapies are needed, and new lines of research are opening up at an accelerating rate. Indeed, in the five years from 2003 to 2007 there were 657 papers published on the topic of "continuous glucose monitoring": as of Jan 2013 there have been 1211 papers published since then. This is a nearly two-fold increase in the rate of report publication on the subject.

Recent work in the field of glucose sensing using non-optical methods has shown great invention and variety. There have been many papers published in recent years describing optimisation and stabilisation of glucose oxidase, including use of gold nanoparticles[10]; ZnO modified gold discs[11]; IrO_x nanoparticle films[12]; magnetic, multi-layered, nanocomposite systems[13]; electroconductive hydrogels[14]; ruthenium-doped TiO_2 sensing films[15]; peptide nanotubes[16]; chitosan–Au nanoplate composite films[17]; the lengthily-named but effective chitosan–Prussian blue–multiwall carbon nanotubes–hollow PtCo nanochains (CS–PB–MWNTs–H-PtCo) films[18]; silver nanowires[19]; TiO_2–Graphene composites[20]; the increasingly ubiquitous carbon nanotubes[21,22,23]; and the carbon networks described as buckypaper[24].

Alternative pathways towards an amperometric glucose biosensor include the use of such materials as nanoporous PtPb networks[25]; microfibers consisting of a copper oxide-doped nickel oxide composite[26]; carbon nanotubes incorporating boron oxide nanoparticles[27]; Ni nanoparticles;[28] and nanocomposite electrodes of CuO nanocubes and graphene[29,30]. A recent paper describes electrochemical analysis of graphene oxide, for the construction of a switchable sensor[31]. Additionally, novel work is being performed using fully non-invasive methods such as breath signal analysis incorporating an array of semiconductor sensors[32]. The interpretation and analysis of these results, and the use of algorithms to make sense of the continuous monitoring data as it pertains to patient control is a field that is developing alongside that of hands-on detection of glucose levels[33,34,] and is an area which will only increase in sophistication as the entire continuous glucose monitoring field develops.

Treatment of insulin-dependent diabetes in the manner requiring fewest invasive events would obviously require implantation of an insulin-regulating device- an ‘artificial pancreas’. This sensor-controller combination is the ideal solution for a diabetic patient, and while great strides are being made in this area of research[35,36,37], the field is both beyond the scope of this project, and is ultimately dependent on progress in the area of glucose monitoring, with which this project is primarily concerned.

Fluorescence spectroscopy possesses attractive and advantageous qualities for blood glucose monitoring. Fluorescence techniques have found many applications in the analytical- and especially the biological- sciences because of their sensitivity, and the ability to detect fluorophores at exceptionally low concentrations, down to a few parts per billion. Applications of fluorescence lifetime spectroscopy are extremely varied. One advantageous aspect of fluorescence lifetime

spectroscopy for biological application is the ability to obtain absolute data. Lifetime measurements are independent of fluorophore concentration, and being a fundamental property of the molecules involved, the lifetime measurements are repeatable and consistent across different instrumentation.

That fluorescence measurements can be performed on a continuous basis is one of the attractive properties in regards to a continuous glucose monitor.

There also exists the possibility of using light itself to interrogate human subjects *in vivo*. Light in the so-called therapeutic window (near infra-red) passes through human skin and could potentially communicate fluorescence information. Implanted sensors in a patient's dermal layer, excited by light of the appropriate wavelengths, could similarly avoid the pain involved with taking blood samples. Currently published research using implanted sensors promises to be just the tip of the glucose monitoring iceberg[38,39]. Widespread use of fluorescence physics in either of these 'smart tattoo' or implanted fibre-optic sensors would redefine minimally-invasive monitoring for diabetes patients[40].

2. Fluorescence photophysics

Fluorescence as a phenomenon has been reported in the scientific literature since the mid-19th century, when Sir John Frederick William Herschel published his 1845 work on the fluorescence of quinine. In the years since that first observation of blue light emission after ultraviolet light excitation, the field has expanded enormously and now occupies a place of prominence in the biological sciences[41].

2.1. Electronic transitions

The absorption of photons by materials is a process which has been understood since the early days of quantum mechanics. The electronic energy levels of an atom or molecule are separated by clearly defined, quantised, energies. Photons of an appropriate corresponding energy can be absorbed by the material and electronic excitation is the result. The energy of a photon is directly related to its frequency (and inversely to its wavelength) by equation 1.

$$E = h\nu = hc/\lambda \qquad (1)$$

where *h* is Planck's constant in $m^2kg.s^{-1}$ and *v* is the light frequency in s^{-1}; *c* is the speed of light in $m.s^{-1}$, and *λ* is the wavelength of the light in m. Absorbance of a photon of energy *E* results in excitation to an energy level *E* Joules above the ground state. The absorbance of a bulk sample is described by the Beer-Lambert law, shown in equation 2.

The transmission of a sample is the intensity of light measured as passing through the sample, compared to the intensity of light entering the sample. Transmission is defined by the ratio of I/I_0 and is logarithmically related to the absorbance as equation 2 describes.

$$A = -\log_{10}\frac{I}{I_0} = \varepsilon c l \qquad (2)$$

A is the absorbance by a sample of incident light, where ε is the molar absorption coefficient in $M^{-1}cm^{-1}$ units, c is the concentration of the sample in M, and l is the path length in cm.

The absorption coefficient is an expression of how likely the sample is to absorb light. It is this absorption of light which excites the sample to a higher electronic energy level. After excitation, there are alternative outcomes for the excitation energy; these are illustrated in figure 2.1.

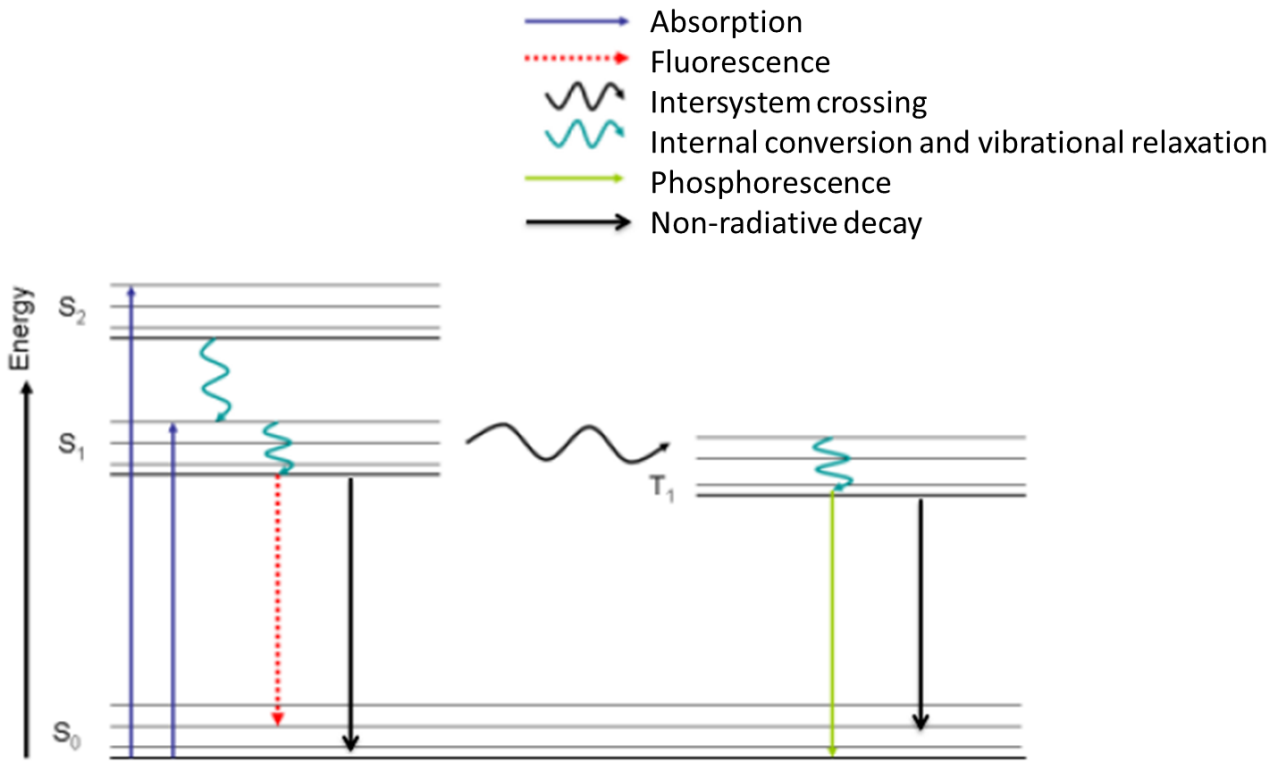

Figure 2.1- A characteristic Jablonski diagram

Immediately following the absorption of a photon, electronic excitation from the S_0 ground state to a higher electronic state takes place. Selection rules dictate that this must be to a vibrational state different from that in the ground state, at a level above the lowest vibrational energy of the excited electronic state. Vibrational relaxations, also known as internal conversions, take place on the picosecond timescale, lowering the energy of the excited state to that of the lowest S_1 (or higher electronic state) energy level. From this state, the energy of the excited state can either be radiated in an emission event, or lost in non-radiative decay processes such as energy transfers and quenching events. The 'inter-system crossing' transition to the quantum mechanically forbidden T_2 and T_1 triplet states is inherently much less likely, and the resulting phosphorescence decay occurs on the order of seconds or longer. The quantum mechanically allowed transition from S_1 state to S_0 state provides us with fluorescence emission. These events take place in the realm of nanoseconds, and it is the study of such fluorescence events that comprise the basis of this report.

It can be observed from the diagram referenced above that as a result of the vibrational and internal conversion energy losses, the fluorescence emission arrow is noticeably smaller than that of the absorption event. This corresponds to a very real loss in energy of the excited state. Accordingly, the relationship between photon energy and wavelength, described in equation 1, dictates that emitted photons are therefore of longer wavelength than the corresponding excitation light.

This change in wavelength is known as the Stokes shift, and the shift is characteristic of the molecule being excited. The absorption and emission spectral profiles of a fluorophore in general mirror each other- this wavelength shift, along with the 'mirroring' effect, is illustrated in figure 2.2.

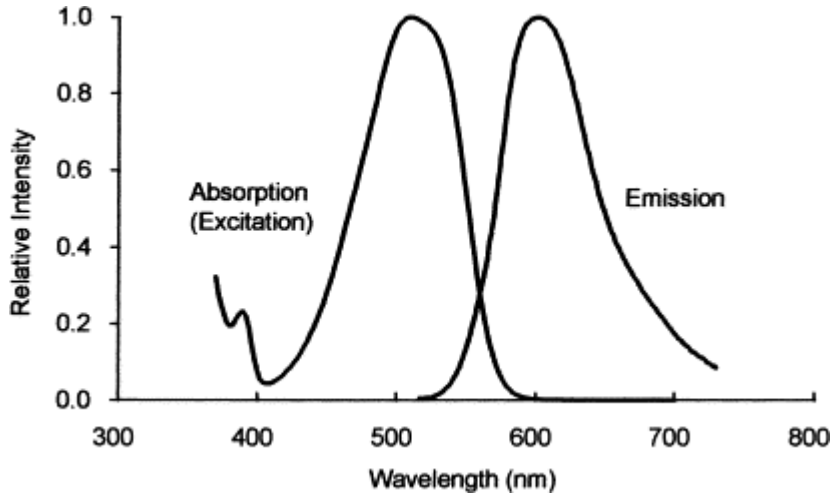

Figure 2.2- Representative absorption and emission spectra of an arbitrary molecule[42]

The wavelength shift in figure 2.2- in this case from around 500nm to around 600nm- is qualitatively representative of the Stokes shift experienced by fluorescent molecules in general, and is a result of the vibrational energy losses in the molecule.

Each luminescent molecule possesses this detectable shift in wavelength on emission. What is also characteristic of that molecule is the time that elapses between excitation and emission. While an electron will be excited to a vibrational and rotational state above the ground level, this quickly 'relaxes' through internal conversion, thermal interactions, and other non-radiative processes before emission of a photon. The rate at which the bulk sample decays from the excited state to the ground state provides the fluorescence lifetime of the sample.

2.2. Fluorescence decay

The excited state population of a fluorophore decays with rate (equation 3)

$$\frac{dn(t)}{dt} = -(k_r + k_{nr})n(t) \tag{3}$$

where k_r represents the radiative decay rate and k_{nr} the non-radiative pathways to energy loss. Fluorescence intensity is proportional to the number of decay events, *n(t)*, and the measured intensity can be represented by the exponential decay (equation 4):

$$I(t) = I_0 \exp(-t/\tau) \tag{4}$$

where

$$\tau = (k_r + k_{nr})^{-1} \tag{5}$$

And the characteristic fluorescence lifetime, τ, is on the nanosecond timescale.

This characteristic time τ is known as the fluorescence lifetime of the sample. While fluorescence decays are quantum mechanical- and thus probabilistic- events, the absolute characteristic lifetime can be accurately obtained by measuring a large enough number of such events.

The radiative pathways of luminescence are of primary interest to the photophysicist. The non-radiative pathways, however, are also of importance in understanding the physics.

2.3. Quantum yield and quenching

Every fluorophore has the potential to undergo non-radiative decay processes, in addition to the radiative (fluorescence emission) processes. The fraction of all processes which result in an emission event is defined as the quantum yield. Mathematically it is described in equation 6:

$$\Phi = \frac{k_r}{k_r + k_{nr}} \tag{6}$$

Where k_r and k_{nr} are the radiative and non-radiative rate parameters respectively. The higher the quantum yield of a fluorophore, the greater the proportion of absorbed photons are emitted, and the more efficient the fluorophore can be judged to be.

Various processes have the potential to decrease the fluorescence intensity of a sample- collectively these are known as quenching of the fluorophore. The molecular interactions which come under the banner of quenching include energy transfers, molecular rearrangements, excited state reactions and the most commonly observed such process- collisional quenching.

Collisional encounters between a fluorophore and a quenching molecule, such as molecular oxygen (which has a quenching effect on nearly all fluorescent compounds), result in an attenuation of the fluorescence in a manner described by the Stern Volmer equation (equation 7).

$$\frac{I_0}{I} = 1 + k_Q \tau_0 [Q] = 1 + K_d [Q] \qquad (7)$$

Where I_0 is the fluorescence intensity in the absence of a quencher, I is the intensity with quencher present, k_Q is the biomolecular quenching constant, τ_0 describes the fluorescence lifetime in the absence of quencher (in s), and $[Q]$ is the concentration of the quencher in M. The term K_d is the product of the lifetime and quenching constant, and is called the Stern-Volmer quenching constant.

2.4. Environmental effects

In this thesis, the effect of local environment is of importance. Environmental effects can have a profound effect on the fluorescence lifetime of some molecules.

Consider the fluorescence lifetime of a molecule given in equation 5, and restated below as equation 8:

$$\tau_M = \frac{1}{k_r + k_{nr}} = \frac{1}{k_M} \qquad (8)$$

Where k_r and k_{nr} are the radiative and non-radiative rate parameters, and k_M is the total decay rate. Environmental factors such as polarity, refractive index, and temperature can directly influence both the radiative and non-radiative rate parameters.

The effects of environment on the emission of fluorophores are complex and are often not resolvable in a quantitative manner[41]. Many factors may influence the emission spectra and quantum yield, including but not limited to both general and specific fluorophore-solvent dipole interactions, solvent viscosity, temperature, changes in both radiative and non-radiative decay rates.

Due to the use of environmentally-sensitive fluorophores in the protein labelling in this project, solvent-fluorophore interactions are taken to be of primary importance.

To a first approximation, assuming that the fluorophore can be represented as a dipole in a continuous medium, excluding hydrogen bonding effects and charge transfer states, the energy difference between the ground and excited states of the fluorophore is affected as described in the Lippert-Magata equation (equation 9):

$$\overline{\nu_A} - \overline{\nu_F} = \frac{2}{hc}\left(\frac{\varepsilon - 1}{2\varepsilon + 1} - \frac{n^2 - 1}{2n^2 + 1}\right)\frac{(\mu_E - \mu_G)^2}{a^3} + constant \qquad (9)$$

The energy difference between the ground and excited states of the fluorophore, $\overline{\nu_A} - \overline{\nu_F}$, expressed in wavenumbers, is seen to be a property of the refractive index (n) and of the dielectric constant (ε) of the solvent, with a dependence on the square of the difference in dipole moments between the ground (μ_G) and excited (μ_E) states.

In the Lippert-Magata equation, h is Planck's constant ($6.626*10^{-27}$ ergs), c is the speed of light in $cm.s^{-1}$, and a is the radius of the cavity in which the fluorophore resides. Worthy of note are the effects of changes in n and ε on the Stokes shift: increasing the refractive index will decrease the $\overline{\nu_A} - \overline{\nu_F}$ energy loss, whereas an increase in the dielectric constant has the opposite effect on these energy changes, and will increase the Stokes shift. As the energy difference between ground and excited states is altered by the solvent environment, so is the fluorescence lifetime. Solvation is the process of attraction and association of solvent molecules with molecules of the solute. Molecules which possess a large dipole moment will share energy with the dipole moments of surrounding solvent molecules, lowering the energy of the excited state. Excitation events happen too quickly

relative to solvent re-orientation to show a strong effect on absorbance spectra. Polar environments, such as water, will encourage this energy loss effect more than non-polar solvents such as pentane. Molecules with a large dipole moment shift upon excitation (the case were $\mu_E - \mu_G$ is large) will also strongly show the effects of solvent interaction upon the emission profile.

The summary of this is that the emission characteristics of fluorophores are not universally invariant- the solvent environment can have a profound impact on how a molecule behaves. Emission spectra from some fluorophores differ drastically depending on environmental factors such as solvent polarity, rates of solvent relaxation, probe-probe interactions, and changes to the decay rates wrought by the solvent. Not every fluorescent molecule is affected by solvent effects, or to the same degree, but those that are can be utilised for analysis of the micro-environment around the fluorophore.

The effects of solvent polarity are important for this project, and can be understood in terms of the molecular dipole moment previously discussed. Excited-state fluorophores have a larger dipole moment than when in the ground state. This excited dipole moment can couple with the dipole moment of the solvent molecules, allowing energy exchange and further relaxation. As a consequence, the susceptible fluorophores in a polar solvent have their emission spectra red-shifted, and the lifetime of the excited state is decreased, both of these effects can be measured and quantised. The degree of dipole interaction can provide information on the quantity and degree of solvent material immediately surrounding the fluorophore.

2.5 FRET

In Förster Resonance Energy Transfer (FRET), an excited donor molecule transfers energy to a ground-state acceptor molecule through dipole-dipole interactions, without any photons being involved. If the emission spectrum of the donor overlaps with absorption spectrum of the acceptor, and the molecules are close enough in space, then FRET will dependably occur. The rate of energy transfer depends on the distance between donor and acceptor- a dependence which allows accurate measurement of the donor-acceptor distances. The distance at which FRET is 50% effective is called the Förster distance (R_0)- this is typically in the nanometre regime. The actual rate of transfer (k_T) is given by equation 10.

$$k_T(r) = \frac{1}{\tau_D}\left(\frac{R_0}{r}\right)^6 \quad (10)$$

Where τ_D is the decay time of the donor in the absence of an acceptor, and *r* is the donor-to-acceptor distance in the sample. The FRET rate is proportional to $1/r^6$, making it useful for distance measurements

2.6 Fluorescence and Glucose Sensing

Although fluorescence spectroscopy enjoys widespread use in the biological sciences, use of fluorescence techniques in glucose monitoring is a non-trivial matter: for the simple reason that glucose itself is a non-fluorescent molecule. Many schemes and methods, some more complex and radical than others, have therefore been investigated for the purpose.

Fluorescence techniques and technologies have found increasing use in the field of glucose sensing, with the rate of publication of relevant papers increasing as does the field itself. Methods and materials appear to vary in popularity from year to year: below I will provide a brief description of protocols used to date. Some of the main optical methods for glucose sensing involve use of fluorescent- and fluorescence-labelled enzymes; boronic acid systems; concanavilin A, and various related glucose binding proteins. In addition, there are increasingly novel techniques being utilised, such as sensors which make us of the near infra-red fluorescence from carbon nanotubes[43].

Immobilised enzymes such as yeast hexokinase and Apo-glucose oxidase have been reported to respond to glucose in a manner which lends itself to fluorescence interrogation[44,45]. Boronic acid derivatives have also shown promise in the field, and there are many examples in the literature of this method of investigation[46,47,48]. These boronic acid derivatives bind to the diols of sugars (such as glucose) and undergo geometric changes upon binding, changes which influence the fluorescence of an attached fluorophore. The lectin Concanavilin A has been exploited in the creation of FRET-based systems: covalent labelling with allophycocyanin[49], ruthenium complexes[50] and the dye Cy5[51] has provided biosensors over a wide range of wavelength regimes. With all of these techniques, there are questions about sensitivity in the human physiological range, and on occasion, issues of reversibility (the process by which the sensor system is restored to initial conditions when glucose concentration is susbequently reduced).

Perhaps the area which has witnessed the greatest growth in recent years has been the use of glucose binding proteins (GBPs). These proteins, derived from bacteria such as E. coli, reversibly bind to glucose and therefore provide the basis for constructing a glucose sensor. The glucose-binding process causes the protein to fold around its central lobe, allowing for different labelling protocols. Labelling the lobes of the protein with donor and acceptor dyes for FRET analysis allowed concentration measurements to be calculated from the degree of protein folding- and therefore the degree of FRET induced by increased donor-acceptor proximity[52,53].

Khan, et al., reported that deliberate placement of environmentally sensitive dyes produces superior changes in the fluorescence profiles compared to FRET systems[54]. Accordingly, interest in the use of environmentally sensitive labelling protocols has increased. Labelling with I-ANS at cysteine position 26 [55], acrylodan at mutation sites located in position 183[39] and 225[56], IANR at various sites[57], and BADAN at position 152[58] show some of the variety in dye identity and location used. In addition, the intrinsic fluorescence of GBP has been used to identify the engineering and mutations that are performed[59], hinting at the possibility of intrinsic fluorescence techniques for glucose concentration measurements.

A fibre-optic clinical sensor has been fabricated using the GBP-BADAN complex, immobilising the protein on agarose and polystyrene beads, and was shown to be reversibly reactive and responsive in the human physiological range[60]. Additional fibre-optic interrogation systems for glucose sensors have been developed[61], and in vivo studies on pigs have shown the hydrogel-immobilised acrolydan-GBP system to be a robust and viable basis for a glucose biosensor[39]. These studies indicate that clinical trials in humans of implanted glucose biosensors are on the horizon, and it is in the interest of all involved in diabetes research to investigate the possible mechanisms and schemes available and conceivable, in order for the research community to develop an efficient and viable non-invasive, continuous glucose sensor.

3 Experimental techniques and instruments

Steady-state fluorescence provides information gathered over the whole period of the scan- it is necessarily averaged over time. There is information that can be derived from the use of fluorescence techniques- such as rates and kinetics of molecular processes- which is unavailable using steady-state fluorimetry. For these data to be obtained, time-domain fluorescence measurements must be considered. Lifetime measurements- that is, determination of the time spent in the excited state- can provide information on the local environment of a molecule, on the size and shape of a molecule, and on inter- and intra-molecular distances.

3.1 Time-resolved fluorescence

Fluorescence lifetimes are measured by exploiting one of two regimes- frequency-domain, or time-domain measurements- also referred to as phase and pulse fluorometry respectively. The frequency-domain, phase fluorometry measurements use amplitude-modulated excitation sources with frequencies around 100MHz. Because of the time lag between absorption and emission, the emission is delayed in time relative to the modulated excitation. The finite time response of the sample also results in demodulation of the emission. Information about the phase difference after emission, and the amplitude modulation changes through fluorescence can both be used to determine the lifetime. The angle by which the phase is shifted or delayed, φ, can be used to calculate the phase lifetime (τ_φ), through the relationship in equations 11 and 12.

$$\tan\phi = \omega\tau_\phi \tag{11}$$

Or

$$\tau_\phi = \omega^{-1}\tan\phi \tag{12}$$

where ω is the modulation frequency in s^{-1}.

The modulation (m) of the emission is measured relative to the excitation as described in equation 13.

$$m = \frac{(B/A)}{(b/a)} \tag{13}$$

where *a* is the average intensity of the incident light, *b* is the peak-to-peak height of the incident light, *A* is the average intensity of the emitted light, and *B* the peak-to-peak height of the emission. The modulation is related the modulation lifetime (τ_m) through equation 14:

$$m = \frac{1}{\sqrt{1+\omega^2\tau_m^2}}, \tag{14}$$

and the modulation lifetime can then obtained, as shown in equation 15:

$$\tau_m = \frac{1}{\omega}\left[\frac{1}{m^2} - 1\right]^{1/2} \tag{15}$$

For a mono-exponential decay, the values of τ_φ and $\tau_{m,}$ are found to be the correct lifetimes. For more complex decay characteristics, these calculated lifetimes represent a weighted average of the decay components.

3.2 Time Correlated Single Photon Counting

The other technique- which is the one used in this project- is time-domain, pulse fluorometry. Samples are excited with a short pulse of light- ideally an infinitely short delta-function, but in practice it is sufficient for the pulse to be shorter than the fluorescence lifetime.

The method of time-domain measurement used in this project was time-correlated single photon counting (TCSPC). As the name suggests, only one excitation-emission event is monitored at each individual instance, yet thousands of events are recorded in total. For each excitation, far fewer than one photon is detected (around 1% of laser pulses give a result)- an intentional set up to prevent allow counting of single, representative photon emission events. If a greater proportion of incident photons cause a fluorescence response, many of the longer lifetimes will not be recorded, and so the overall recorded lifetime will appear to be shorter than in reality. A pulse of light from a laser, LED, or flash-lamp, is used to excite the sample, and the time delay between the excitation pulse and

emission of each received photon is recorded. These data are collected and used to build up the intensity profile. The time taken for the intensity profile to fall to 1/e of initial intensity provides the fluorescence lifetime.

The layout of a TCSPC kit is illustrated in figure 3.1.

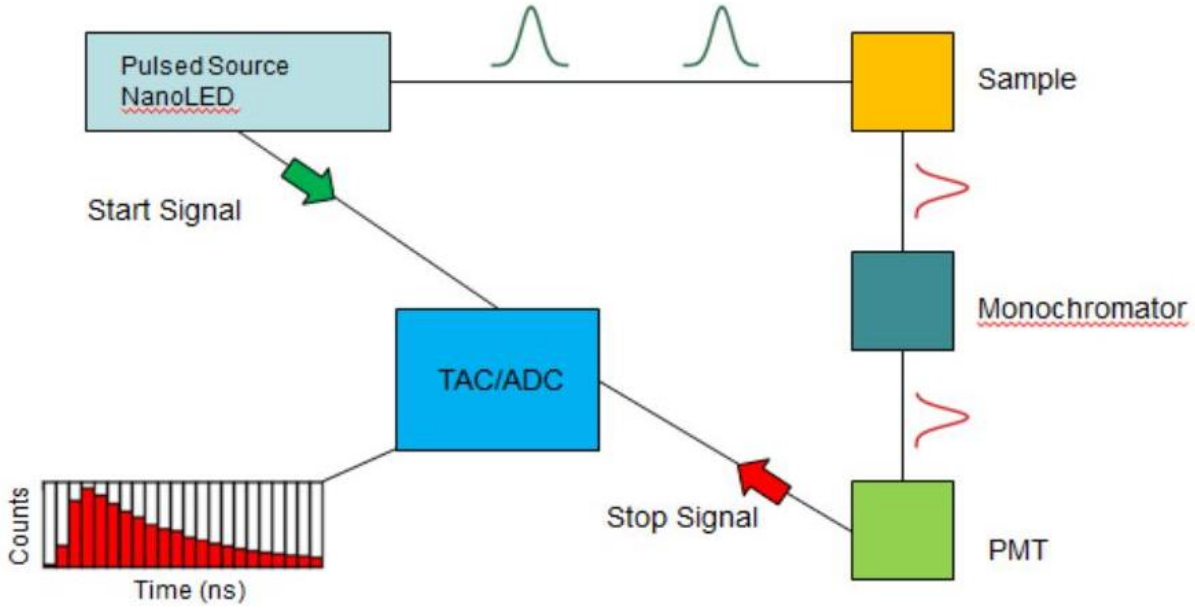

Figure 3.1- Outline of a generic TCSPC kit[62]

The pulsed light source excites the sample as previously discussed, and a photo-detector (PMT) picks up the emitted light and issues the 'stop' signal. Simultaneous to the excitation pulse production, a synchronising 'start' pulse is also generated. This 'start' pulse provides the zero-time value from which the emission time is measured. The number of photons collected- and therefore the number of emission events- for each sub-unit of time channel is collated into a histogram. This plot, exhibiting a characteristic decay curve (which can be modelled as a combination of exponential decays) is used to calculate the lifetime parameters.

3.3 Data analysis

TCSPC intensity decays are fit to the multi-exponential model described in equation 16:

$$I(t) = \sum_i \alpha_i \exp(-t/\tau_i) \qquad (16)$$

Where α_i is the pre-exponential weighting factor for the component, t is the time in seconds, τ is defined as in equation 5, and the sum is normalised to unity.

Data analysis in TCSPC is complicated by the finite duration of the time response of the fluorometer. It was earlier stated that the ideal excitation pulse was a δ-function, but the pulse widths of real sources are larger than this idealised situation, and photon detector responses are also non-instantaneous. Most instrument response functions are 0.5 ns to 2 ns wide, which requires a degree of data analysis in order to retrieve the impulse response of the sample.

The solution is to use convolution analysis whereby the excitation pulse is considered to be composed of a series of δ-functions and the fluorescence decay a linear superposition of the corresponding fluorescence impulse responses, as expressed in equation 17.

$$N_c(t) = \int_0^t P(t')I(t-t')dt' \tag{17}$$

Where $N_c(t)$ is the calculated, expected, fluorescence decay, which is broader than the fluorescence impulse response $I(t-t')$ because of the effect of the finite instrumental response or prompt function $P(t')$. The variable t' is a moving time delay that defines the instant at which each δ-function component of the instrumental pulse generates the start of a fluorescence response. $P(t')$ is usually measured by tuning the fluorescence monochromator to the excitation wavelength and replacing the fluorescent sample with a colloid that simulates the isotropic nature of fluorescence by diffuse scattering of the excitation pulse. In this project LUDOX silica was used to determine the $P(t')$ for each measurement.

Using equation 17 to analyse fluorescence decay requires numerical analysis using reconvolution rather than deconvolution. That is to say, the term $I(t-t')$ in equation 17 is iterated to give τ from equation 16 when the calculated decay $N_c(t)$ best describes the measured decay data $N(t_k)$.

The closeness of the match between the measured and modelled intensity decays is shown by the 'goodness of fit'; calculated using the non-linear least squares (NLLS) method. The goodness-of-fit parameter, or 'χ^2 value', is given in equation 18.

$$\chi^2 = \sum_{k=1}^{n} \frac{1}{\sigma_k^2}\left[N(t_k) - N_c(t_k)\right]^2 = \sum_{k=1}^{n} \frac{\left[N(t_k) - N_c(t_k)\right]^2}{N(t_k)} \quad (18)$$

Where $N(t_k)$ are the measured data, $N_c(t_k)$ are the calculated decay data, and σ_k is the standard deviation of each data point. The standard deviation is calculated as shown in equation 19.

$$\sigma_k = \sqrt{N(t_k)} \quad (19)$$

The value of χ^2 depends on the number of data points- to normalise for this, the slightly altered reduced χ^2 value is used to judge the goodness of fit. If the reduced value of χ^2 is close to unity, then the fit is determined to be good- if the model does not fit the data, then the χ^2 value will be much greater than 1. Generally, a value of approximately 1.2 or better denotes a good fit to the data. χ^2 values greater than 1.2 indicate an inappropriate model being used to fit the data, or a systematic error in the experiment.

The weighted residuals, W_t described in equation 20, are also often presented as their distribution underpins the χ^2 values; random rather than systematic deviations being taken to indicate a good fit to the data.

$$W_t = \frac{N_c(t) - N(t)}{\sqrt{N_c}} \quad (20)$$

The weighted residuals of a plot are a straightforward method of indicating the goodness of fit of a model, as they especially highlight areas of the plot where more than random noise fluctuations are influencing the result.

Figure 3.2 shows an example of curve fitting to a fluorescence lifetime decay profile, which was recorded using Horiba DAS6 software.

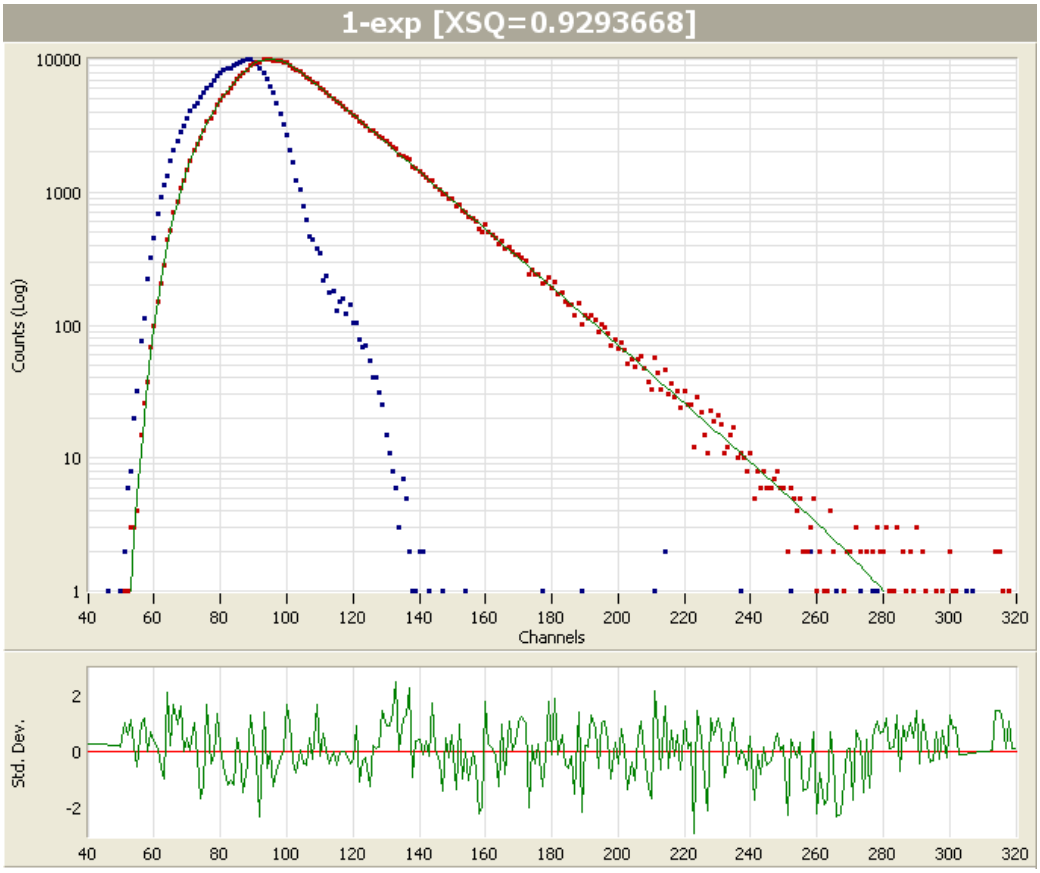

Fig 3.2- Example fluorescence lifetime decay with a single exponential fit to the data

The red data points are the observed number of counts per channel for the fluorescence decay (channels providing a measure of time), the blue points are the recorded counts for the excitation pulse prompt function, and the green line shows the fitted function. The lower section of the graph displays the weighted residuals- in this case the random fluctuations reveal the deviations to be due to random noise, rather than systematic error.

3.4 Anisotropy

Exciting a sample of fluorescent molecules with polarised light can provide information on how isotropic the sample may be. Using light polarised in one orientation will excite the molecular dipoles in the sample which possess the same orientation. By analysis of the fluorescence emission at parallel and perpendicular orientations to the excitation pulse, the extent and speed of depolarisation is measured. This depolarisation can be a result of various mechanisms, but in the simplest case (a homogeneous solution of fluorophores), the depolarisation time is a measurement of rotational diffusion. For an ideal rigid molecule, the speed at which fluorophores rotate gives a clear indication of the size of the molecule- or the molecule to which the fluorophore is attached.

The anisotropy decay is also affected by the rigidity and segmental flexibility of the macromolecule. Independent motions of the fluorophore relative to the macromolecule will be on a shorter timescale than the rotation of the molecule as whole, and anisotropy measurements of such a system will reveal a shortened correlation time. This is a relevant factor when considering protein labelling- deviations from the assumption of the system as a rigid rotor will influence the measured anisotropy decay time.

Fluorescence anisotropy is defined as shown in equation 21.

$$r = \frac{I_{\parallel} - I_{\perp}}{I_{\parallel} + 2I_{\perp}} \tag{21}$$

Where $I_{\parallel}$ is the intensity of fluorescence which is vertically polarised and $I_{\perp}$ is the horizontal fluorescence intensity.

By experimentally recording vertically (*V*) and horizontally (*H*) polarized fluorescence decay curves, $I_{VV}(t)$ and $I_{VH}(t)$, orthogonal to vertically (*V*) polarized excitation, a time-resolved anisotropy function $r(t)$ of a sample is generated as shown in equation 22.

$$r(t) = \frac{I_{VV}(t) - GI_{VH}(t)}{I_{VV}(t) + 2GI_{VH}(t)} \tag{22}$$

Where *G* is a factor ($G = I_{HV}(t)/I_{HH}(t)$) determined for horizontal orientation of the excitation polarizer in order to correct for differences in the polarization transmissions of the fluorescence detection channel at *V* and *H*, which are largely due to the emission monochromator. The factor of 2 in the denominator arises because there is a plane in the direction of the excitation in which depolarization of fluorescence is not detected, but is identical to that detected in the emission channel

Because the denominator in equation 20 describes all three planes of polarization it actually also describes the fluorescence decay undistorted by any polarization bias. This can be seen by inserting equations 23 and 24 into equation 22.

$$I_{VV}(t) = \exp(-t/\tau_f)\left[1 + 2r_0\exp(-t/\tau_c)\right] \tag{23}$$

$$I_{VH}(t) = \exp(-t/\tau_f)\left[1 - r_0 \exp(-t/\tau_c)\right] \quad (24)$$

As a result of which, we obtain equation 25, describing the anisotropy in terms of rotational correlation time:

$$r(t) = r_0 \exp\left(-\frac{t}{\tau_c}\right) \quad (25)$$

Where is r_0 the initial anisotropy at t = 0, which has a maximum value of 0.4, and τ_c is the rotational correlation time, which describes the rate of depolarization due to isotropic rotation.

From equation 25, the term denoted τ_c is the rotational correlation time. Mathematically, it is given as

$$\tau_c = \frac{\eta V}{k_B T} \quad (26)$$

Where η is the solvent viscosity in $kg.m^{-1}.s^{-1}$, V is the volume of the rotating sphere in m^3, k_B is the Boltzmann constant ($1.38*10^{-23}$ $J.K^{-1}$), and T is the temperature in Kelvin of the solution. This relationship between rotational correlation time and rotating sphere volume allows for calculation of the radius of the rotating sphere, according to the relationship

$$r^3 = \frac{3\tau_c k_B T}{4\pi\eta} \quad (27)$$

The radius of the assumed sphere gives a strong indication of the actual size of the rotating structure of which the fluorophore is a component. The relationship between anisotropy decay and rotational volume therefore allows for comparisons of size; a relevant calculation when studying folding of proteins.

Non-linear least squares (NLLS) analysis of the anisotropy decay data is used in an analogous manner to that previously described for fluorescence lifetime analysis. Re-arrangement of equation 22 provides equation 28.

$$d_t = r(t)\left[I_{VV}(t) + 2GI_{VH}(t)\right] = I_{VV}(t) - GI_{VH}(t) \qquad (28)$$

The function in brackets in equation 28 is the fluorescence decay, which we can fit to separately using as many decay parameters as required to give a good fit in order to obtain the fluorescence impulse response *i(t)* and then keep it fixed . The function on the right hand side of equation 28 contains the difference data d_t that carries the rotational information and which can be iteratively fitted to using NLLS reconvolution of the prompt function *P(t)* with appropriate anisotropy impulse response functions *r(t)*.

From this iterative process, the values of anisotropy and rotational correlation time are calculated, with the χ^2 again providing a measure of the goodness of fit. In this case, χ^2 is given as in equation 29.

$$\chi^2 = \sum_{\substack{Data \\ channels}} \left[\frac{d_t - P(t) \otimes r(t)i(t)}{\sqrt{d_t}}\right]^2 \qquad (29)$$

Figure 3.3 shows a representative anisotropy decay for a single rigid rotor.

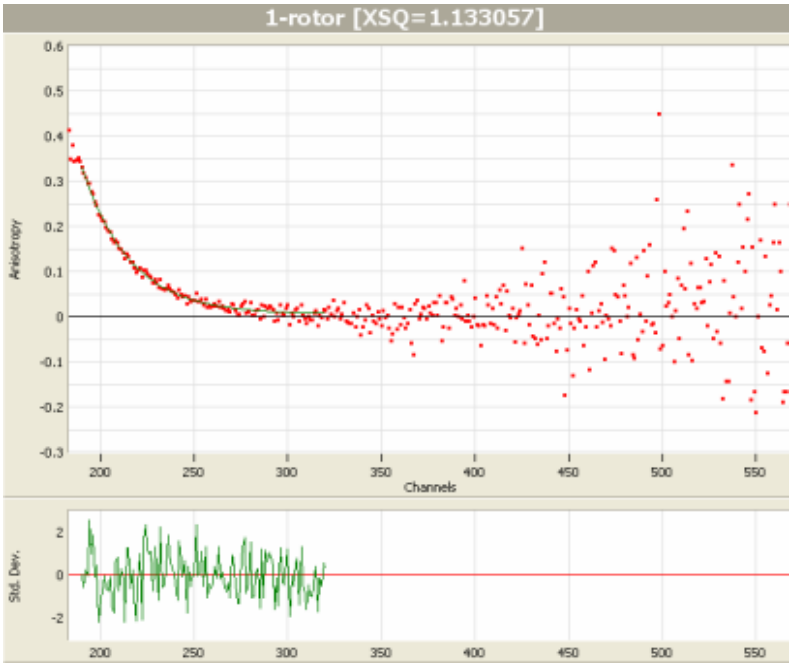

Figure 3.3- Example anisotropy decay of a single rigid rotor

The red data points are the calculated anisotropy values at each channel. The green line is a single-exponential decay which was fir to the data. The anisotropy value at *t=0* (the r_0 value) is very close to the theoretical maximum value of 0.4, and at longer timescales the values are noisy, but distributed in an even manner around an anisotropy value of zero, which is how the anisotropy of rigid rotors appears in practice.

3.5 Laboratory Equipment

Absorbance measurements were made on the Jasco V660 absorbance spectrometer. Fluorescence emission scans were recorded on the HORIBA Scientific Fluorolog 3 spectrometer. Given the small sample volumes available in this project, repeat experiments could not be conducted, and errors in the absorbance and emission values are therefore taken to be negligible for the purposes of this project, with the understanding that in reality this is not the case.

TCSPC data were recorded on a Horiba Scientific Fluorocube, using both NanoLED diodes and DeltDiodes for excitation; with double monochromators utilised to selectively excite the samples, and to isolate the emitted light. Lifetime analyses were performed on the Horiba DAS6 software, which calculated standard deviations in both lifetimes and relative amplitudes of pre-exponential factors. Errors in this report, denoted σ in each instance, are reported to 3 standard deviations.

When analysing the fluorescence lifetimes, in many cases involving 2-exponential decays the lifetimes were fixed at a constant value and the DAS6 software was used to calculate the relative amplitudes of the pre-exponential factors as the experiment progressed. Calculation of a 2-exponential lifetime decay is an iterative process involving both lifetimes and their pre-exponential factors, and so holding 2 of the variables (the lifetimes) constant prevents the iterations finding a minimised χ^2 value which is not physically useful. Keeping the lifetimes constant ensures that the variations seen between samples are expressed solely in the relative amplitudes of the pre-exponential factors. If these vary in a manner that makes sense, then the system displays just one set of varying numbers in response to glucose- a rather more desirable outcome when glucose-sensing is the goal. This constrained fitting was often used to compare samples in the same experiment.

Anisotropy decays were recorded on the Horiba Scientific Fluorocube, using the same NanoLED and DeltaDiode excitation sources as for TCSPC experiments. Anisotropy decay rates and rotational correlation times were calculated using the Horiba DAS6 software, which also provided the standard deviations. Errors in the anisotropy data (σ) are given to 3 standard deviations.

All samples were analysed in quartz cuvettes procured from Starna Scientific. Experiments using free dye were performed in 3 ml cuvettes, with a path length of 1 cm. Protein studies were performed using quartz micro-cuvettes with a geometric volume of 65 µL, which translates to a fluid volume of 70 µL. The microcuvettes possessed a path length of 10 mm, and a sample width of 2 mm.

3.6 Materials

All chemicals were procured from Sigma-Aldrich. Triple mutant H152C/A213R/L238S glucose binding protein (mGBP) samples were generously provided by Dr. Faaizah Khan of the diabetes research group at Guy's Hospital, London. Iodoacetamide nile red (IANR) was prepared in the chemistry department at Strathclyde University, with the help of Mr. Alan Hutton. 9-Fluorenyl methoxycarbonyl-tyrosine-leucine (FMOC-YL) samples were provided by Dr. Nadeem Javid of the chemistry department at Strathclyde University.

3.7 Protein labelling protocol

Triple mutant glucose binding protein was labelled with the fluorophore 6-Bromoacetyl-2-Dimethylaminonaphthalene (BADAN) according to the protocol described by Khan, et. al[58], which is summarised as follows. BADAN dye was dissolved in dimethyl formamide (DMF) until a concentration of 2.6 mM was reached: this figure being calculated from the Beer-Lambert law (equation 2), with the absorption coefficient at 380 nm taken to be $2.1*10^4 M^{-1}cm^{-1}$. The reducing agent tris(2-carboxyethyl)phosphine (TCEP) (2.5uL, 0.5M) was combined with concentrated mGBP stock (40 µL, 750 µM) and PBS (440 µL) and left for 30 min to allow the reduction of the protein to take place. After 30 min the BADAN stock was added (10 µL) and the sample was mixed and left overnight at 4 ^{o}C. During this time the BADAN dye is assumed to bind to the reduced protein.

In order to separate the labelled protein from any unattached dye, a gel filtration column was utilised. Larger protein molecules process more quickly through the medium than do smaller dye molecules- this separation allows for removal of the free dye. Sephadex G25 beads (10 g) were left overnight in PBS (100 ml) to reach full saturation. The prepared beads were carefully loaded into the column by Pasteur pipette, ensuring a compact arrangement of the beads, free from air pockets, in

an arrangement approximately 30 cm in length. With the column ready for filtration, the mGBP-BADAN solution was delicately placed on top of the Sephadex 'bed' and allowed to settle. The column cap was attached to a length of tubing which was run through a peristaltic pump. The pump was set to produce a constant flow rate (0.25 ml/min) and the gel filtration process was started. Filtration fractions were collected in 500 µL Eppendorf tubes. The labelled protein presented in the 20th fraction and was completely through the gel by the 34th fraction, as determined by spectroscopic measurements of the fractions. The free dye itself only appeared after the equivalent of 100 similarly sized fractions.

The fractions were collected in individual 500 µl eppendorf tubes. The labelled protein started to be found in the 20th collected fraction, and was present in the next 10 fractions After filtration, the samples were concentrated on a centrifuge using Vivaspin 6 concentrator tubes. The centrifuge was used to produce a spin rate of 3000 rpm for 15 min, reducing the sample volume from 10 ml to 500 µL in this time.

The same labelling protocol was used for the attachment of both alternative fluorophores, namely Texas Red IANR.

3.8 IANR synthesis

The fluorophore IANR was prepared in the chemistry department, with the help of Alan Hutton. Starting from the initial compound of 9-Diethylamino- 2-hydroxy-5H-benz[a]phenoxazin-5-one the scheme shown in figure 3.4 was followed to completion, providing a product which was assumed to be IANR[79].

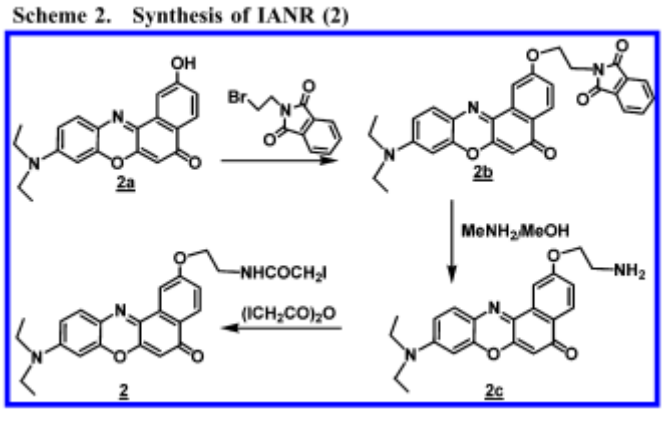

Figure 3.4- Chemical reaction scheme for IANR, adapted from Thomas, et al. [79]

3.9 Sol gel preparation

Silica sol gels were prepared as described in the literature[63,64].

Using tetramethyl orthosilicate (TMOS) as a precursor, the procedure was as follows. TMOS (4.5 ml) was added to de-ionised water (5 ml). Hydrochloric acid (0.1 M, 0.1 ml) was added to the sample, and the batch was sonically agitated for 30min. The sample was removed from the sonic bath, and stored at 4 ^{o}C for 120 h. The hydrolysis was assumed to be complete at this stage, and so the sol was removed from storage, and placed in a rotary evaporator at 50 ^{o}C. From the referenced work by MacMillan *et al.*,[63] five minutes on the rotary evaporator was known to remove the alcohol. The sol mix was then combined with phosphate buffered saline (15 ml) and borate buffered saline (15 ml), at which point gelation began. Both buffer solutions were required to ensure a neutral pH in the finished sol. At this stage, the biological molecules were added to the measurement cuvette, along with the buffered sol mix. Within 5 minutes, gelation was typically complete.

The tetraethyl orthosilicate (TEOS) protocol was slightly different in practice, but conceptually the same. TEOS (9 ml) was added to de-ionised water (3 ml) and hydrochloric acid (0.01 M, 0.2 ml) in a centrifuge tube. The sample tube was sonically agitated for 1 h, keeping the bath at room temperature or lower, before storage at -18 ^{o}C for 28 days. After the 28 day period, when the solution was both clear and monophasic, hydrolysis was judged to be complete. The sol was then heated on the rotary evaporator for a 3, 4, 5, or 6 minutes at 50 ^{o}C, in order to determine the optimal evaporation time. From this point onwards, the procedure was identical to that for TMOS-mixing with buffer solutions and biomolecules, followed by gelation.

3.10 Hydrogel preparation

Work was performed in the Strathclyde University Chemistry Department with the help of Nadeem Javid; with the task being creation of an appropriate hydrogel for protein encapsulation. The labelled protein was encapsulated in an FMOC-YL hydrogel. To create the gel, 5.2 mg of FMOC-YL were combined with 500 µL of phosphate buffer (100 mM) and alternately stirred and sonically agitated until any bubbles were removed and the mixture was uniform. This hydrogel mixture was combined with the labelled protein in a 65 µL cuvette and mixed again. The encapsulated protein was then left

for 24 hours to produce a solid gel with FMOC-YL concentration of 20 mM and labelled protein concentration of 10 μM.

4 Glucose Binding Protein

Bacterially-derived glucose/galactose binding protein (GBP) from *E.Coli* is known to bind to glucose molecules- undergoing a conformational change. The two lobes of the protein molecule fold around the glucose molecule. This reaction is reversible and the proportion of folded protein molecules correlates with the concentration of glucose in the sample, paving the way for use as a glucose sensor. Figure 4.1 shows a representation of the conformational changes of wild-type glucose binding protein when binding to glucose. . The lattice parameters of GBP determined by high-resolution X-ray diffraction are *a= 61.26 Å, b=36.58 Å, c =64.94 Å*, and *α=90.00°, β=107.19°, γ=90.00°* for GBP bound to glucose. (from the Protein Data Base, http://www.pdb.org DOI: 2210/pdb2hph/pdb)

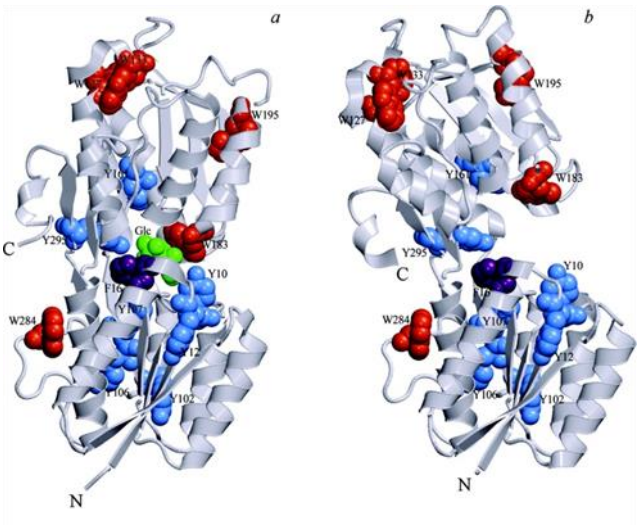

Figure 4.1- 3D structure of wild type GBP when complexed to glucose (a), and in the absence of glucose (b). Adapted from Stepanenko *et al.* [65].

From these structural representations, the conformational change is clear. The wild-type GBP has a binding constant for glucose in the micromolar region, which is orders of magnitude smaller than needed for clinical testing in the millimolar regime. Site-directed mutagenesis by the diabetes research group at Guy's Hospital has produced the triple mutant H152C/A213R/L238S with a binding constant of 11 mM. This protein is reactive to micromolar concentrations of glucose: which is the human physiological regime[58]. In addition, the cysteine mutation at the H152C site provides a platform for covalent labelling in close proximity to the glucose binding site. The structure of the mGBP protein is shown in figure 4.2.

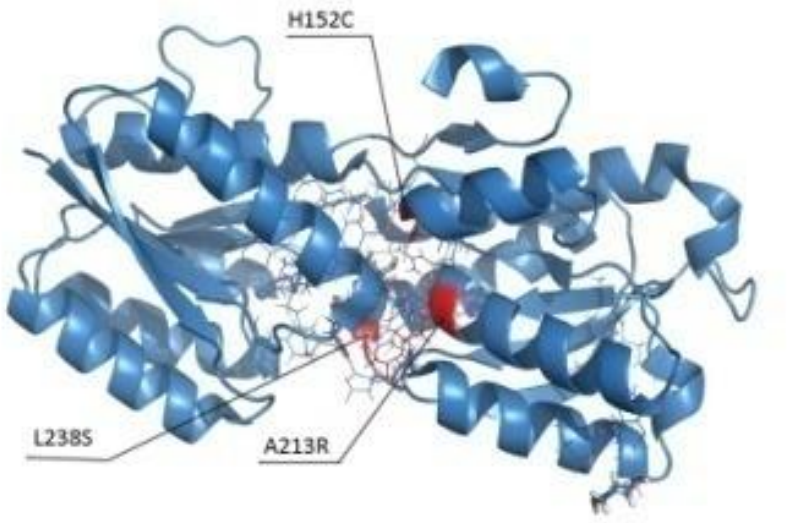

4.2- Molecular structure of triple mutant H152C/A213R/L238S glucose/galactose binding protein

Triple mutant H152C/A213R/L238S-GBP was generously provided by Dr. Faaizah Khan of the diabetes research group at Guy's Hospital, and this was the protein used for the experiments in this project.

4.1 Intrinsic fluorescence

The mGBP protein molecule itself contains fluorescent amino acids- 7 tyrosine and 5 tryptophan residues. These amino acids were investigated for intrinsic fluorescence response to glucose concentration. Intrinsic fluorescence of proteins is dominated by tryptophan, which displays a larger extinction coefficient than tyrosine. Energy absorbed by tyrosine is often transferred to the tryptophan residues in the same protein, leading to a single emission peak around 350nm. This tryptophan emission is sensitive to local environment[41].

4.2 mGBP absorbance

The absorbance spectrum of the mGBP sample was recorded. The resulting spectrum is displayed in figure 4.3.

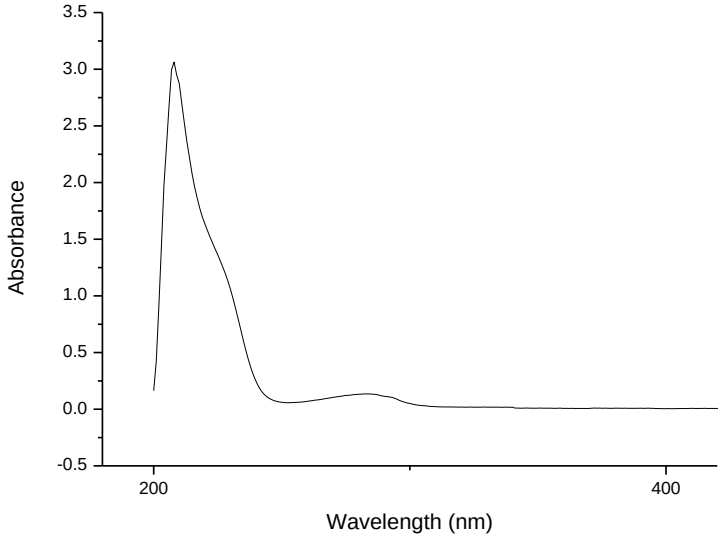

Figure 4.3- Absorbance spectrum of mGBP

The spectrum exhibits both the near-ubiquitous peptide bond absorbance at 220 nm, and a broad absorbance covering 250-300 nm, peaking around 280 nm, which corresponds to photon absorption by both amino acids. Tyrosine absorbance is seen to fall to zero at 295nm, which allows selective excitation of the tryptophan residues which continue to absorb at this increased wavelength. While the peak at 220 nm is much larger, the fluorescent amino acid peak is clearly visible in figure 4.3.

4.3 mGBP emission

With two fluorescent amino acids present in the protein, two excitation wavelengths were investigated when considering the intrinsic fluorescence. Light of wavelength 280nm was used to excite both tyrosine and tryptophan residues, while light of wavelength 295nm excited the tryptophan amino acids alone. Sample emission was measured while increasing the glucose concentration.

The fluorescence emission spectrum of the mGBP sample is shown in figure 4.4, displaying the spectra obtained when exciting at both 280 nm and 295 nm.

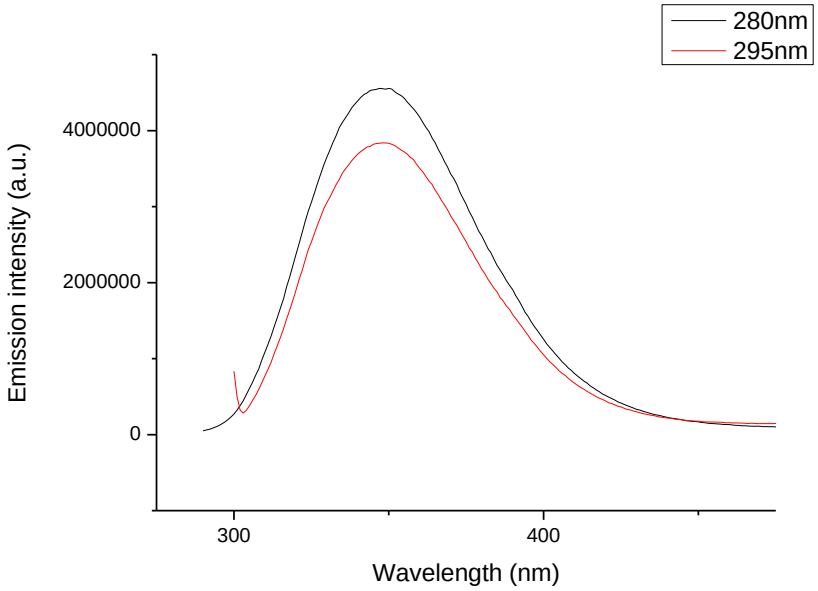

Figure 4.4- Emission spectra of mGBP when excited at both 280 nm and 295 nm

Excitation at both wavelengths leads to an emission peak at 348nm- that recognised as the characteristic tryptophan wavelength. The peak obtained when excitation takes place at 280 nm- the emission profile which includes tyrosine residues as well as tryptophan residues- shows fluorescence emission at 348 nm. The single emission peak indicates the expected energy transfer between the amino acids.

When all twelve amino acids are excited at 280nm, the emission intensity is seen to be only slightly greater than when only five tryptophan amino acids are excited. This is indicative of the tryptophan dominance in protein fluorescence[41].

Measuring the changes in intrinsic fluorescence emission intensity with respect to glucose concentration yielded the data displayed in figure 4.5. The small number of concentrations measured is due to the long time necessary for data collection. Recording all of the data for one single glucose concentration took a full week of laboratory time, and so information in the physiological glucose range was prioritised.

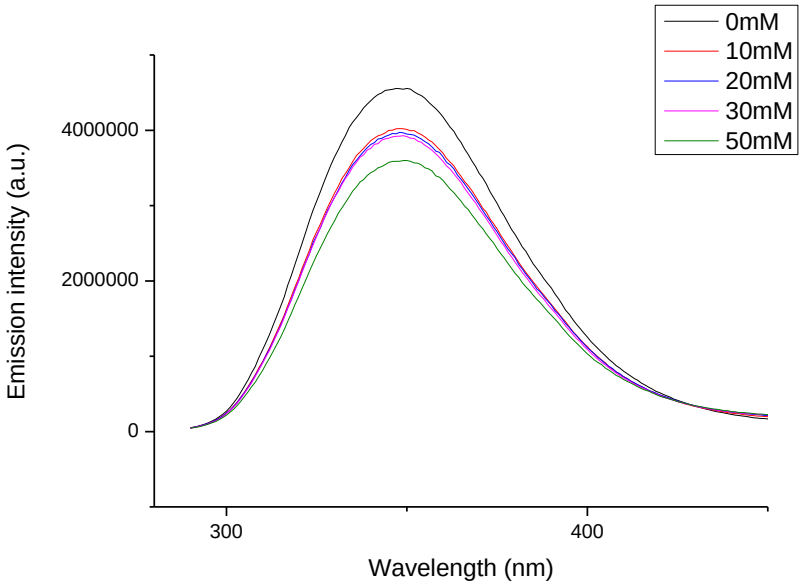

Figure 4.5- Emission spectra of GBP with glucose when excited at 280 nm

When exciting the sample at 280 nm, the fluorescence intensity decreases with increasing glucose concentration, although in a non-linear manner. It can be assumed that the amino acids are exposed to the solvent environment in a different manner with protein folding- a manner which inhibits the overall fluorescence emission.

Exciting samples at 295 nm provided the results shown in figure 4.6.

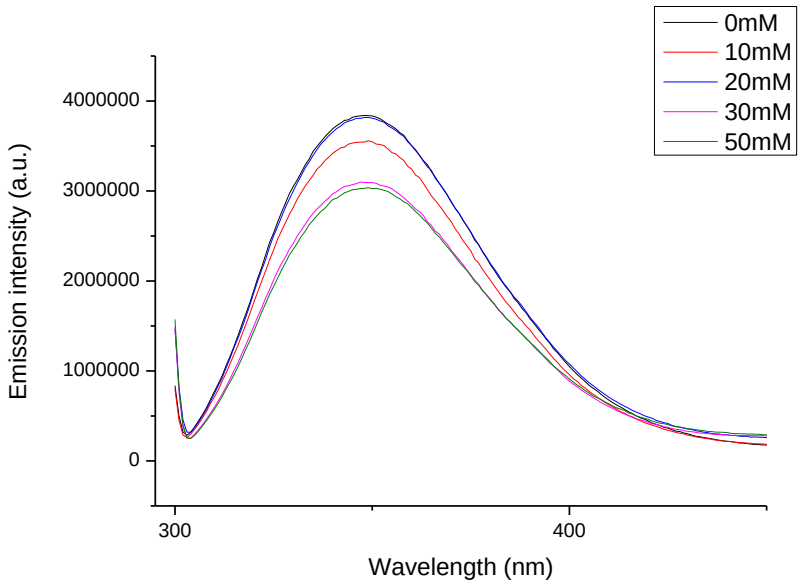

Figure 4.6- Emission spectra of GBP with glucose when excited at 295 nm

At both excitation wavelengths, the emission intensity decreases with glucose concentration without linearity. Given the large number of intrinsic fluorophores present in different locations on the molecule, discerning which specific tyrosine or tryptophan residues have their emission inhibited would be a task too complex to resolve with the data obtained.

4.4 mGBP lifetimes

The fluorescence lifetimes with increasing glucose concentration were measured. Figure 4.7 shows the recorded fluorescence decay profile for mGBP when the 295nm excitation pulse was used.

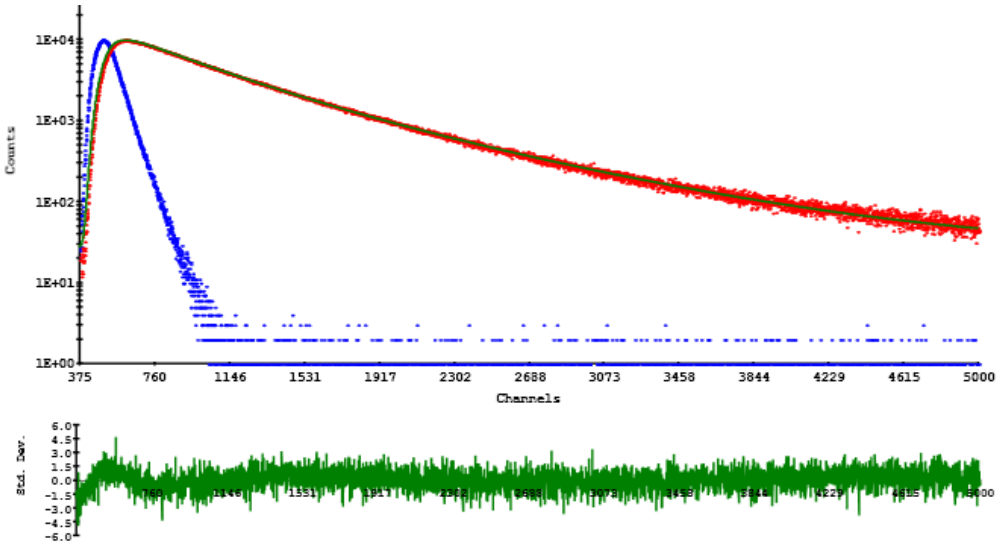

Fig 4.7- mGBP decay curve when exciting at 295nm

The recorded decay curves were fitted to 2- and 3-exponential decays, and the best-fitting parameters calculated. With 280 nm excitation, the calculated parameters are shown in table 4.1, and table 4.2 shows the results when excitation occurs at 295 nm.

mGBP: Intrinsic fluorescence when exciting at 280nm									
Glucose conc./mM	**T1/ns**	**σ/ns**	**T2/ns**	**σ/ns**	**B1**	**σ**	**B2**	**σ**	**χ2**
0	3.40	0.09	5.91	0.10	63.13	0.47	36.87	0.80	1.03
10	3.31	0.14	5.91	0.09	57.70	0.51	42.30	0.69	1.05
20	3.08	0.09	5.85	0.08	55.47	0.49	44.53	0.61	1.00
30	3.52	0.06	7.10	0.12	70.72	0.38	29.28	0.90	1.08
50	3.15	0.09	6.50	0.09	60.23	0.43	39.77	0.66	1.06

Table 4.1- 2-exponential lifetime decays of mGBP, excited at 280 nm

mGBP: Intrinsic fluorescence when exciting at 295nm									
Glucose conc./mM	**T1/ns**	**σ/ns**	**T2/ns**	**σ/ns**	**B1**	**σ**	**B2**	**σ**	**χ2**
0	3.30	0.16	5.80	0.09	63.01	0.51	36.99	0.80	1.03
10	3.02	0.13	5.69	0.08	55.97	0.53	44.03	0.63	1.11
20	2.82	0.12	5.65	0.06	48.76	0.57	51.24	0.52	1.13
30	2.98	0.12	5.86	0.07	56.08	0.53	43.92	0.55	1.06
50	2.62	0.08	5.56	0.06	50.23	0.63	49.77	0.51	1.00

Table 4.2- 2-exponential lifetime decays of mGBP, excited at 295 nm

What is apparent from tables 4.1 and 4.2 is that, judging from the χ^2 values, the 2-exponential decay model is a good fit to the experimental data. What is less apparent is why this might be so. There are 7 tyrosine residues assumed to be absorbing at 280 nm, 5 tryptophan residues assumed to be absorbing at 295 nm, and the emission is assumed to be from the 5 tryptophan residues. In other words, there are assumed to be at least 5 amino acids contributing to the fluorescence- yet the overall fluorescence decays are well modelled by 2-exponential decay models. There is no improvement in the quality of fit when adding an extra exponential factor to the calculated parameters.

One possible explanation is that for each situation- whether the protein is folded or unfolded- there are only two distinct classes of environment in which the amino acids find themselves. The relative proportions of these alternative regimes change with protein folding, but not in a linear manner. It could be the case that as certain amino acids move into a micro-environment which increases the fluorescence lifetime, other amino acids simultaneously move into a micro-environment which decreases the lifetime. The overall effect therefore shows change- but not in the direction of any particular trend.

To investigate any trends which might be useful for glucose sensing, the data were plotted to fit to fixed lifetime values. At each excitation wavelength the lifetime values in the absence of glucose were used, and the relative amplitudes collected are presented in tables 4.3 and 4.4.

mGBP: Intrinsic fluorescence when exciting at 280nm							
Glucose conc./mM	T1/ns	T2/ns	B1	σ	B2	σ	χ2
0	3.40	5.90	60.13	0.47	39.87	0.72	1.06
10	3.40	5.90	57.53	0.51	42.47	0.67	1.05
20	3.40	5.90	61.85	0.48	38.15	0.77	1.09
30	3.40	5.90	55.14	0.56	44.86	0.70	1.08
50	3.40	5.90	62.41	0.55	37.59	0.81	1.32

Table 4.3- 2-exponential lifetime decays of mGBP with fixed lifetimes, excited at 280 nm

mGBP: Intrinsic fluorescence when exciting at 295nm							
Glucose conc./mM	T1/ns	T2/ns	B1	σ	B2	σ	χ2
0	3.30	5.80	53.45	0.50	46.55	0.58	1.24
10	3.30	5.80	56.21	0.50	43.79	0.62	1.12
20	3.30	5.80	55.10	0.54	44.90	0.61	1.15
30	3.30	5.80	50.50	0.67	49.50	0.58	1.06
50	3.30	5.80	59.80	0.56	40.20	0.68	1.24

Table 4.4- 2-exponential lifetime decays of mGBP with lifetimes fixed, excited at 295 nm

The tables show that there is no real trend in the relative amplitudes. Again, although the overall fluorescence decays fit well to 2-exponential plots, the complexity of the intrinsic fluorescence makes deriving sensible information a complicated endeavour.

4.5 mGBP anisotropy

The fluorescence anisotropy of the samples was investigated with excitation at 280nm and 295nm. The anisotropy decay profile of mGBP in the absence of glucose, when exciting at 295nm, is shown in figure 4.8.

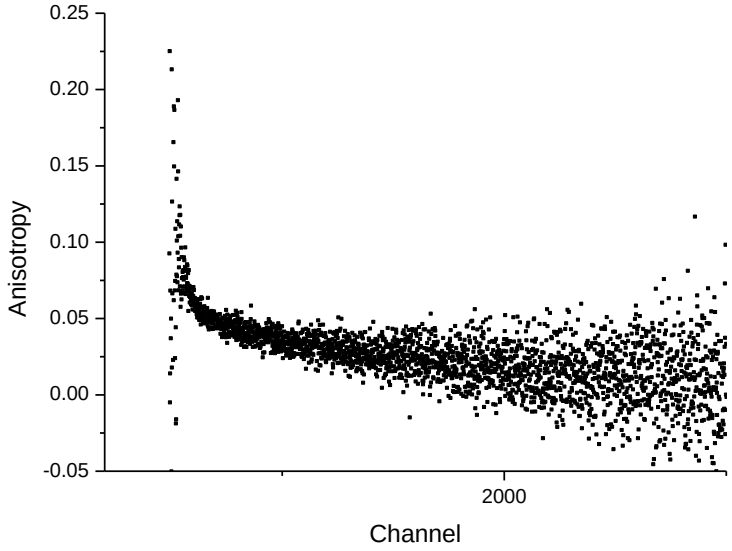

Figure 4.8-Anisotropy decay for mGBP with 295nm excitation

The measurements at both wavelengths- 280 nm and 295 nm excitation- were analysed, and provided the mono-exponential fits that are displayed in tables 4.5 and 4.6. The hydrodynamic diameters in each case were calculated according to equation 26.

mGBP Intrinsic Fluorescence: Single exponential rotational times with 280nm excitation					
Glucose conc./mM	T/ns	σ/ns	χ2	Diameter (nm)	σ/nm
0	6.03	0.28	1.09	3.59	0.17
10	5.70	0.38	1.09	3.53	0.24
20	4.91	0.33	1.11	3.36	0.23
30	4.62	0.26	1.09	3.29	0.19
50	4.16	0.24	1.16	3.18	0.18

Table 4.5- Anisotropy measurements on mGBP with 280 nm excitation

mGBP Intrinsic Fluorescence: Single exponential rotational times with 295nm excitation					
Glucose conc./mM	T/ns	σ	χ2	Diameter (nm)	σ/nm
0	9.43	0.60	1.13	4.17	0.27
10	9.10	0.61	1.07	4.12	0.28
20	8.80	0.71	1.17	4.08	0.33
30	8.14	8.59	1.12	3.97	0.42
50	6.54	4.74	1.29	3.69	0.27

Table 4.6- Anisotropy measurements on mGBP with 295 nm excitation

The anisotropy data clearly show the hydrodynamic diameters of the proteins decreasing with increasing glucose concentration. This result is a clearer one than the decay lifetime parameters

obtained- with increasing glucose concentration the protein size is seen to decrease at both excitation wavelengths, entirely as expected with increasing glucose concentration.

The apparent rotational time obtained, and the apparent diameter observed, with 280 nm excitation is noticeably shorter than that obtained at 295 nm. The protein appears to be 0.58 nm smaller when calculated using the data from the 280 nm excitation, most likely an effect emanating from the very quick energy transfer processes between amino acids prior to emission. The apparent rotational times provide calculated diameters smaller than the known lattice parameters described earlier in the chapter. X-ray diffraction shows a mean dimension of 5.43 nm, in contrast to the calculated diameter of 3.69 nm for the bound protein, this likely being a result of the sensitivity to protein conformation, and the tendency for tryptophan to transfer energy to nearby groups in the protein[41].

4.6 Conclusions

The intrinsic fluorescence of mGBP was investigated through excitation at both 280 nm and 295 nm. The decreases in the fluorescence emission intensity values when exciting at both wavelengths show that information on micro-environment changes can theoretically be obtained from the intrinsic fluorescence of the binding protein itself. The presumed complexity of the lifetime data appears to result in a 2-exponential decay curve on analysis- but one which shows little meaningful trend. The reduction in hydrodynamic diameter observed from the depolarisation data shows that the protein is folding under the experimental conditions- a more sophisticated method of analysis would be required to tease out meaningful information from the lifetime decay curves.

5 A short-wavelength fluorophore

The fluorophore 6-Bromoacetyl-2-Dimethylaminonaphthalene (BADAN), shown in figure 5.1, is known to be environmentally sensitive, with solvent polarity having an effect on fluorescence emission intensity and lifetime decays.

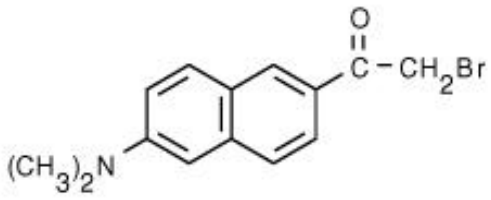

Figure 5.1- Chemical structure of BADAN

The molecule dipole moment is evidently large, as seen by the number of covalent bonds between the amide and carbonyl functional groups. The excited state of BADAN exhibits a charge transfer from the amide to the carbonyl group, involving twisting of the dimethyl amino group. This twisted conformation, or twisted internal charge transfer state (TICT), increases the dipole moment of the excited state yet further, contributing to the great tendency of BADAN to interact with the surrounding solvent polarity. This large dipole moment allows for strong solvent interactions. It is this property which makes it useful as an environmental indicator[66,67,68].

Labelling of bacterially-derived glucose binding protein to produce a glucose sensor has been described by Khan, et al[58]. The labelling protocol attaches the environmentally sensitive BADAN to a strategically useful binding site, theoretically providing the ability to monitor glucose concentration by way of the fluorescence interactions between BADAN and the surrounding polar solvent. Figure 5.2 illustrates the conceptual basis for this.

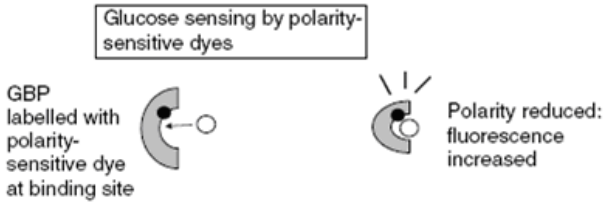

Figure 5.2- Mechanism of labelled GBP response to glucose, adapted from Pickup, *et al*. [69]

5.1 BADAN fluorescence

Before exploring the use of the labelled protein, characterisation studies of BADAN were performed in order to more fully understand the properties and performance of GBP-BADAN as a glucose sensor.

5.1.1 BADAN absorption

A few grains of BADAN dye were dissolved in dimethyl-formamide (DMF), and this stock solution was diluted in a range of solvents- n-Pentane, DMF, methanol, and phosphate buffered saline (PBS). The samples were diluted to give an absorbance value of ~0.1. The effect of the DMF on the other solvents was minimised by using the smallest possible volumes of DMF- approximately 1 µL of stock in 3 ml of solvent. The absorbance spectra were recorded, and these are shown in figure 5.3.

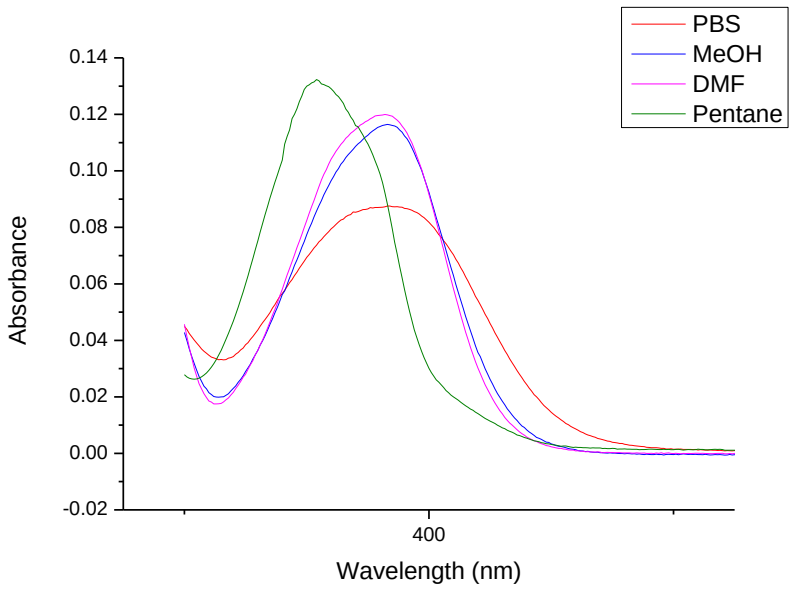

Figure 5.3- Absorbance spectra of BADAN in solvents

The absorbance spectra reveal the environmentally-sensitive nature of the BADAN absorption profile, and provide the relevant wavelengths for excitation.

5.1.2 BADAN emission

Each one of these solvent preparations was electronically excited at their absorption maximum wavelength. The emission profiles of BADAN in these solvents are shown in figure 5.4.

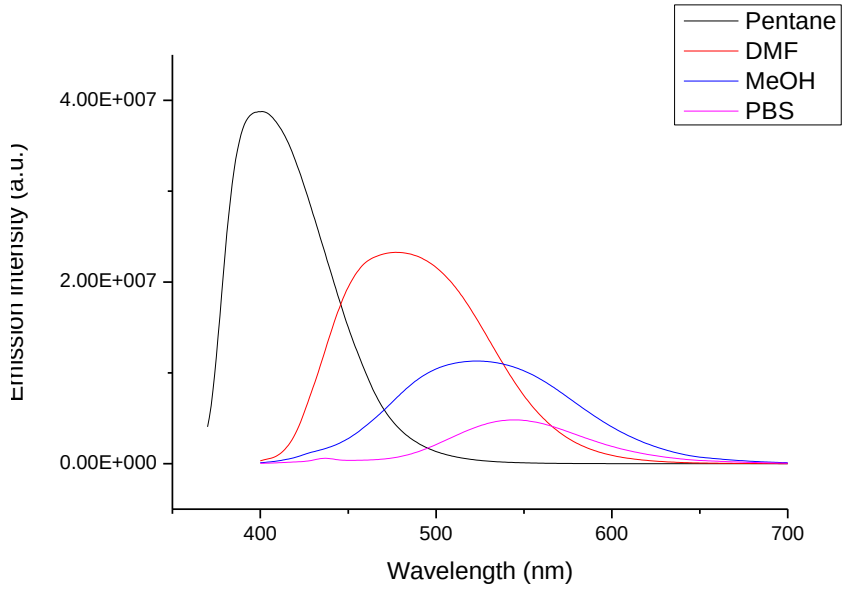

Figure 5.4- Emission profiles of BADAN in solvents of varying polarity

As can be seen from figure 5.4, the dye has the lowest emission intensity in PBS- the most polar solvent tested- and the highest intensity in n-Pentane- the least polar solvent in the experiment. The emission wavelength is also noticeably red-shifted with increasing solvent polarity.

5.1.3 BADAN lifetimes

The fluorescence lifetime decays of the above BADAN samples were measured, exciting at a wavelength of 400 nm for PBS, MeOH, and DMF, and at a wavelength of 360 nm for pentane. The best-fitting exponential functions are presented in table 5.1.

Solvent	1-exponential decay			2-exponential decay								
	T1/ns	σ/ns	χ2	T1/ns	σ/ns	T2/ns	σ/ns	B1	σ	B2	σ	χ2
PBS	1.05	0.01	4.59	0.67	0.05	1.74	0.07	64.69	1.40	35.31	1.96	1.19
MeOH	2.89	0.01	6.07	1.50	0.07	3.60	0.03	30.94	1.16	69.06	0.54	1.03
DMF	3.61	0.00	1.10	3.27	0.31	4.38	0.22	66.82	1.21	33.18	2.48	1.02
Pentane	3.52	0.00	1.11	3.47	0.05	6.61	0.03	51.47	2.66	48.53	0.05	1.08

Table 5.1: 1- and 2-exponential decay plots for BADAN in different solvents

The pattern that appears to be emerging is one of the BADAN decay curves becoming more mono-exponential in character as the solvent polarity decreases. As the solvent becomes less polar, there

will be less variation in the polarity of the microenvironment surrounding the dye, so the dye molecules on aggregate will increasingly present only one lifetime. Running alongside that observation is the increase in the fluorescence lifetime with decreasing polarity. As the solvents become less polar in nature, there are weaker interactions between the BADAN dipole and the solvent molecules.

5.1.4 BADAN response to glucose

The fluorescence response of free BADAN dye with changing glucose concentration was measured. The fluorescence emission spectra were measured at glucose concentrations comparable to those used in later protein studies. The emission spectra are shown in figure 5.5.

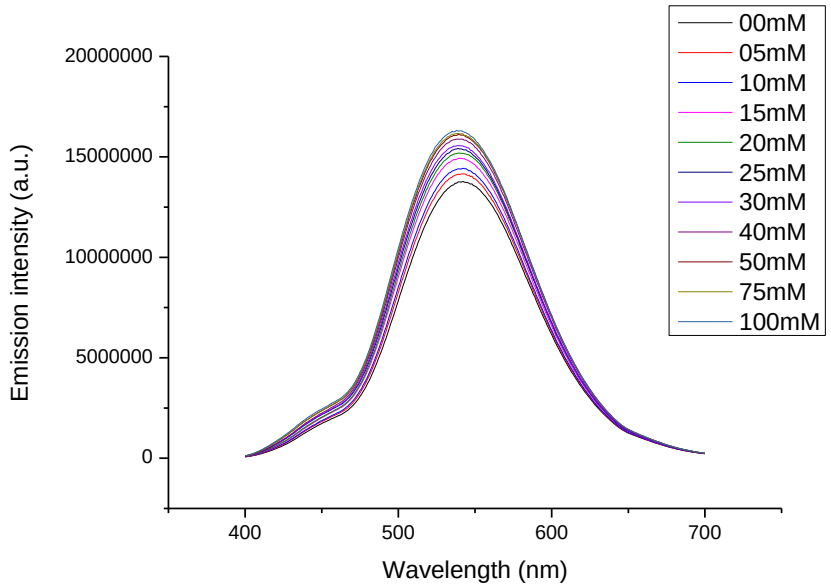

Figure 5.5: Emission spectra of BADAN in PBS with increasing glucose concentration

There is clearly a variation in emission spectral profiles. A plot of emission intensity against glucose concentration is shown in figure 5.6.

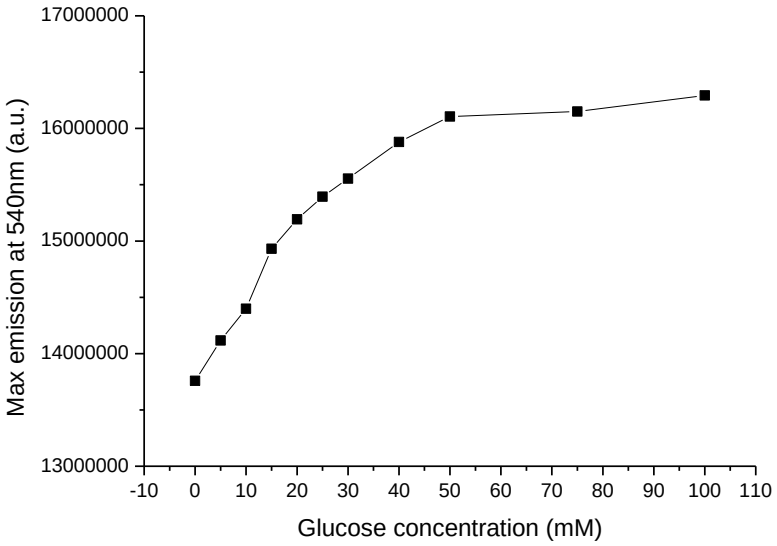

Figure 5.6: BADAN in PBS; emission intensity changes with glucose concentration

What is clear from figure 5.6 is that there is an apparent increase in emission intensity with increasing glucose concentration. This increase is from $1.38*10^{-7}$ a.u. to $1.63*10^{-7}$ a.u.- an increase of 18%. This effect- where the dye is not being affected by any protein actions, or by solvent polarity to any great extent- is curious. While the refractive index of the solvent influences fluorescence as shown in equation 9, over the glucose range studied *n* changes by only 0.0021, or 0.2%[70]. Changes in the dielectric constant of ~2% over this glucose range have been reported[71], which is a factor that must be considered. Some combination of these solvent effects contributes to the observed increase in recorded fluorescence, although it should be noted that changes in refractive index, for example, can alter the recorded fluorescence of a sample by directing a greater proportion of the emitted light onto the detector.

The fluorescence lifetimes of BADAN in buffer were recorded as the glucose concentration was increased, using a 400 nm excitation source. The best-fitting plots were found to be two-exponential. These data are presented in table 5.2.

Fluorescent lifetimes of BADAN in PBS									
Glucose conc./mM	T1/ns	σ/ns	T2/ns	σ/ns	B1	σ	B2	σ	χ^2
0	0.68	0.03	1.79	0.03	53.10	1.14	46.90	1.28	0.99
5	0.67	0.03	1.81	0.04	54.48	1.12	45.52	1.33	1.03
10	0.64	0.03	1.75	0.04	52.88	1.17	47.12	1.28	1.18
15	0.61	0.03	1.70	0.03	53.20	1.20	46.80	1.27	1.13
20	0.62	0.03	1.74	0.03	53.18	1.15	46.82	1.30	1.11
25	0.61	0.03	1.70	0.03	51.12	1.18	48.88	1.15	1.09
30	0.63	0.03	1.74	0.03	53.45	1.13	46.55	1.25	1.10
50	0.65	0.04	1.73	0.04	55.20	1.09	44.80	1.36	1.11
100	0.65	0.03	1.71	0.03	52.98	1.11	47.02	1.29	1.15

Table 5.2: BADAN in PBS; lifetime changes with glucose concentration

As can be seen from table 5.2, there is little change in the lifetimes with increases in glucose concentration. This contrasts with the noticeable increases in emission intensity over the same concentration range- increases which would have been hypothesised to result only from fewer dye-solvent interactions.

It is well known that the polarity of a solvent will have an effect on the fluorescence emission and lifetime decay of the dye BADAN. This fact was confirmed in the work above. The effect of glucose concentration on the fluorescence characteristics of the dye were investigated, and the results are intriguing. Neither the refractive index changes nor any variation in solvent dielectric constant can account for the increase in fluorescence intensity. However, the expected corresponding lifetime changes quite conclusively failed to materialise.

5.2 mGBP-BADAN fluorescence

The labelled protein sample was examined to confirm the success of the process.

After the labelling protocol was complete, the absorbance profile of the sample was measured. This spectrum is shown in figure 5.7.

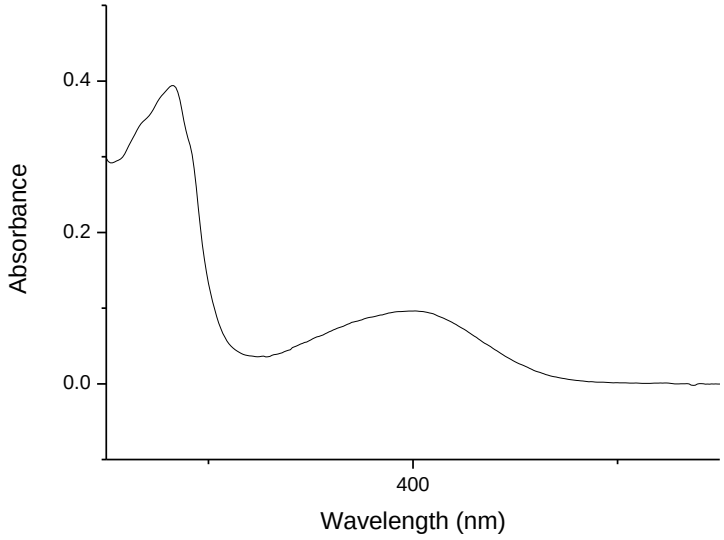

Figure 5.7: Absorbance spectrum of mGBP-BADAN after labelling

From the plot in figure 5.7, the two absorbance bands are evident- one at 280 nm, and one at 380 nm. These correspond to the expected spectral regions of intrinsic optical absorption at 280 nm for tryptophan, and at 380 nm for the extrinsic dye BADAN. The absorbance value at 280 nm is seen to be 0.394, and at 400 nm it is 0.096. The molar absorption coefficient of glucose binding protein is $4.623*10^4$ $M^{-1}cm^{-1}$ as calculated by the method described by Gill and von Hippel[72]. With the molar absorption coefficient of BADAN know to be $2.1*10^4$ $M^{-1}cm^{-1}$, and using the Beer-Lambert law (equation 2), it can be calculated that the degree of binding is 43%. That is, 43 % of mGBP molecules are labelled with a molecule of BADAN dye.

5.2.1 mGBP-BADAN emission

This mGBP-BADAN sample was fluorescently excited at 400 nm and the emission spectrum was recorded. This spectrum is presented in figure 5.8.

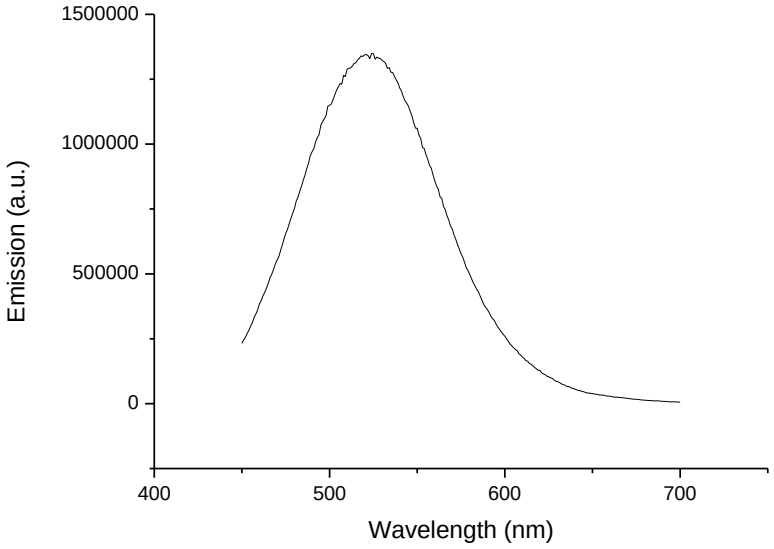

Figure 5.8- Emission spectrum of mGBP-BADAN, excited at 400 nm.

The emission peak is present at 530 nm, compared with the emission peak of 544 nm for free BADAN dye in water. With the reasoning (see figure 5.4) that increasing solvent polarity red-shifts the emission wavelength of BADAN, it can be concluded that the binding process- or at least, having the dye in the bound state- protects the dye to some degree from the solvent polarity.

With protein folding, this process is hypothesised to continue. The mGBP molecule folds in response to glucose, so the glucose concentration of the sample was increased, and the resulting emission spectra measured and recorded. The results of this investigation are shown in figure 5.9.

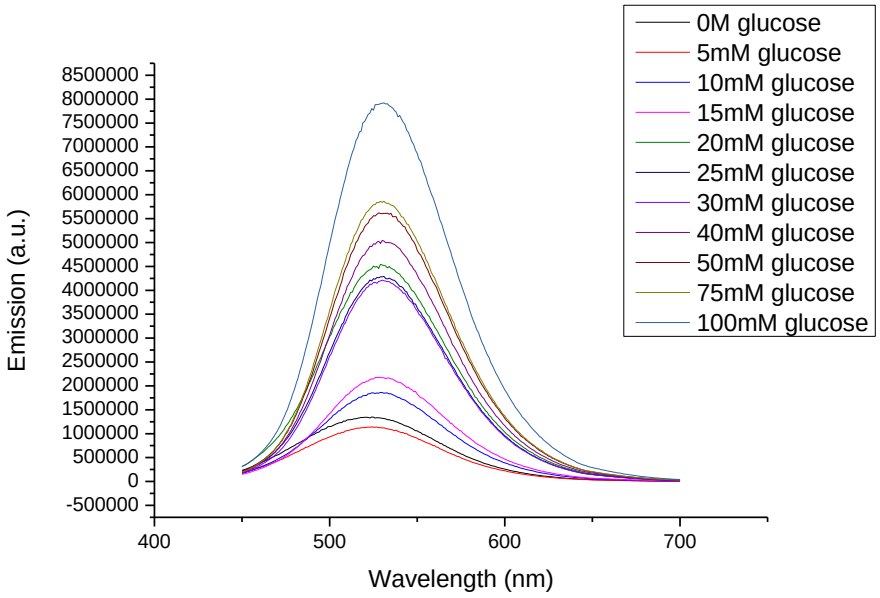

Figure 5.9- Emission spectra of mGBP-BADAN with increasing glucose concentration

Emission intensity clearly increases with increasing glucose concentration. The increases in emission intensity at 530nm from figure 5.9 are illustrated in figure 5.10.

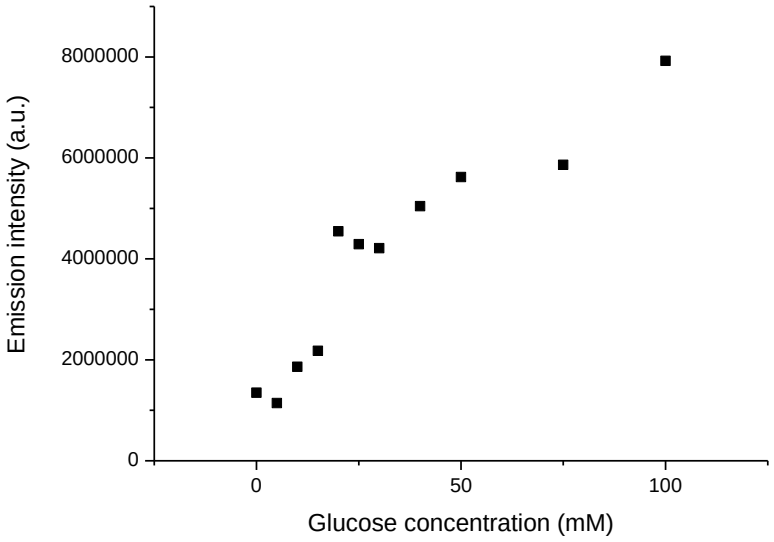

Figure 5.10- Emission intensities at 530nm of mGBP-BADAN with increasing glucose concentration

As the glucose concentration increases, so does the degree of glucose binding and protein folding, and therefore- according to the theory- so does the degree of protection for the fluorophore. With increasing protection from the polar solvent environment, the emission intensity increases as expected. Plotting the dose-response curve of fluorescence increase against logarithmic

concentration for these data as described by Khan *et al.*[58] did not provide a good sigmoidal fit, and the Origin software could not resolve a value for K_d.

From figure 5.9, there appears to be a slight wavelength shift of the peak emission value with intensity. A plot of emission peak wavelength against glucose concentration is shown in figure 5.11, with the peak wavelengths determined by careful examination of the spectral profiles.

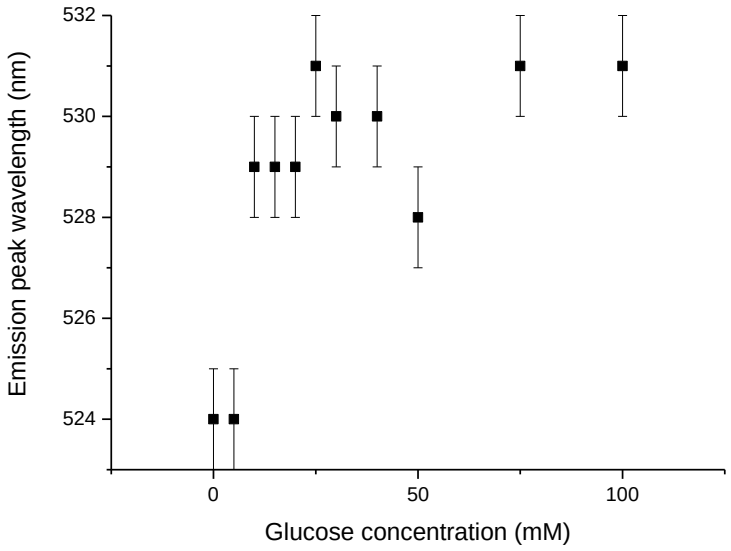

Figure 5.11- Emission peak wavelength of mGBP-BADAN at increasing glucose concentration

There is a change in the peak position, as seen in figure 5.11. The peak emission wavelength shifts from 524 nm to 531 nm over the range 0-100 mM (although it reaches that point at 25 mM glucose). This red-shifting is slight, and unexpected. As figure 5.4 clearly illustrated, less polar environments and therefore fewer dye-solvent interactions, allow free BADAN to fluoresce with greater intensity, and also at shorter wavelengths. What is found with the mGBP-BADAN complex is that when glucose concentration is increased, the dye label fluoresces with greater intensity, but at longer wavelengths. These facts appear to be inconsistent with each other, but since the relative change in emission intensity is rather greater than the relative wavelength change, the emission intensity will be given greater importance in analysis.

The spectra were analysed as a group- each spectrum was 'normalised' to the values of one chosen spectrum. Point-by-point the emission intensities were divided by the emission intensity at one specific glucose concentration- and the ratiometric size differences were then plotted. This method

was used to take away the similarities between spectral shape from sample to sample. Figure 5.12 shows the case where the 0 mM glucose sample is taken as the reference spectrum, and every other glucose concentration spectrum is divided by the values of the 0 mM plot.

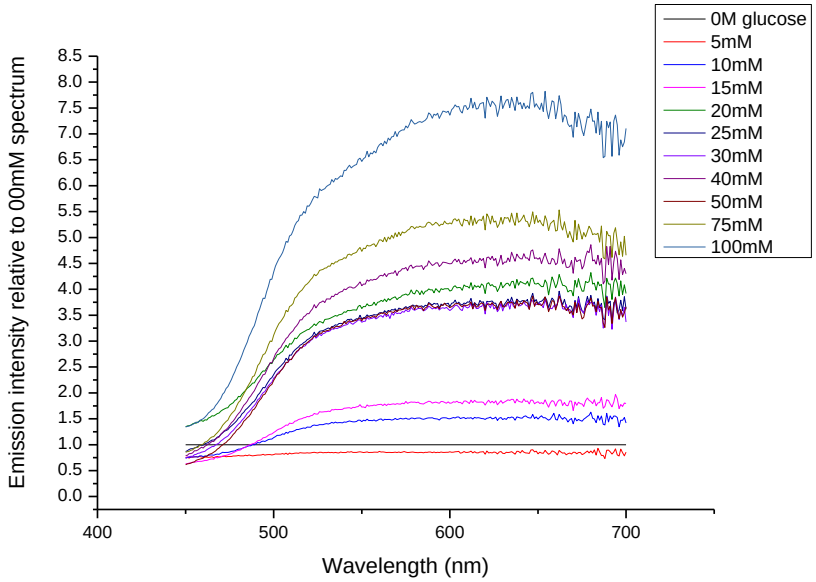

Figure 5.12- mGBP-BADAN spectra normalised to 0 mM sample values

This manipulation was performed at each sample concentration, and it was seen that the case which produced the longest-wavelength range plateaus was when 50mM was used as reference. The graph of this is shown in figure 5.13.

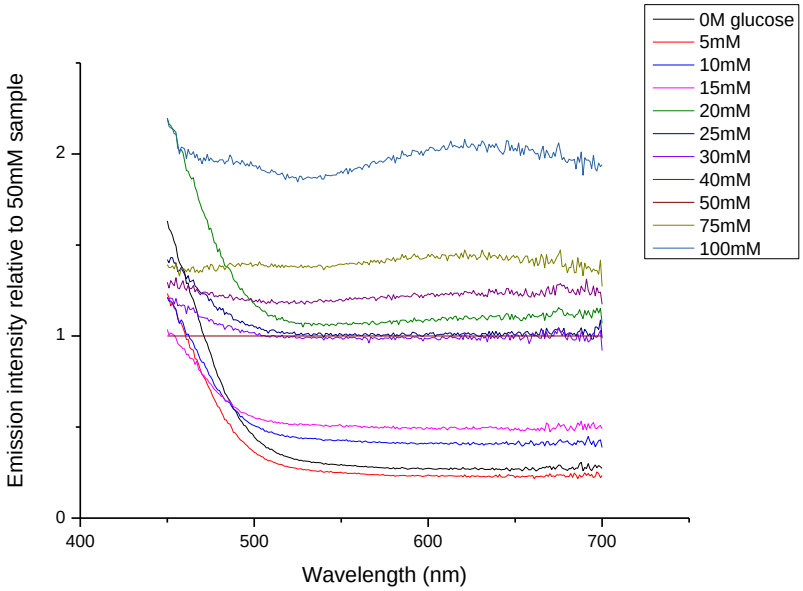

Figure 5.13- mGBP-BADAN spectra normalised to 50 mM sample values

Figure 5.13 shows that the difference between spectra extends over a long wavelength range- the contrasts at different concentrations are just as strong at 700 nm as they are at 530 nm. Figure 5.14 provides a contracted view of this situation.

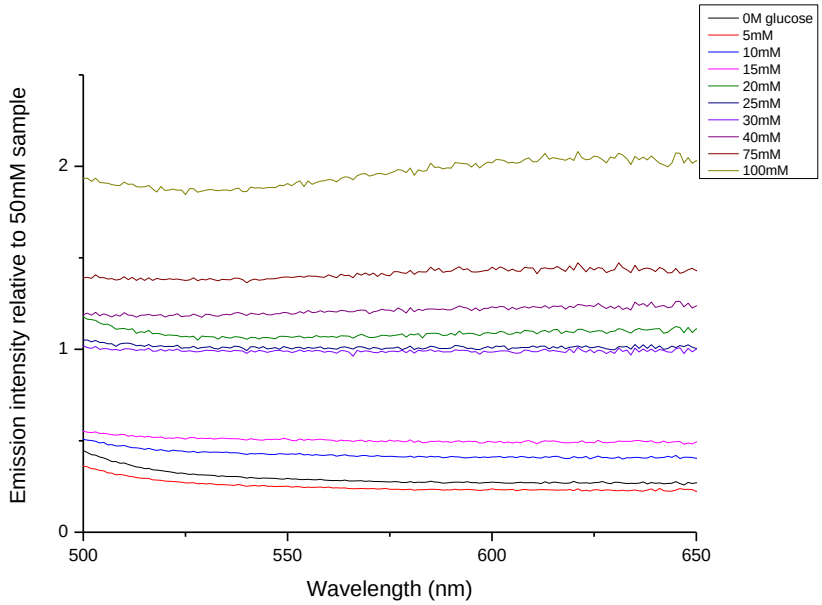

Figure 5.14- mGBP-BADAN spectra normalised to 50 mM sample values: detail

Given that the 50 mM straight line at unity is being used as reference, it has been excluded from the figure. The figure shows that the calculated fluorescence emission values over the range 500-650 nm are constant, implying that emission detection could be performed at any wavelength on this range, provided that calibrations were correctly performed.

5.2.2 mGBP-BADAN lifetimes

The TCSPC fluorescence lifetime decays of GBP-BADAN with glucose addition were recorded with excitation at 379nm. Figure 5.15 shows the decay profile recorded at 100mM glucose concentration

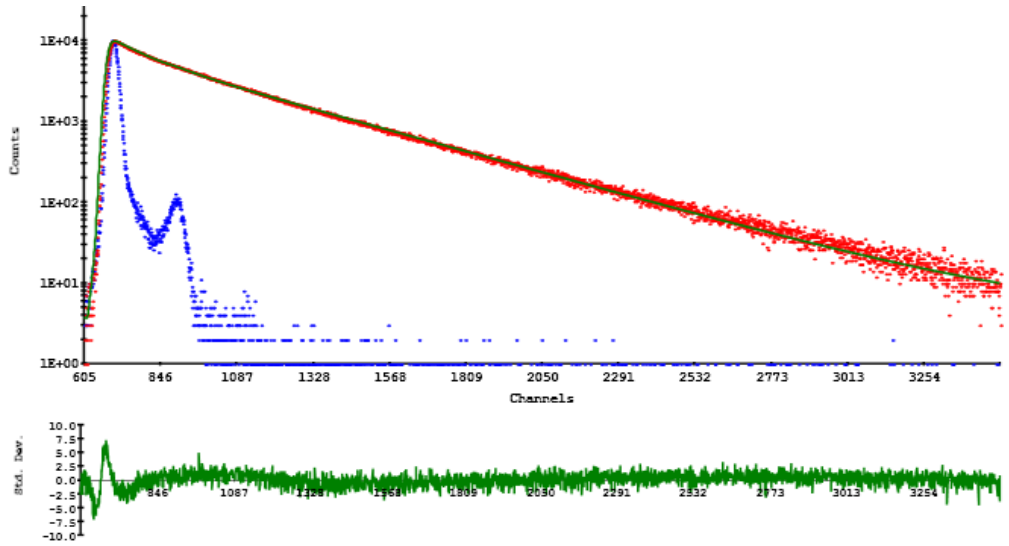

Figure 5.15 –TCSPC data for mGBP-BADAN at 100mM glucose concentration

Figure 5.16 shows the fluorescence lifetime data recorded in the presence of both 0mM and 100mM glucose.

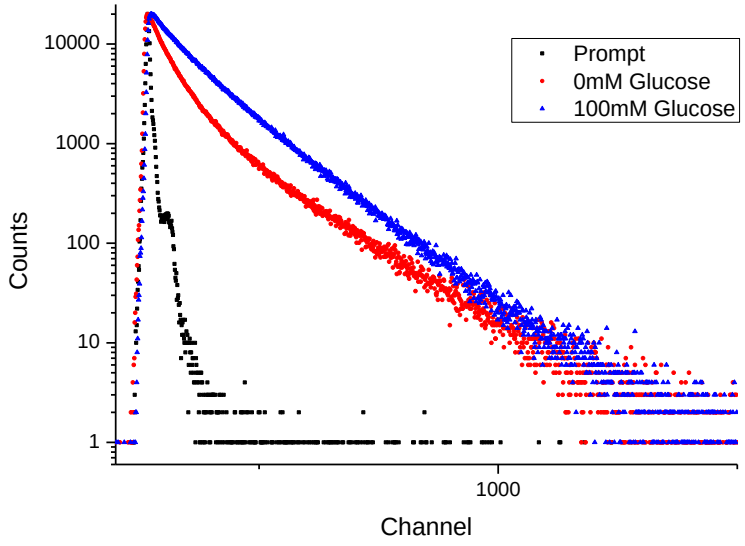

Figure 5.16- TCSPC decay curves for mGBP-BADAN at glucose concentrations of both 0mM and 100mM

Mono-exponential curves fit to the data with poor correspondence- χ^2> 15. 2- and 3- exponential fits to the data were calculated, with the quality of fit χ^2 value improving by only ~0.1 units when adding the third exponential factor. The χ^2 value of the 2-exponential plots was ~1.1. Combining these two observations with literature values[58], the decay plots were taken to be well represented by a 2-exponential model.

As glucose concentration in the sample changed, the fluorescence decay curves changed. The variations in calculated lifetimes and in calculated pre-exponential factors are shown in table 5.3.

mGBP-BADAN fluorescent lifetimes									
Glucose conc./mM	T1/ns	σ/ns	T2/ns	σ/ns	B1	σ	B2	σ	χ^2
0	0.89	0.02	3.48	0.02	40.27	0.72	59.73	0.44	1.17
5	0.84	0.02	3.33	0.02	37.53	0.73	62.47	0.40	1.29
10	1.11	0.04	3.26	0.02	32.97	0.10	67.03	0.41	1.12
15	0.97	0.04	3.11	0.02	24.92	1.13	75.08	0.37	1.10
20	0.97	0.04	3.09	0.02	21.08	1.21	78.92	0.33	1.15
25	0.97	0.05	3.04	0.01	20.52	1.31	79.48	0.33	1.15
30	1.30	0.01	3.13	0.02	40.06	1.29	59.94	0.40	1.08
40	1.30	0.01	3.11	0.02	38.79	1.33	61.21	0.40	1.13
50	1.30	0.02	3.11	0.02	38.28	1.36	61.72	0.40	1.07
75	1.30	0.02	3.10	0.02	37.06	1.40	62.94	0.39	1.05
100	1.31	0.07	3.10	0.02	36.92	1.41	63.08	0.40	1.11

Table 5.3- Calculated 2-exponential fits to mGBP-BADAN with increasing glucose concentration

The short lifetime- T1- is seen to steadily increase with glucose concentration, as the longer lifetime- T2- is seen to steadily decrease in a corresponding manner. The changes in lifetime are displayed graphically in figure 5.17.

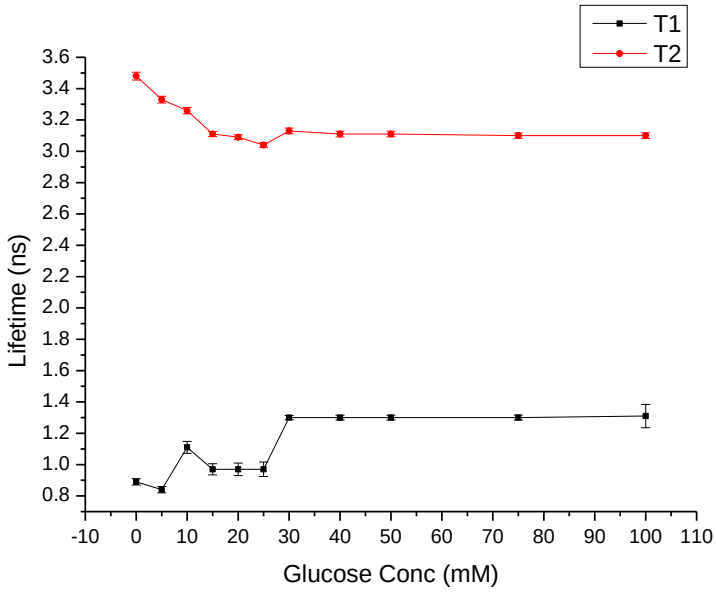

Figure 5.17- Changes in fluorescence lifetimes of mGBP-BADAN with increasing glucose concentration

The lifetimes change noticeably in magnitude over the glucose concentration range 0-30mM (conveniently the human physiological range), but after that, the changes 'flatline'. This lack of response is also in contrast to the emission intensity results seen in figures 5.9 and 5.10- where the emission intensity continued to increase with glucose concentration over the entire 0-100 mM

range. Similarly, the amplitude of the pre-exponential factors B1 and B2 changes with glucose concentration- although in a less clear manner. The changes are shown graphically in figure 5.18.

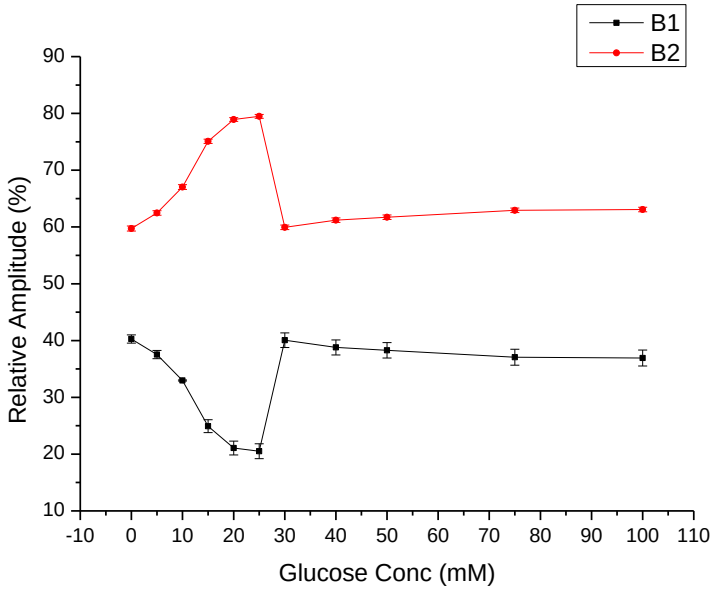

Figure 5.18- Amplitude of pre-exponential factors B1 and B2 calculated for mGBP-BADAN with increasing glucose concentration

The relative amplitude of the pre-exponential factors changes noticeably over the same concentration range for which the lifetimes themselves vary. After that point, what happens is less clear. Both the lifetimes and the relative amplitudes are changing in the same experiment, so drawing clear conclusions from either one is non-trivial.

With glucose sensing being the end goal, having one set of varying parameters which changes with glucose concentration is desirable. Forcing the decay plots to fit to a certain pair of lifetimes, and measuring the changes in the amplitude of the pre-exponential factors, would provide such a solution. Indeed, this was the method used by Khan, et al[58].

Fitting the data to the same constant lifetimes (0.90 ns and 3.20 ns) as reported in literature, the changes in pre-exponential factors were calculated on the DAS6 software. These changes are reported in table 5.4.

mGBP-BADAN fluorescent lifetime decay parameters with fixed lifetimes							
Glucose conc./mM	T1/ns	T2/ns	B1	σ	B2	σ	χ^2
0	0.90	3.20	37.86	0.86	62.14	0.44	1.72
5	0.90	3.20	35.09	0.89	64.91	0.42	1.49
10	0.90	3.20	28.69	0.98	71.31	0.37	1.16
15	0.90	3.20	24.35	1.00	75.65	0.34	1.42
20	0.90	3.20	21.38	1.06	78.62	0.32	1.54
25	0.90	3.20	20.99	1.07	79.01	0.32	1.86
30	0.90	3.20	20.29	1.07	79.71	0.31	1.99
40	0.90	3.20	19.83	1.08	80.17	0.31	2.15
50	0.90	3.20	19.57	1.09	80.43	0.31	2.10
75	0.90	3.20	19.17	1.10	80.83	0.31	2.12
100	0.90	3.20	19.17	1.09	80.83	0.31	2.27

Table 5.4- Calculated 2-exponential fits to mGBP-BADAN with increasing glucose concentration, when holding lifetimes constant

The change in pre-exponential amplitudes is apparent from table 5.4. This variation is represented graphically in figure 5.19.

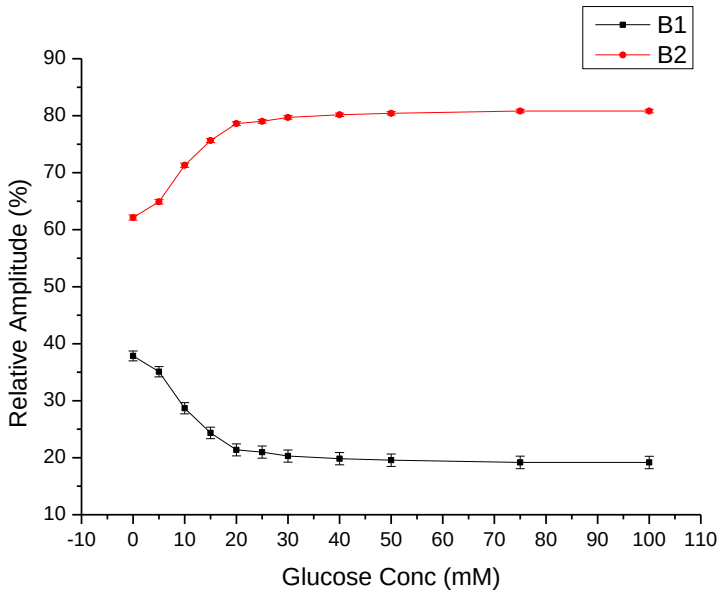

Figure 5.19- Amplitude of pre-exponential factors B1 and B2 calculated for mGBP-BADAN with increasing glucose concentration when lifetimes are held constant

Compared to the 'free' best fits in figure 5.18, figure 5.19 shows a progressive trend. The relative amplitude of the 3.2 ns component grows larger with increasing glucose concentration. The increase in relative amplitude continues past the 30 mM 'plateau' region found in figure 5.17, but with a much reduced variation between successive measurements. The literature values show a change in relative amplitudes of ~30%, levelling off around 50 mM- this experiment shows a change in relative

amplitudes of 18%, levelling off around 30 mM. This difference between laboratories may be a result of less efficient labelling (43%) in this project compared to that conducted in other locations.

The trend is a consistent one, and with the lifetimes themselves held constant, a progressive change in relative amplitudes is seen with increasing glucose concentration. This would appear to be a sound basis for a glucose sensor.

Other forced fits to chosen lifetimes were also calculated for comparison purposes, while analysing the same experimental data as before. Using the lifetimes of 1.00 ns and 3.25 ns, relative amplitudes were calculated and these data are shown in table 5.5.

mGBP-BADAN fluorescent lifetime decay parameters with fixed lifetimes							
Glucose conc./mM	T1/ns	T2/ns	B1	σ	B2	σ	χ^2
0	1.00	3.25	60.34	1.27	39.66	0.49	1.39
5	1.00	3.25	45.56	1.31	54.44	0.47	1.25
10	1.00	3.25	28.47	1.30	71.53	0.42	1.08
15	1.00	3.25	22.01	1.22	77.99	0.39	1.26
20	1.00	3.25	19.40	1.36	80.60	0.37	1.38
25	1.00	3.25	19.81	1.27	80.19	0.37	1.61
30	1.00	3.25	19.51	1.26	80.49	0.36	1.69
40	1.00	3.25	18.32	1.35	81.68	0.36	1.56
50	1.00	3.25	18.18	1.37	81.82	0.36	1.50
75	1.00	3.25	18.83	1.28	81.17	0.35	1.81
100	1.00	3.25	18.99	1.27	81.01	0.35	1.93

Table 5.5- Calculated 2-exponential fits to mGBP-BADAN with increasing glucose concentration, when holding lifetimes constant

A graphical representation of this table is shown in figure 5.20.

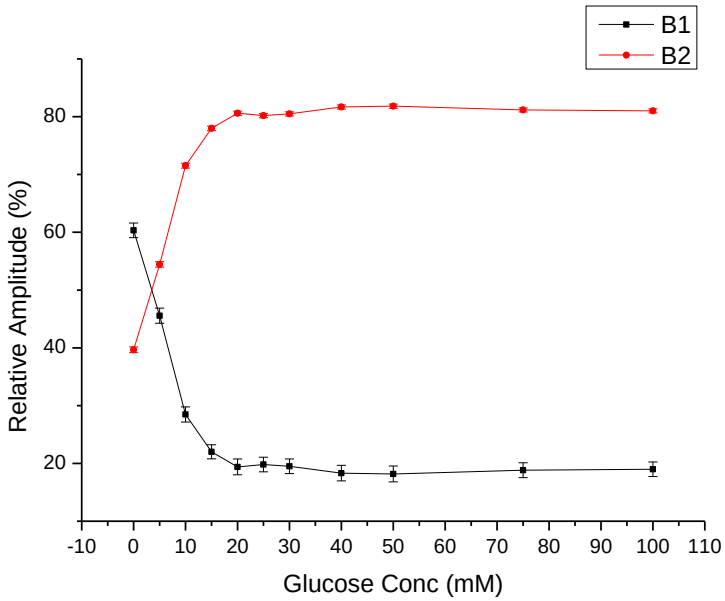

Figure 5.20- Amplitude of pre-exponential factors B1 and B2 calculated for mGBP-BADAN with increasing glucose concentration when lifetimes are held constant

When the lifetimes are forced to these slightly larger values, the response at low glucose concentrations is very strong, but these plots rapidly reach a value at 20 mM glucose from which it barely changes with respect to further glucose addition. For lower glucose concentrations this selection of lifetimes may provide greater contrast- a potentially useful feature for glucose sensing at low metabolite concentrations. After all, the data above ~30 mM glucose would be of no use in a functioning glucose sensor in a live patient.

These results confirm the potential of both fluorescence intensity and lifetime measurements of mGBP-BADAN in the construction of a viable biosensor. The results obtained fit with the reported literature values, while the lifetime analysis with different parameters held constant indicates the potential for greater sensitivity in certain concentration ranges with some fine-tuning of the analysis.

5.2.3 mGBP-BADAN anisotropy

The fluorescence anisotropy measurements were performed on the same samples as were used for the lifetime decay readings. The raw data recorded with a glucose concentration of 100 mM are shown in figure 5.21

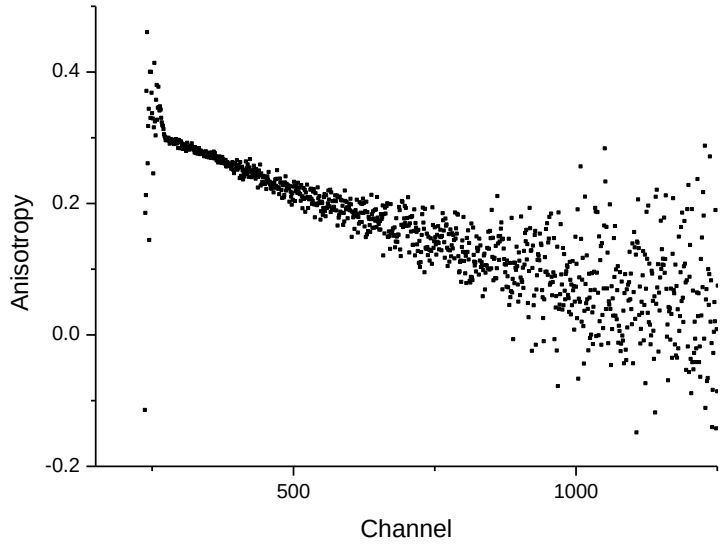

Figure 5.21- Anisotropy decay of mGPB-BADAN with glucose concentration of 100mM

After data analysis, it was seen that a mono-exponential decay was the most appropriate model for understanding the depolarisation. Table 5.6 shows the rotational correlation times of the mGBP-BADAN complex for increasing concentrations of glucose, along with the calculated hydrodynamic diameter.

mGBP-BADAN 1-exponential rotational times					
Glucose conc./mM	T/ns	σ/ns	χ2	Diameter/nm	σ/nm
0	33.44	3.23	1.19	6.36	0.61
10	38.31	4.18	1.34	6.66	0.73
20	28.00	4.48	1.24	6.00	0.96
30	26.60	2.36	1.24	5.90	0.52
40	29.50	4.69	1.12	6.10	0.97
50	24.80	2.08	1.10	5.76	0.48
75	23.40	2.72	1.15	5.65	0.66
100	23.10	2.62	1.12	5.62	0.64

Table 5.6- Anisotropy measurements of mGBP-BADAN with increasing glucose concentration

Table 5.6 reveals a consistent decrease in the rotational time from 33.4 ns to 23.1 ns over the glucose range 0-100 mM. This corresponds to a decrease in apparent hydrodynamic diameter from 6.4 nm to 5.6 nm- a finding consistent with the protein folding in response to glucose concentration. The greater the concentration of glucose, the greater is the proportion of protein molecules that fold in response, and the smaller is the average size of the protein molecules themselves. These numbers compare favourably with the crystal lattice parameters obtained by x-ray diffraction, and mentioned

in chapter 4 (*a= 61.26 Å, b=36.58 Å, c =64.94 Å)*. The recorded decrease in rotational time is illustrated with a line graph in figure 5.22.

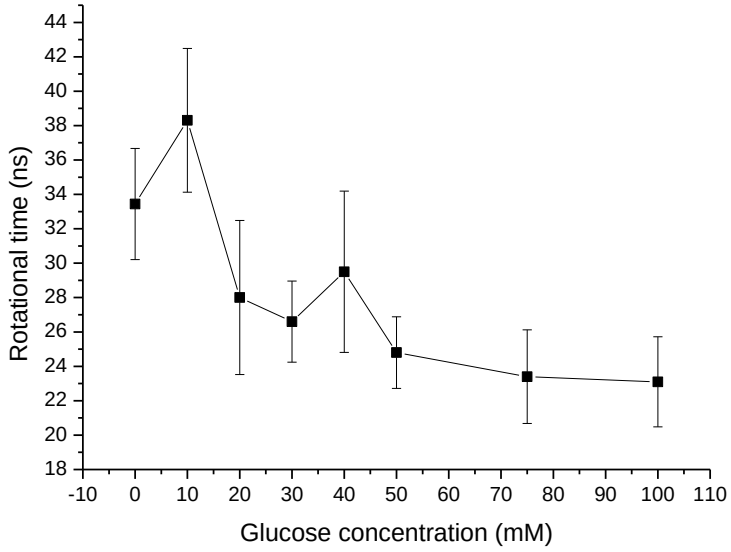

Figure 5.22- Anisotropy measurements of mGBP-BADAN with increasing glucose concentration

Although there are two anomalously high results in figure 5.23, the uncertainties in these measurements are also large. The trend of decreasing rotational correlation time is a valid one, given the size of the measured uncertainties. The overall decrease in rotational time- and therefore in protein size- is evident from this figure. This confirms the proposed mechanism of protein folding by which the sensor operates.

5.3 Conclusions

The fluorescent dye BADAN is known to be environmentally sensitive- especially to the effects of solvent polarity. What we have shown is that the dye is sensitive to the level of exposure to a solvent environment when the solvent polarity does not change. Labelling mGBP with the dye produced a complex which showed a change in fluorescence emission intensity of 500% in the presence of saturating glucose. The fluorescence lifetimes similarly showed a response to glucose concentration, with the long lifetime component of a 2-exponential decay becoming increasingly dominant as concentration was increased. Anisotropy studies of the labelled protein revealed a calculated hydrodynamic diameter comparable to the lattice parameters observed in x-ray diffraction. This

calculated diameter decreased with increasing glucose concentration, confirming the action of protein folding by which the mGBP is understood to function.

6 Robustness of mGBP-BADAN

Glucose binding protein is known to bind very strongly to glucose and galactose. What is unclear from literature is how strongly it might bind to other sugars involved in human metabolism. The concentration of glucose in human blood is approximately two orders of magnitude greater than other carbohydrates, but quantification of the effect of these low concentration sugars was considered desirable. Two sugars were chosen for investigation- fructose and lactose.

D-(-)-Fructose is a simple sugar with the same molecular weight as glucose (180g/mol). The molecular structure of D-(-)-fructose is shown in figure 6.1. All further references in this chapter to fructose refer to the D-(-)-fructose molecule.

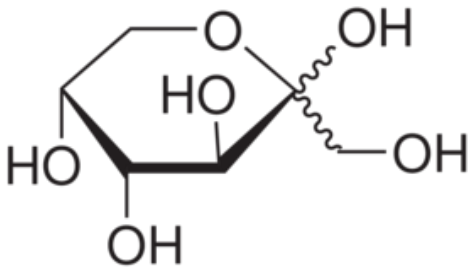

Figure 6.1- Molecular structure of D-(-)-fructose

D-Lactose is also a simple sugar, one that is almost twice the molecular weight of glucose and fructose, weighing in at 342 g/mol. A molecule of lactose is broken down in the body into one glucose and one galactose molecule- this relationship is apparent from the molecular structure, shown in figure 6.2. All further references in this chapter to lactose refer to the D-lactose molecule.

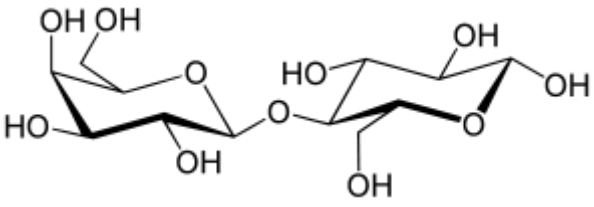

Figure 6.2- Molecular structure of D-lactose

The effect of temperature on the mGBP-BADAN response to glucose was also investigated. Two temperatures were chosen to illustrate the concept- 37 ^{o}C and 50 ^{o}C. 37 ^{o}C was chosen for its link to

body temperature, and 50 ^{o}C was chosen as a roughly similar 'jump' as was expressed between room temperature and body temperature.

After the system was tested at temperatures outside of the normal functioning range, it was decided to also test the system in solutions of varying pH. The phosphate buffered saline used in the previous experiments has a pH value of 7.4, the same as found in serum. The buffer solutions chosen for comparison were the commonly-available borate buffer (pH 9.2) and phthalate buffer (pH 4.0).

The excitation wavelength for all fluorescence emission spectra in the chapter was 380 nm, and for lifetime decays a 379 nm source was used.

6.1 Alternative Sugars

mGBP-BADAN samples were investigated for changes in fluorescence properties with the two alternative sugars. 10 µM GBP-BADAN samples had aliquots of either fructose or lactose solution added until the concentration of that sugar was 100 mM in the sample cuvette. At this assumed saturation sugar concentration, the concentration of glucose in the sample was then steadily increased from 0 mM to 100 mM- with the goal of examining the specificity of the mGBP, and particularly whether the presence of two of the most common carbohydrate metabolites might affect the protein function.

6.1.1 Fructose response: emission

Fructose, with the same molecular weight as glucose, was examined first. The samples were excited at 380 nm and the emission spectra were recorded. The fluorescence emission intensities at the peak wavelength (530 nm) were collated.

Figure 6.3 shows a plot of fluorescence emission intensity against total sugar concentration. The first 100 mM of sugar added were fructose, and the second 100 mM were glucose. The values were ratiometrically adjusted to take account of sample dilution. No changes were observed in the wavelength of maximum emission intensity with increasing fructose concentration.

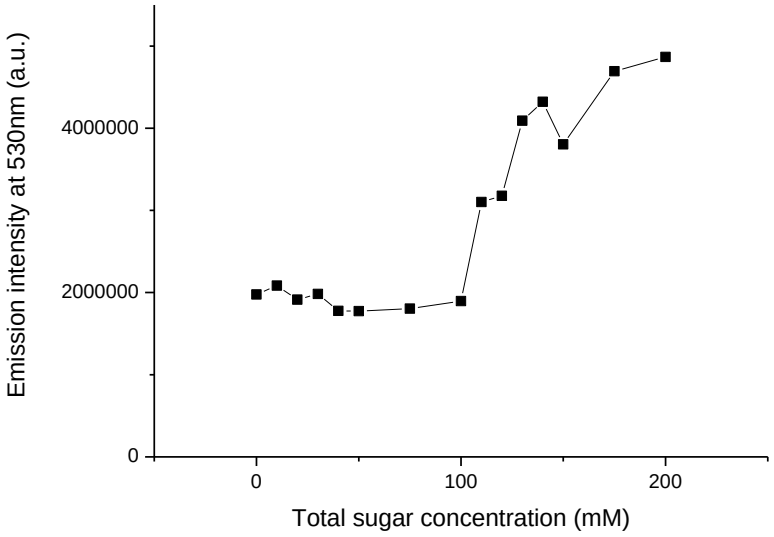

Figure 6.3- Emission intensities at 530nm of mGBP-BADAN with increasing total sugar (fructose then glucose) concentration

The figure shows that when fructose concentration is increased, the emission intensity does not increase- in fact; it decreases slightly over this range. At total sugar concentration of 100mM, there is saturation level of fructose and no glucose at all. From 110 mM onwards, there is glucose present in the sample and the emission intensity correspondingly increases noticeably.

This suggests that the specificity of mGBP for binding to glucose is very high. There is little noticeable effect on emission intensity corresponding to fructose addition, but even with a high concentration of fructose in the solution, the mGBP-BADAN system shows a strong response to glucose addition.

Plotting a sigmoidal dose-response function to the data provides the graph shown in figure 6.4.

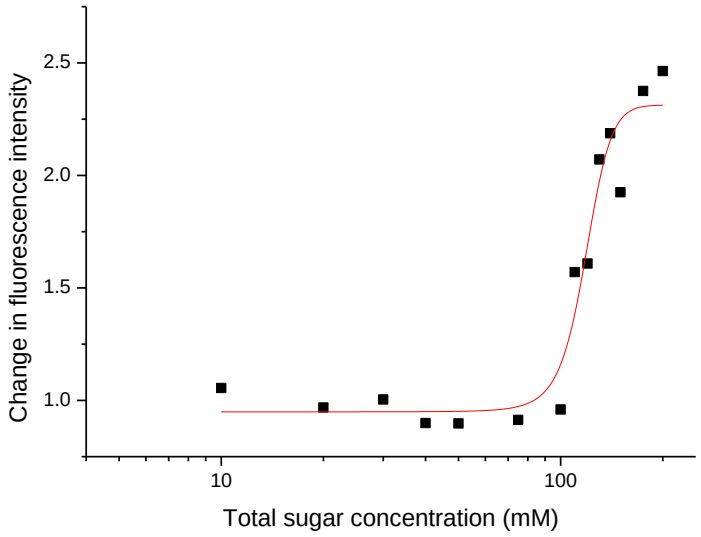

Figure 6.4- Dose response curve of mGBP-BADAN in saturating fructose concentration

Analysis of the data, performed using the Origin software, reveals a K_d value of 118.16 (±3.72) mM for total sugar concentration, or 18.16 (±3.72) mM for glucose response in the presence of saturating fructose. This is seen to be higher than the K_d of 11mM reported for the glucose response alone.

6.1.2 Fructose response: lifetimes

The fluorescence lifetimes for each of these samples were also recorded. Table 6.1 shows the changes in the 2-exponential decay lifetimes with the addition of the fructose solution aliquots. Table 6.2 shows the differences found in the 2-exponential decay lifetimes with glucose addition- in the presence of 100 mM concentration of fructose.

mGBP-BADAN fluorescence lifetimes with increasing fructose concentration									
Fructose conc./mM	T1/ns	σ/ns	T2/ns	σ/ns	B1	σ	B2	σ	χ2
0	0.79	0.02	2.75	0.04	54.71	0.77	45.29	0.79	1.47
10	0.71	0.02	2.88	0.04	48.66	0.67	51.34	0.68	2.11
20	0.70	0.02	2.89	0.04	49.07	0.66	50.93	0.66	2.30
30	0.71	0.02	2.89	0.04	49.24	0.66	50.76	0.66	2.12
40	0.71	0.02	2.86	0.04	49.20	0.66	50.80	0.66	2.10
50	0.70	0.02	2.83	0.04	49.47	0.67	50.53	0.66	2.25
75	0.69	0.02	2.79	0.04	49.19	0.67	50.81	0.68	2.26
100	0.70	0.02	2.79	0.04	49.78	0.67	50.22	0.67	2.14

Table 6.1- 2-exponential lifetime changes of mGBP-BADAN with fructose addition

mGBP-BADAN fluorescence lifetimes with increasing glucose concentration									
Fructose concentration of 100mM throughout									
Glucose conc./mM	T1/ns	σ/ns	T2/ns	σ/ns	B1	σ	B2	σ	χ2
0	0.70	0.02	2.79	0.04	49.78	0.67	50.22	0.68	2.14
10	0.88	0.03	3.12	0.02	24.46	1.04	75.54	0.40	1.22
20	0.94	0.04	3.16	0.02	22.45	1.14	77.55	0.39	1.18
30	0.96	0.04	3.14	0.02	21.11	1.21	78.89	0.39	1.14
40	0.97	0.05	3.14	0.02	20.41	1.25	79.59	0.38	1.13
50	0.99	0.05	3.15	0.02	20.69	1.24	79.31	0.39	1.23
75	1.00	0.05	3.15	0.02	19.92	1.31	80.08	0.39	1.10
100	1.01	0.05	3.16	0.02	19.98	1.30	80.02	0.39	1.23

Table 6.2- 2-exponential lifetime changes of fructose-saturated mGBP-BADAN with glucose addition

Table 6.1 shows the best-fitting 2-exponential lifetime decays when the fructose concentration was increased. Over the range of 0-100 mM fructose, there appears to be negligible change in either the lifetimes or the relative amplitudes of the pre-exponential factors. This contrasts with the addition of glucose to mGBP-BADAN as explored in chapter 5. The lack of fluorescence lifetime response to fructose concentration strongly implies that the protein itself is not responding (binding) to the sugar.

With fructose concentration held high, the mGBP-BADAN fluorescence lifetime response to glucose addition is clear from table 6.2. With the best-fitting 2-exponential plots to the decays, changes in fluorescence lifetimes and in the relative amplitudes of the pre-exponential factors are clear. The greatest alteration in response is seen with the first change in glucose concentration- from 0 mM to 10 mM. This initial addition of glucose is responsible for 85% of the change in relative amplitudes. The response over this range is more rapid than is seen for the mGBP-BADAN without fructose present.

It would appear that the binding protein is being primed in some way by the presence of fructose- although there is no reaction, subsequent responses to glucose are stronger than would be predicted. However, given the orders of magnitude variation between the metabolites in the human body, such information should likely not impede progress in construction of a glucose sensor.

6.1.3 Lactose response: emission

The fluorescence response to lactose was then examined. As with the fructose experiments, the lactose concentration was increased from 0 mM to 100 mM, and then the glucose concentration of this sample was subsequently increased from 0 mM to 100 mM.

Fluorescence emission spectra were recorded and the emission maximal intensities at the peak wavelength (530 nm) were collated, and are shown in figure 6.4. The intensity values have been adjusted ratiometrically to take account of changes in sample volume, and as in figure 6.3 the sequence is lactose addition to saturation first, then glucose addition. No changes were observed in the wavelength of maximum emission intensity with increasing fructose concentration.

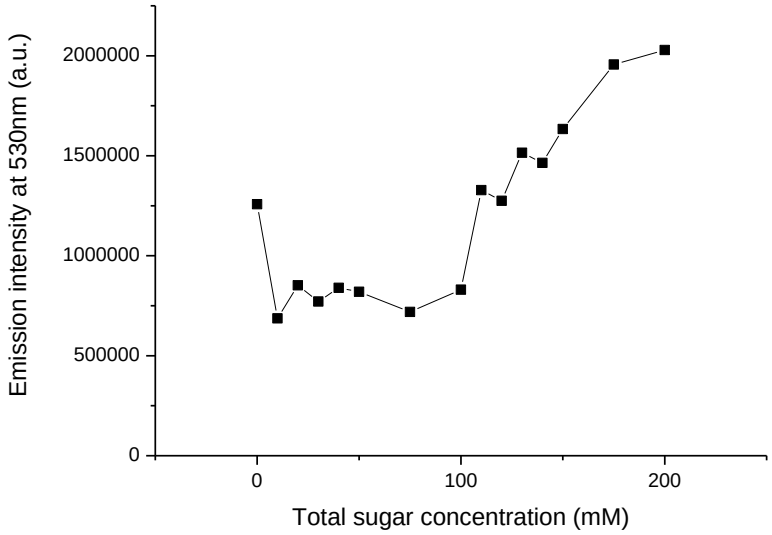

Figure 6.5- Emission intensities at 530nm of mGBP-BADAN with increasing total sugar (lactose then glucose) concentration

Figure 6.5 shows that for the lactose concentration 10 mM to 100 mM, there is very little noticeable change in emission intensity. Between 0 mM and 10 mM lactose, there is a strong decrease in emission intensity, for reasons unclear. Unfortunately, the low stocks of mGBP precluded a repeat of this experiment. Repetition of these measurements would account for any anomalously, perhaps erroneously, high or low readings. In contrast with the data from figure 6.3 which showed an emission intensity at zero glucose concentration of $2*10^6$, the intensity recorded in figure 6.5 is seen to be $1.25*10^6$. Once again, repeat experiments would reveal more about this situation.

Plotting a sigmoidal dose-response function to the data provides the graph shown in figure 6.6.

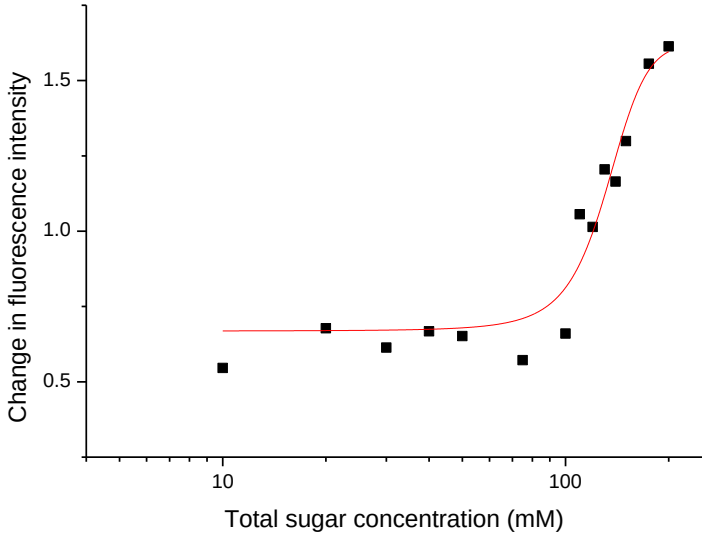

Figure 6.6- Dose response curve of mGBP-BADAN in saturating fructose concentration

Analysis of the data, performed using the Origin software, reveals a K_d value of 106.14 (±9.45) mM for total sugar concentration, or 6.14 (±9.45) mM for glucose response in the presence of saturating fructose. The literature value for the K_d of 11mM reported for the glucose response alone is within the calculated uncertainty of this experimental result.

6.1.4 Lactose response: lifetimes

Each of the above lactose/glucose samples was investigated for fluorescence lifetime decay changes in the same manner as were the fructose/glucose samples. The changes in the 2-exponential decay functions over the range 0 mM to 100 mM lactose are shown in table 6.3. Table 6.4 shows the changes when the lactose concentration was 100 mM, and the glucose concentration ranged from 0 mM to 100 mM.

mGBP-BADAN fluorescence lifetimes with increasing lactose concentration									
Lactose conc./mM	**T1/ns**	**σ/ns**	**T2/ns**	**σ/ns**	**B1**	**σ**	**B2**	**σ**	**χ2**
0	0.83	0.02	3.09	0.04	55.63	0.61	44.37	0.70	1.54
10	0.83	0.02	3.08	0.04	55.88	0.61	44.12	0.70	1.50
20	0.84	0.02	3.08	0.04	57.28	0.60	42.72	0.72	1.56
30	0.81	0.02	2.96	0.04	56.16	0.62	43.84	0.71	1.56
40	0.83	0.02	2.95	0.04	57.18	0.62	42.82	0.74	1.43
50	0.81	0.02	2.92	0.04	56.31	0.63	43.69	0.72	1.52
75	0.81	0.02	2.85	0.04	56.57	0.64	43.43	0.73	1.53
100	0.80	0.02	2.86	0.04	55.47	0.79	44.53	0.81	1.57

Table 6.3- 2-exponential lifetime changes of mGBP-BADAN with lactose addition

mGBP-BADAN fluorescence lifetimes with increasing glucose concentration									
Lactose concentration of 100mM throughout									
Glucose conc./mM	T1/ns	σ/ns	T2/ns	σ/ns	B1	σ	B2	σ	χ2
0	0.79	0.02	2.86	0.04	55.47	0.79	44.53	0.81	1.57
10	0.74	0.03	2.93	0.02	24.34	1.09	75.66	0.43	1.41
20	0.73	0.03	2.91	0.02	22.65	1.15	77.35	0.42	1.31
30	0.76	0.04	2.92	0.02	22.69	1.15	77.31	0.42	1.40
40	0.77	0.03	2.93	0.02	21.42	1.20	78.58	0.41	1.28
50	0.77	0.03	2.93	0.02	20.59	1.23	79.41	0.40	1.33
75	0.74	0.04	2.90	0.02	18.97	1.31	81.03	0.39	1.40
100	0.75	0.04	2.92	0.02	18.97	1.32	81.03	0.39	1.40

Table 6.4- 2-exponential lifetime changes of lactose-saturated mGBP-BADAN with glucose addition

In comparison with figure 6.4, table 6.3 shows no change in fluorescence response with lactose addition. The lifetimes and relative amplitudes both show negligible change over the entire range of lactose concentrations- including the 0-10 mM range. There is no change in fluorescence lifetime response of the GBP-BADAN when lactose is present, strongly implying- as was the case with fructose- that the protein is not binding to the alternative sugar.

Table 6.4 reveals that the relative amplitudes of the pre-exponential factors change dramatically over the 0-10 mM glucose range, and show incremental changes after that point. The analysis here mirrors that for the fructose experiment- that the sensor molecule shows no response to the alternative sugar, but that the response to glucose is more rapid than would be expected. As with fructose, however, the greatly exaggerated nature of the lactose concentration in this experiment should not unduly worry those conducting experiments on blood itself.

After this work, it is evident that the glucose binding protein is very efficient in its job. Similarly sized and structured sugar molecules elicit no response- showing the high selectivity of the protein for binding to glucose.

6.2 Changes in temperature

The effect of temperature on the mGBP-BADAN complex was investigated. For these experiments the sample cuvettes were held at the appropriate temperature using water baths connected to the spectrometer sample holders. The samples were held at elevated temperature for half an hour before the first measurement, and then held constant for the duration of the experiment- with the exception of the few seconds required to change between measurement devices.

The laboratory temperature was measured at arbitrary, semi-regular, intervals over the six months preceding these experiments, and was found to vary between 19 °C and 21 °C during that time, depending on weather and ambient conditions. Lab temperature for these experiments was 21 °C.

6.2.1 37 °C emission

The sample chamber of the emission spectrometer was held steady at 37 °C, and the emission spectral changes were recorded in response to glucose. Figure 6.7 shows the emission spectra recorded.

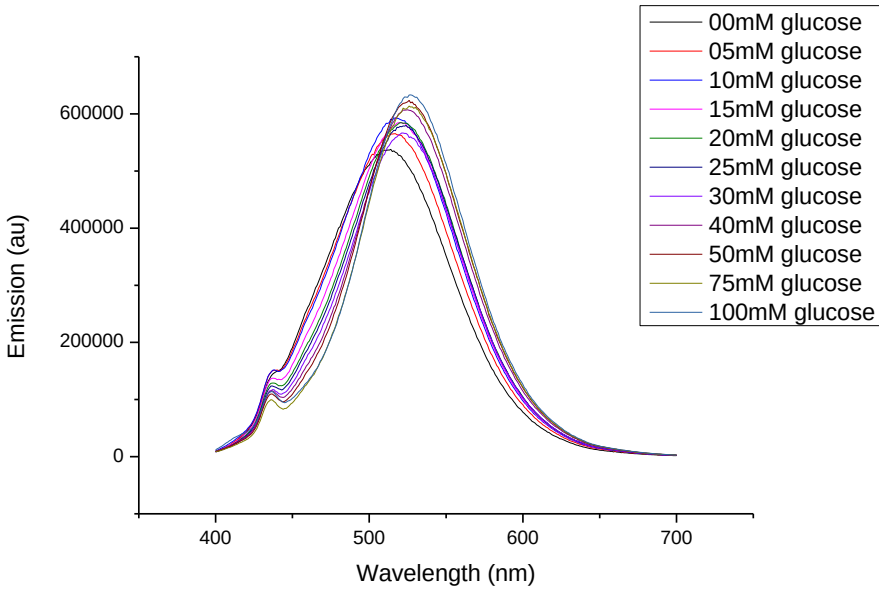

Figure 6.7- Emission spectra of mGBP-BADAN at 37 °C with glucose addition

Figure 6.7 appears to show a less pronounced emission increase with glucose at 37 °C than was seen at 21 °C (see figure 5.10). Plotting the emission intensities against glucose concentration provides the data for figure 6.8.

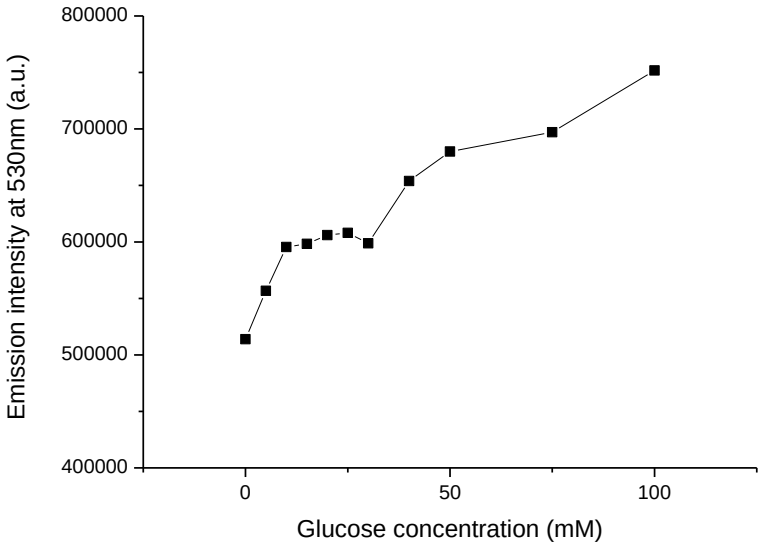

Figure 6.8- Emission intensities at 530nm of mGBP-BADAN at 37 ^{o}C, with changing glucose concentration

From figure 6.8 it is clear that there is an increase in emission intensity with glucose concentration, but that the response is less marked than at room temperature. At room temperature the fluorescence emission showed a 400% increase in intensity over the studied glucose range- at 37 ^{o}C the intensity shows a 50 % increase only. A reduced response at body temperature might raise questions as to the suitability of the system as a bio-sensor, when studying emission intensity. However, the trend is still clear, as the emission intensity increases over the measured range of glucose concentration.

6.2.2 37 ^{o}C lifetimes

TCSPC measurements on the samples were made at each glucose concentration, again holding the temperature constant at 37 ^{o}C. The χ^2-minimised 2-exponential fits to these data are shown in table 6.5.

mGBP-BADAN fluorescence lifetimes at 37°C									
Glucose conc./mM	**T1/ns**	**σ/ns**	**T2/ns**	**σ/ns**	**B1**	**σ**	**B2**	**σ**	**χ^2**
0	0.87	0.02	3.52	0.03	76.06	0.75	23.94	0.47	1.14
5	0.98	0.03	3.43	0.03	70.09	1.04	29.91	0.50	1.04
10	1.01	0.03	3.45	0.03	69.37	1.01	30.63	0.51	1.10
15	1.05	0.03	3.43	0.03	68.03	1.00	31.97	0.51	1.12
20	1.06	0.03	3.37	0.03	66.52	1.04	33.48	0.51	1.10
25	1.08	0.03	3.35	0.03	65.48	1.04	34.52	0.51	1.06
30	1.04	0.04	3.27	0.02	66.27	1.04	33.73	0.47	1.06
40	1.09	0.03	3.24	0.02	63.15	1.03	36.85	0.46	1.05
50	1.13	0.04	3.23	0.02	61.94	0.97	38.06	0.46	1.08
75	1.13	0.04	3.15	0.02	58.46	1.04	41.54	0.45	1.08
100	1.19	0.06	3.16	0.02	57.31	1.05	42.69	0.45	1.13

Table 6.5- 2-exponential lifetime analysis of mGBP-BADAN at 37 ^{o}C with changing glucose concentration

From the table, it can be seen that the lifetimes and relative amplitudes of the pre-exponential factors both vary with glucose concentration over the range 0-100 mM. The T1 value increases from 0.87 ns to 1.19 ns at 37 ^{o}C- the values calculated at room temperature show an increase from 0.89 ns to 1.31 ns. The T2 value at 37 ^{o}C falls from 3.52 ns to 3.16 ns; at room temperature the corresponding decrease is from 3.48 ns to 3.10 ns. These values correspond closely, indicating similar performance from the sensor at the two temperatures when fluorescence lifetimes are considered.

For further comparison with the room temperature experiments, the lifetimes were fixed at 0.9 ns and 3.2 ns, and the relative amplitudes of the pre-exponential factors were recalculated at each glucose concentration. These results can be seen in table 6.6.

mGBP-BADAN fluorescence lifetime parameters at 37°C							
Glucose conc./mM	T1/ns	T2/ns	B1	σ	B2	σ	χ^2
0	0.90	3.20	71.02	0.87	28.98	0.48	1.88
5	0.90	3.20	68.35	1.16	31.65	0.48	1.18
10	0.90	3.20	67.55	1.24	32.45	0.47	1.22
15	0.90	3.20	47.78	1.17	52.22	0.46	1.21
20	0.90	3.20	37.70	1.14	62.30	0.46	1.17
25	0.90	3.20	34.20	1.12	65.80	0.46	1.12
30	0.90	3.20	34.54	1.06	65.46	0.44	1.12
40	0.90	3.20	30.47	1.00	69.53	0.41	1.16
50	0.90	3.20	29.82	0.98	70.18	0.41	1.25
75	0.90	3.20	28.61	0.95	71.39	0.40	1.41
100	0.90	3.20	27.99	1.01	72.01	0.38	1.61

Table 6.6- Fixed lifetime 2-exponential lifetime analysis of mGBP-BADAN at 37 °C with changing glucose concentration

Interestingly, doing the calculations with fixed lifetimes shows a change in relative amplitude of 43 % over the glucose concentration range: this is a larger change than the 18% observed at 21 °C (see table 5.4).

The results from table 6.6 are shown in figure 6.9.

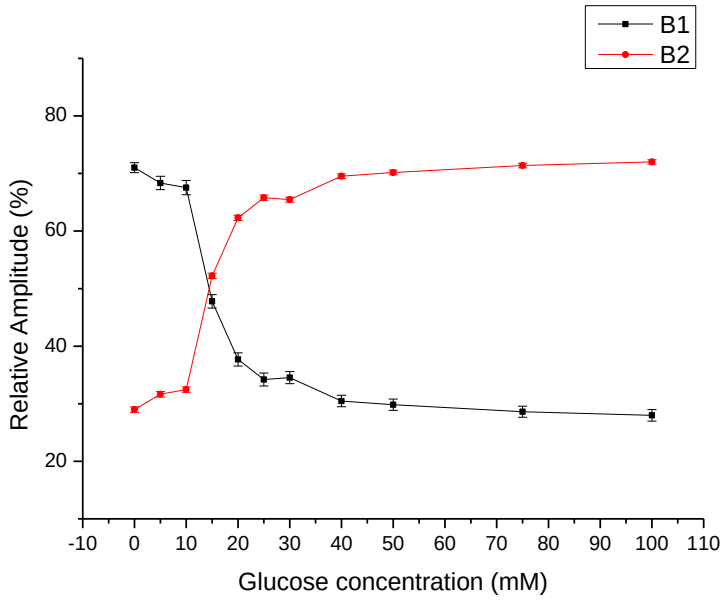

Figure 6.9- Relative amplitudes of pre-exponential factors of mGBP-BADAN at 37 °C, with fixed lifetimes

This result may not be surprising, when one considers the optimal functioning temperature of many biomolecules is closer to 37 ^{o}C than 21 ^{o}C. At the least, it is evident that the sensor which functions at room temperature also does so at human body temperature- indeed, it appears to show a greater response at 37 ^{o}C

6.2.3 50 ^{o}C emission

The second temperature investigated was 50 ^{o}C, and results were collected as before, holding the chamber temperature at 50 ^{o}C. The emission spectra collected with increasing glucose concentration are presented in figure 6.10.

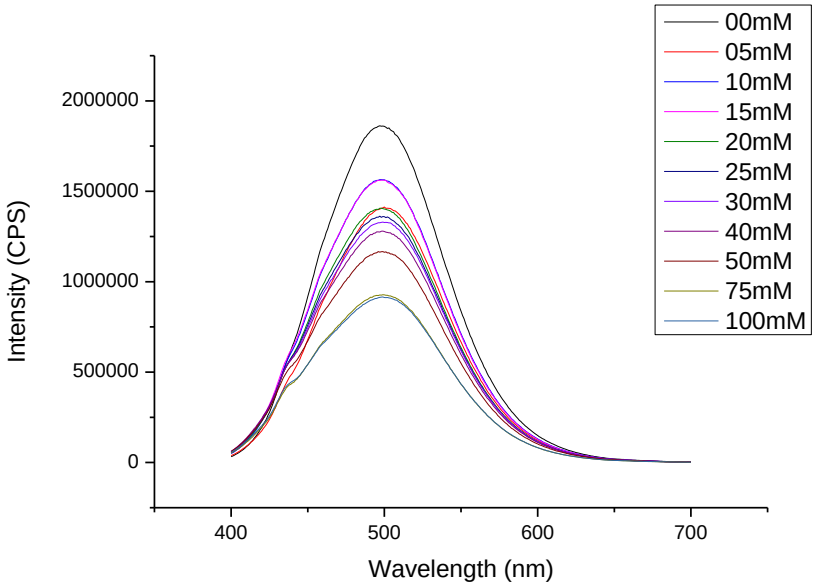

Figure 6.10- Emission spectra of mGBP-BADAN with glucose at 50 ^{o}C

There is evidently a change in emission intensity as the experiment progresses- the trend appears to be in the opposite direction to that which was expected. Plotting emission maximum intensity against glucose concentration provides the results seen in figure 6.11.

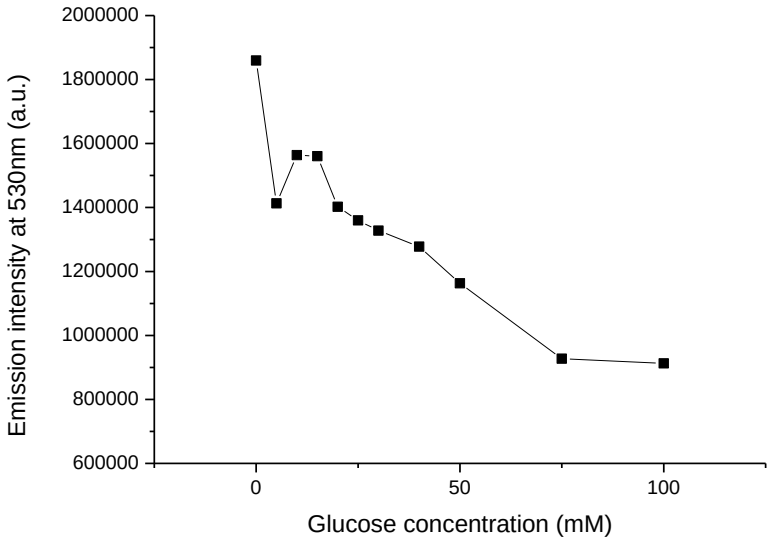

Figure 6.11- Emission intensities at 530nm with glucose of GBP-BADAN at 50 ^{o}C

The pattern is clear- with increasing glucose concentration, the emission intensity decreases. Or certainly, as the experiment progresses, the emission intensity decreases. It is possible that the elevated temperature negatively affects the mGBP-BADAN complex in an increasing manner- that is, the longer it is held at 50 ^{o}C, the more degraded the system becomes. Further experiments- holding the concentration constant and temperature elevated for increasing periods- would be needed for full analysis. For the purposes of this project, it is enough to conclude that the fluorescence emission of the system is negatively affected by the temperature of 50 ^{o}C.

6.2.4 50 ^{o}C lifetimes

On each of the samples used for fluorescence spectral measurements, the fluorescence lifetime decays were also investigated. The results of the best-fitting (minimised χ^2) plots are shown in table 6.7.

mGBP-BADAN fluorescence lifetimes at 50°C									
Glucose conc./mM	T1/ns	σ/ns	T2/ns	σ/ns	B1	σ	B2	σ	χ^2
0	0.78	0.03	2.77	0.04	40.44	1.25	59.56	0.75	1.31
5	0.77	0.03	2.80	0.03	37.43	1.30	62.57	0.73	1.19
10	1.26	0.06	3.37	0.04	59.92	1.31	40.08	0.69	1.16
15	1.24	0.06	3.38	0.03	59.86	1.38	40.14	0.68	1.09
20	1.27	0.06	3.39	0.04	59.78	1.29	40.22	0.70	1.04
25	1.24	0.06	3.39	0.03	60.21	1.40	39.79	0.69	1.01
30	1.28	0.06	3.44	0.04	60.99	1.29	39.01	0.72	1.22
40	1.25	0.05	3.43	0.04	60.91	0.80	39.09	0.72	1.03
50	1.22	0.05	3.42	0.04	61.54	0.84	38.46	0.70	1.03
75	1.25	0.00	3.46	0.04	61.97	0.79	38.03	0.73	0.99
100	1.25	0.01	3.50	0.04	62.96	0.75	37.04	0.75	1.12

Table 6.7- 2-exponential lifetime analysis of mGBP-BADAN at 50 °C with increasing glucose concentration

Interestingly, over the range of increasing glucose concentrations, the short-lifetime component comes to dominate- the opposite of what is seen at room temperature and at 37 °C, where the long-lifetime component grows increasingly dominant. Closer examination reveals that there is really just one step-change between two near-plateaus, between 5 mM and 10 mM. Either side of this large step, the relative amplitudes change very little.

Re-analysing the data with the lifetimes fixed at 0.9 ns and 3.2 ns provides the data shown in table 6.8.

mGBP-BADAN fluorescence lifetime parameters at 50°C							
Glucose conc./mM	T1/ns	T2/ns	B1	σ	B2	σ	χ^2
0	0.90	3.20	48.33	0.98	51.67	0.48	1.72
5	0.90	3.20	45.88	1.04	54.12	0.48	1.55
10	0.90	3.20	31.45	1.29	68.55	0.47	1.34
15	0.90	3.20	31.82	1.33	68.18	0.46	1.29
20	0.90	3.20	31.10	1.33	68.90	0.46	1.24
25	0.90	3.20	31.30	1.33	68.70	0.46	1.24
30	0.90	3.20	31.08	1.35	68.92	0.44	1.44
40	0.90	3.20	31.29	1.37	68.71	0.41	1.25
50	0.90	3.20	32.82	1.51	67.18	0.41	1.32
75	0.90	3.20	31.61	1.25	68.39	0.40	1.27
100	0.90	3.20	32.35	1.42	67.65	0.38	1.38

Table 6.8- Fixed lifetime 2-exponential lifetime analysis of mGBP-BADAN at 50 °C with increasing glucose concentration

Once again, there is not much change (0.80 % for a ten-fold glucose concentration increase) in amplitude over the range 10-100 mM. In contrast with the results obtained at room temperature and at 37 °C, the system does not show much response to glucose concentration outside of the single large shift in relative amplitudes. Figure 6.12 provides a graphical representation of these results.

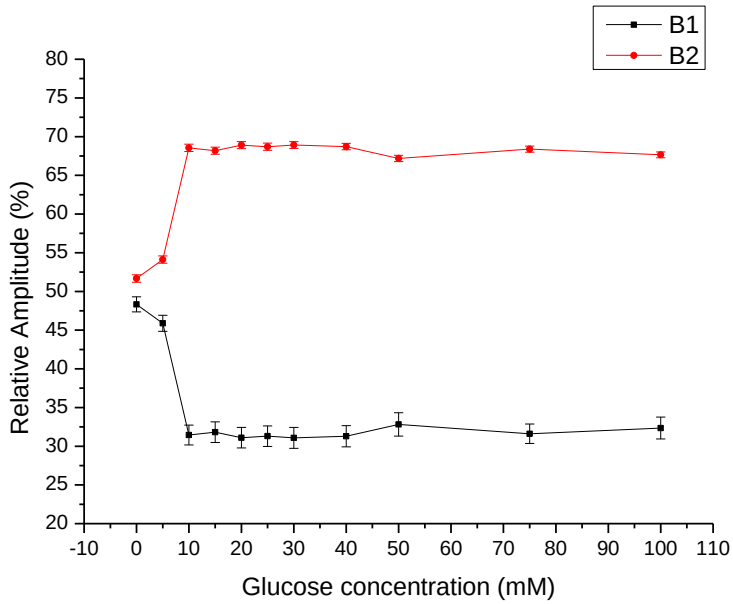

Figure 6.12- Relative amplitudes of pre-exponential factors of mGBP-BADAN at 37°C, with fixed lifetimes

Figure 6.12 shows a limited response to glucose concentration at 50 °C. These results are in line with the emission spectra- there appears to be a lack of functioning, or a degradation, of the system when it is held at a temperature elevated above normal physiological function. It appears that the GBPBADAN system is ineffective as a glucose sensor at 50 °C. However, this temperature is one that is never present in a functioning human body, so it is unlikely to have a relevant impact on proceedings.

6.3 Changes in pH

With the alternative buffer solutions replacing PBS, the experiments on glucose response were conducted at room temperature as before. The only alteration was one further emission and lifetime measurement recorded at saturation concentration one hour after the first saturation measurement. It was hoped that this additional measurement might give an indication of fluorescence changes with time in the more acidic or basic conditions.

6.3.1 pH 9.2 emission

Borate buffer (pH 9.2) replaced PBS for this experiment. The fluorescence emission spectra with glucose concentration were recorded as before. These are shown in figure 6.13.

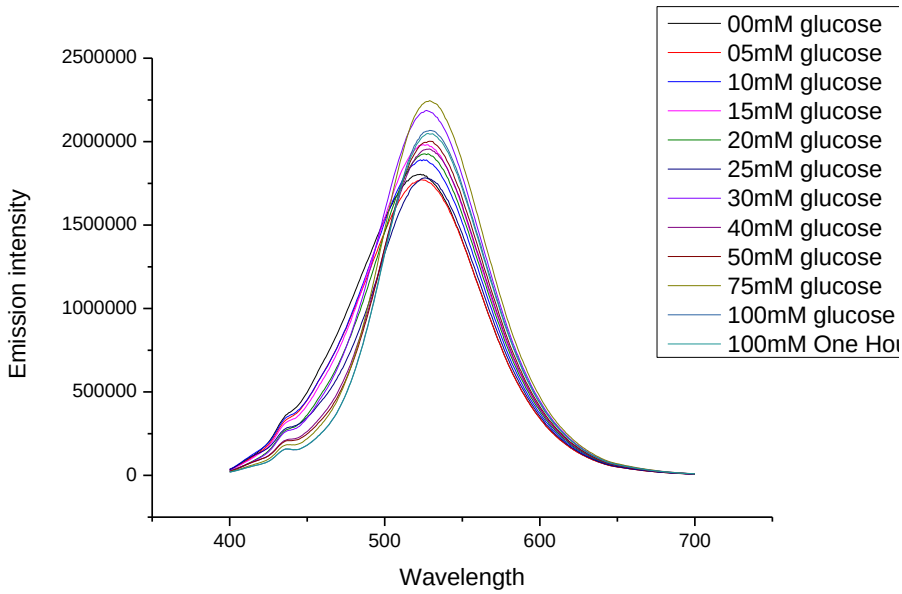

Figure 6.13- Fluorescence emission spectra of mGBP-BADAN in borate buffer

The emission maxima with respect to glucose concentration are plotted in figure 6.14. It is worth noting that there is a <1% decrease in emission intensity between the two measurements made at 100mM glucose: the difference between them being one solely of time spent in the buffer. This minimal change suggests minimal degradation of the fluorophore in one hour at pH 9.2.

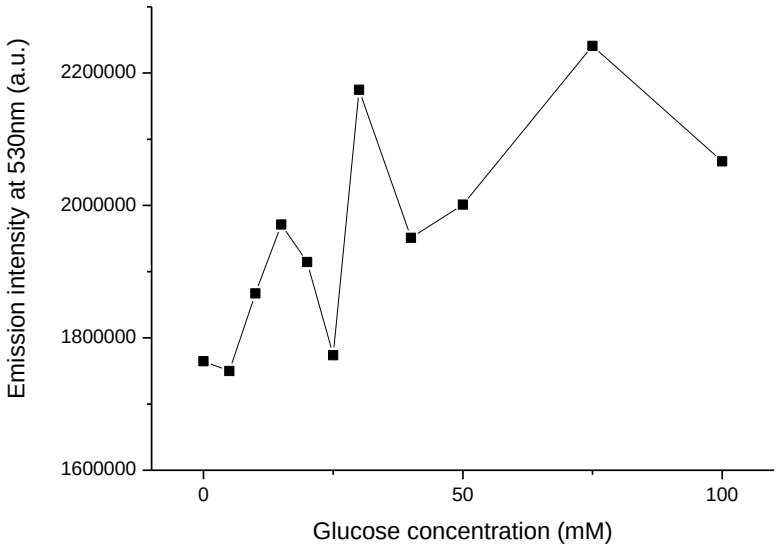

Figure 6.14- Fluorescence emission intensities of mGBP-BADAN in borate buffer

It appears that there is a marginal response to the glucose, but that the response is not as great in basic conditions as in neutral conditions. It also appears that there is a very slight reduction in emission intensity when the sample was left for an hour, but that this reduction is not dramatic.

6.3.2 pH 9.2 lifetimes

The fluorescence lifetime decays were recorded, and the best fitting 2-exponential plot parameters are shown in table 6.9.

mGBP-BADAN fluorescence lifetimes in borate buffer									
Glucose conc./mM	**T1/ns**	**σ/ns**	**T2/ns**	**σ/ns**	**B1**	**σ**	**B2**	**σ**	**χ2**
0	1.05	0.02	3.75	0.03	70.33	0.62	29.67	0.55	1.21
5	1.05	0.02	3.70	0.03	68.89	0.64	31.11	0.54	1.16
10	1.06	0.02	3.63	0.03	66.19	0.67	33.81	0.52	1.17
15	1.08	0.02	3.54	0.02	61.94	0.56	38.06	0.49	1.17
20	1.09	0.03	3.50	0.02	59.97	0.74	40.03	0.47	1.18
25	1.10	0.03	3.42	0.02	56.54	0.79	43.46	0.45	1.08
30	1.11	0.03	3.38	0.02	54.13	0.84	45.87	0.49	1.17
40	1.13	0.03	3.30	0.02	48.63	0.93	51.37	0.45	1.09
50	1.13	0.04	3.23	0.02	45.71	1.00	54.29	0.44	1.10
75	1.17	0.04	3.19	0.02	42.17	1.09	57.83	0.43	1.10
100	1.22	0.05	3.17	0.02	40.01	0.23	59.99	0.40	1.11
100mM- one hour later	1.18	0.05	3.15	0.02	40.40	0.22	59.60	0.40	1.18

Table 6.9- mGBP-BADAN in borate buffer; 2-exponential lifetime decays

It can be seen from the table that the T1 value increases from 1.05 ns to 1.18 ns, and the T2 value decreases from 3.75 ns to 3.17 ns. In PBS the T1 value rises from 0.89 ns to 1.31 ns, and the T2 value falls from 3.48 ns to 3.10 ns. The changes in calculated lifetimes are not as great in the lower pH buffer solution as they are in PBS.

Fixing the lifetimes to the values used throughout the project of 0.9 ns and 3.2 ns, the figures obtained for the relative amplitudes are given in table 6.10.

mGBP-BADAN fluorescence lifetimes fixed in borate buffer							
Glucose conc./mM	**T1/ns**	**T2/ns**	**B1**	**σ**	**B2**	**σ**	**χ^2**
0	0.90	3.20	64.91	0.78	35.09	0.48	1.74
5	0.90	3.20	46.91	0.79	53.09	0.48	1.68
10	0.90	3.20	42.66	0.81	57.34	0.46	1.56
15	0.90	3.20	37.72	0.85	62.28	0.49	1.45
20	0.90	3.20	34.91	0.87	65.09	0.42	1.39
25	0.90	3.20	32.34	0.90	67.66	0.43	1.20
30	0.90	3.20	30.38	0.92	69.62	0.40	1.26
40	0.90	3.20	26.33	0.97	73.67	1.12	1.18
50	0.90	3.20	25.00	0.97	75.00	0.37	1.28
75	0.90	3.20	23.09	1.02	76.91	0.36	1.43
100	0.90	3.20	22.17	1.02	77.83	0.35	1.70
100mM- one hour later	0.90	3.20	22.85	1.00	77.15	0.32	1.75

Table 6.10- mGBP-BADAN in borate buffer; 2-exponential lifetime decays when lifetimes are fixed

Here there is again a fluorescence response to glucose- the change in pre-exponential factors between 0 mM and 100 mM glucose is 42 %. This compares unexpectedly favourably with the relative amplitude change seen in PBS- that figure being 18 %. The efficacy of the system as a fluorescence-lifetime glucose sensor is not diminished in a more basic solution. The relative amplitude changes are displayed in figure 6.15.

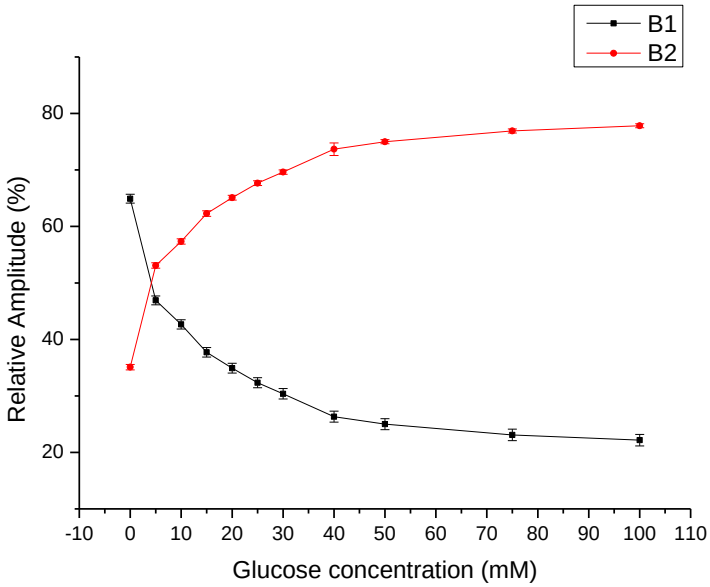

Figure 6.15- - Relative amplitudes of fixed-lifetime pre-exponential factors of mGBP-BADAN in borate buffer

Figure 6.15 shows that in borate buffer the pre-exponential factors of the fluorescence lifetime decay curves change in the presence of glucose- that the long lifetime component becomes increasingly dominant with increasing glucose concentration, as observed when measuring in PBS.

The sensor system evidently can withstand a slight increase in the environmental pH. Slightly more basic conditions do not appear to trouble the binding protein when it comes to fluorescence lifetimes.

6.3.3 pH 4.0 Emission

Phthalate buffer (pH 4.0) replaced PBS for the next experiment conducted at room temperature. The fluorescence emission spectra with glucose concentration were recorded as before. These are shown in figure 6.16.

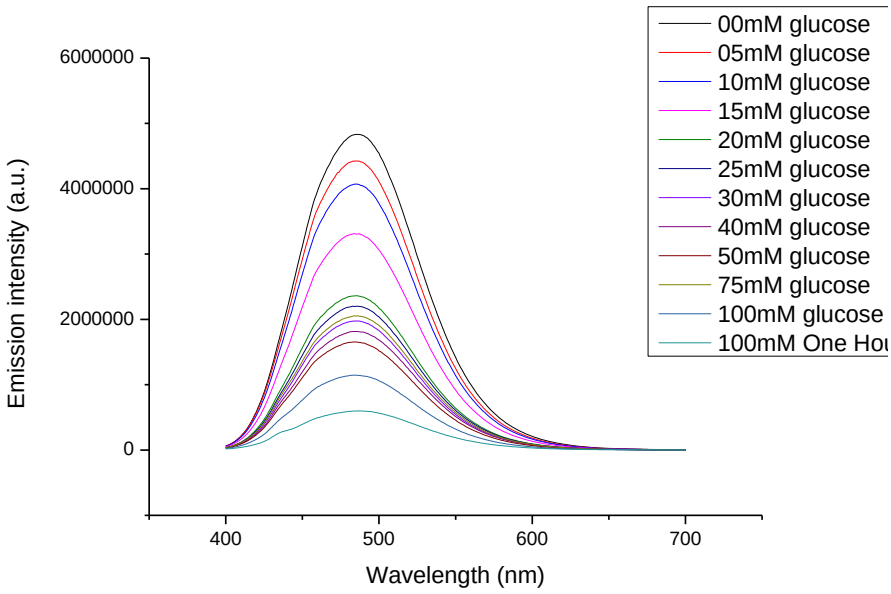

Figure 6.16- Fluorescence emission spectra of mGBP-BADAN in phthalate buffer

Comparing figure 6.16 to figure 5.10, a blue-shift in the emission wavelength is clear when the buffer is acidic. The peak emission intensity was found at 530 nm in PBS, yet is observed at 495nm in phthalate buffer. The emission intensity also changes with glucose concentration- plotting these emission maxima against glucose concentration results in figure 6.17.

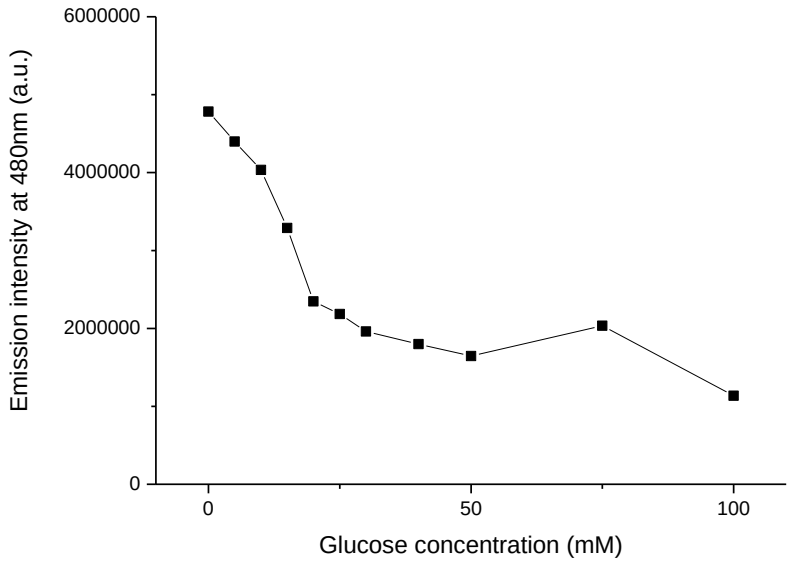

Figure 6.17- Fluorescence emission maxima of mGBP-BADAN in phthalate buffer

The emission intensity decreases over the whole measured range of glucose concentrations. In comparison with the borate buffer results, the emission intensity in phthalate continues to fall between measurements of the same concentration separated by time. The measurement taken one hour after 100mM is reached was the lowest intensity reading taken. There is a 48% decrease in emission intensity in that hour. The implication of this is that the acidic buffer solution is degrading the mGBP-BADAN complex regardless of glucose concentration. The fluorescence emission intensity response is not the same as in neutral buffer, and is not a valid parameter for glucose sensing in such an acidic environment.

6.3.4 pH 4.0 Lifetimes

The fluorescence lifetime decays of the phthalate buffer were recorded, and the 2-exponential fits with the minimised χ^2 value for this buffer are presented in table 6.11.

mGBP-BADAN fluorescence lifetimes in phthalate buffer									
Glucose conc./mM	**T1/ns**	**σ/ns**	**T2/ns**	**σ/ns**	**B1**	**σ**	**B2**	**σ**	**χ2**
0	1.24	0.06	3.02	0.02	40.57	1.30	59.43	1.30	1.09
5	1.26	0.06	3.01	0.02	41.83	1.25	58.17	1.25	1.11
10	1.27	0.05	3.03	0.02	43.00	1.20	57.00	1.20	1.07
15	1.29	0.05	3.04	0.02	43.85	1.18	56.15	1.18	1.02
20	1.25	0.05	3.01	0.02	44.38	1.27	55.62	1.27	1.02
25	1.25	0.06	2.99	0.02	44.30	1.18	55.70	1.18	1.12
30	1.25	0.06	3.00	0.02	45.89	1.21	54.11	1.21	1.09
40	1.22	0.06	2.95	0.02	44.86	1.24	55.14	1.24	1.04
50	1.24	0.06	2.96	0.02	45.96	1.23	54.04	1.23	1.03
75	1.24	0.05	2.97	0.02	46.76	1.14	53.24	1.14	1.07
100	1.23	0.05	2.96	0.02	47.68	1.20	52.32	1.20	1.01
100mM- one hour later	1.19	0.05	2.97	0.02	48.31	1.18	51.69	1.18	1.03

Table 6.11- 2-exponential lifetime decays of mGBP-BADAN in phthalate buffer

The changes are less pronounced than those seen in other solvent environments – the short lifetime decreases by 0.05 ns over the experiment, compared to a 0.42 ns increase in PBS; similarly the longer lifetime component decreases by 0.05 ns, contrasting with the 0.38 ns decrease in the phosphate buffer. It is apparent that in contrast to neutral and slightly basic solutions, there is minimal response to glucose concentration in the acidic buffer.

For a more direct comparison with previous results, the experimental data were re-fitted to fixed lifetime parameters of 0.9 ns and 3.2 ns. The changes in these parameters are shown in table 6.12.

GBP-BADAN fluorescence lifetimes fixed in phthalate buffer							
Glucose conc./mM	**T1/ns**	**T2/ns**	**B1**	**σ**	**B2**	**σ**	**χ2**
0	0.90	3.20	24.71	1.00	75.29	0.35	2.62
5	0.90	3.20	25.64	0.96	74.36	0.36	2.93
10	0.90	3.20	26.47	0.93	73.53	0.36	2.88
15	0.90	3.20	26.57	0.93	73.43	0.36	2.87
20	0.90	3.20	27.44	0.92	72.56	0.38	2.81
25	0.90	3.20	27.65	0.93	72.35	0.39	3.03
30	0.90	3.20	28.42	0.91	71.58	0.40	2.98
40	0.90	3.20	28.86	0.91	71.14	0.40	3.06
50	0.90	3.20	29.32	0.88	70.68	0.40	3.20
75	0.90	3.20	30.02	0.85	69.98	0.41	3.19
100	0.90	3.20	30.35	0.88	69.65	0.41	3.13
100mM- one hour later	0.90	3.20	30.73	0.87	69.27	0.42	2.78

Table 6.12- 2-exponential fixed-lifetime decays of mGBP-BADAN in phthalate buffer

Keeping the lifetimes to the same values as used previously, it can be seen that the fits are less good- χ^2 values ranging between 2.62 and 3.19 are observed. The change in relative amplitudes in the acidic buffer is 5.64 % over the range 0-100 mM, contrasted with an 18 % change observed in PBS. These results are plotted against glucose concentration in figure 6.18.

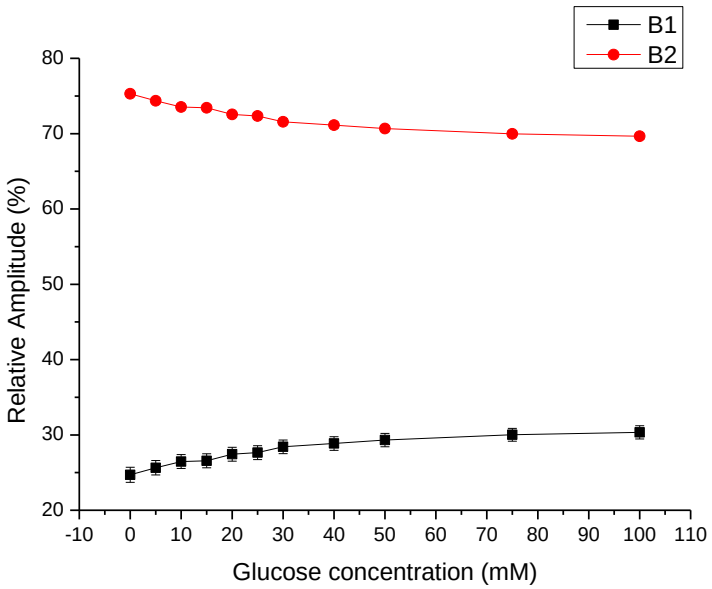

Figure 6.16- Relative amplitudes of fixed-lifetime pre-exponential factors of mGBP-BADAN in phthalate buffer

The results in figure 6.18 show that the short-lifetime component becomes increasingly dominat over the concentration range, but that the response itself (6%) is minimal.

6.4 Conclusions

From these experiments it can be concluded that the glucose sensing system using mGBP-BADAN is selective for glucose, as it does not show a fluorescence response to fructose or lactose concentrations when measuring emission intensity or lifetime data. It was observed that even with supra-physiological concentrations of both alternative sugars, the mGBP-BADAN sensor responded positively to glucose concentration- in effect, ignoring the other metabolites to show a positive response to glucose.

The labelled protein was found to retain efficacy at body temperature (37 °C), and continues to show a fluorescence response in solution of pH 9.2 comparable to that observed at pH 7.4. However, the more aggressive environments investigated, those of 50 ^{o}C and pH 4.0 respectively, both impair the fluorescence response to glucose, rendering the system ineffective in these environments.

It is clear that large deviations of the system from physiological conditions result in degradation of the system. This decreased or ineffective response to glucose when the temperature and acidity are increased is not a surprise, given the biological origin of the sensor molecule, but confirmation of this fact was worthwhile.

7 Long-wavelength fluorophores

Despite its apparent efficiency, one potential drawback of BADAN as a biosensor is the potential for interference from protein auto-fluorescence. A longer wavelength dye could avoid this issue, and a dye in the infrared region could potentially pass through human skin in the previously mentioned 'therapeutic window'. Unfortunately, very few fluorophores are available which are both environmentally sensitive and thiol-reactive. Thiol-reactivity, possessed by BADAN but not all fluorophores, is the phenomenon which allows straightforward covalent binding to the mutant cysteine group near the glucose binding site. Exploration of the longer wavelength regime will therefore be a non-trivial matter.

7.1 Texas Red

Texas Red, illustrated in figure 7.1, is a thiol-reactive dye which absorbs and emits light around 600 nm- absorption at 595 nm, and emission at 615 nm[73]. Texas Red is not known to have fluorescence properties which depend on solvent environment, and so it was thought that negative response from such a dye would provide useful confirmation of the environmental response which made mGBP-BADAN an effective sensor. If a dye such as Texas Red bound to the mGBP showed no response to glucose concentration, while occupying the same binding site as BADAN, then the solvent-response would be the main point of difference between the systems, and therefore the reason for the glucose response. Texas Red has the same thiol-reactive binding properties as BADAN, and therefore the labelling protocol which exploited the thiol-reactivity of BADAN was employed for labelling with Texas Red.

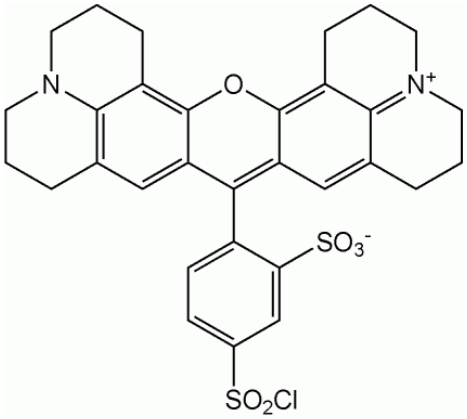

Figure 7.1- Chemical structure of Texas Red[74]

7.1.1 Texas Red fluorescence

The absorbance spectrum of Texas Red dissolved in DMF was recorded and is presented in figure 7.2.

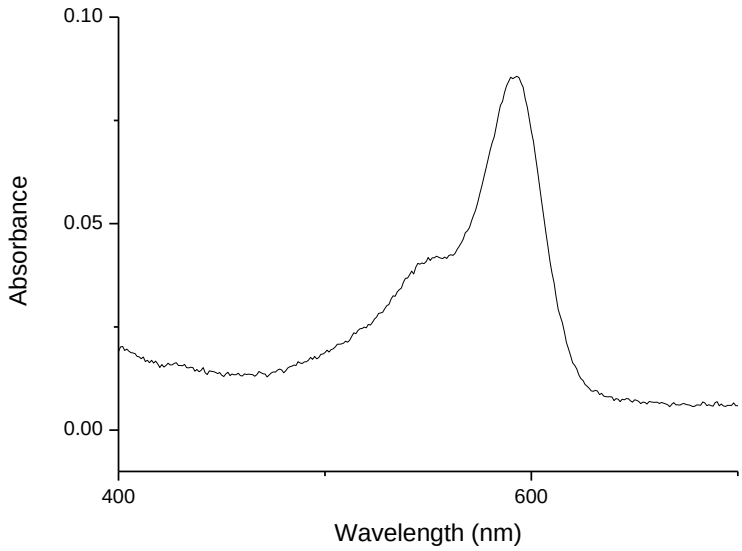

Figure 7.2- Absorbance spectrum of Texas Red dye in DMF

Exciting the dye at the absorbance band observed at 595 nm provided a fluorescence emission spectrum which is shown in figure 7.3.

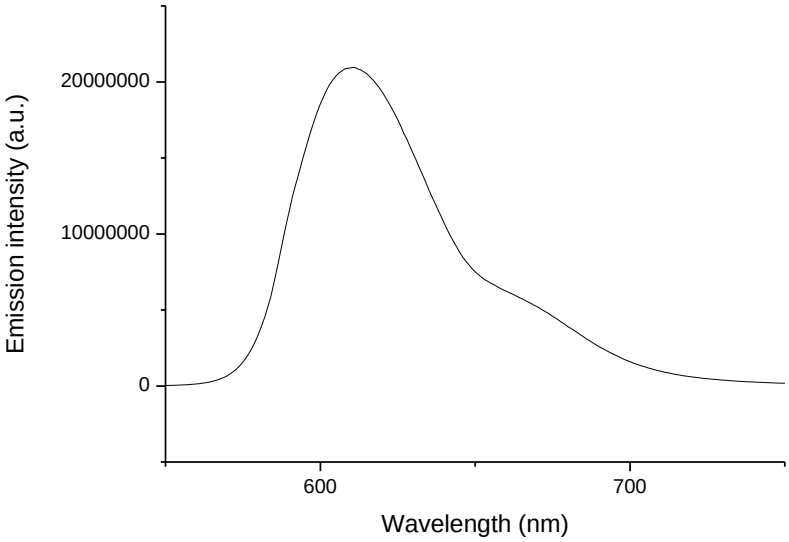

Figure 7.3- Emission spectrum of Texas Red dye in DMF

The fluorescence lifetime of the dye in DMF was recorded, with excitation at 590 nm. With a χ^2 value of 1.02, the mono-exponential lifetime decay provided a lifetime of 4.05ns.

7.1.2 mGBP-Texas Red labelling

Mutant glucose binding protein was labelled with Texas Red, using the protocol successfully employed for binding BADAN to the protein. After gel filtration, the two bands containing the bound and the free dye were clearly, visibly, separated. The dye molecules were too small to have made it through the Sephadex beads at the same rate as the protein. After centrifugally concentrating the filtered sample, the absorbance spectrum of the sample was recorded. The spectrum is shown in figure 7.4.

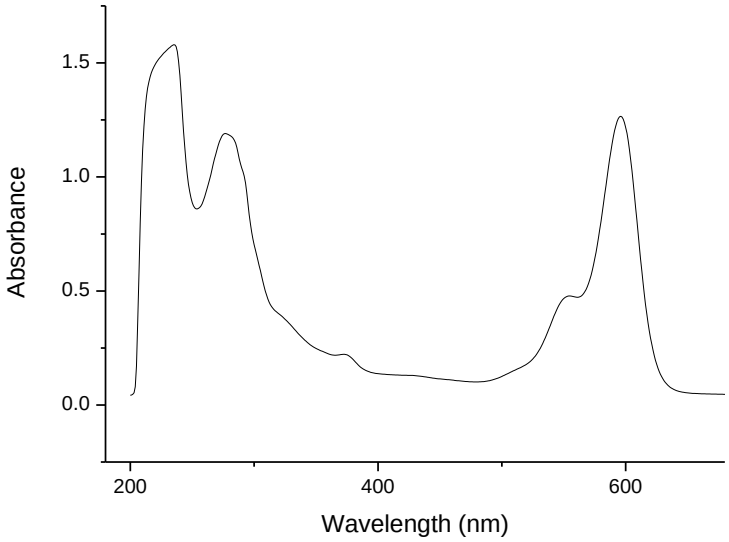

Figure 7.4- Absorbance spectrum of mGBP labelled with Texas Red.

The characteristic protein peaks at 220 nm and 280 nm, present alongside the extrinsic dye absorption peak at 595 nm, in a sample where the free dye has been filtered off, indicate that the labelling was successful. Beer-Lambert calculations (for Texas Red $\varepsilon=8.5*10^4$ $M^{-1}cm^{-1}$) based on the above spectrum reveals that 47.0% of the mGBP molecules are labelled with the dye.

7.1.3 mGBP-Texas Red emission

Exciting at 595 nm, the emission spectrum obtained is presented in figure 7.5.

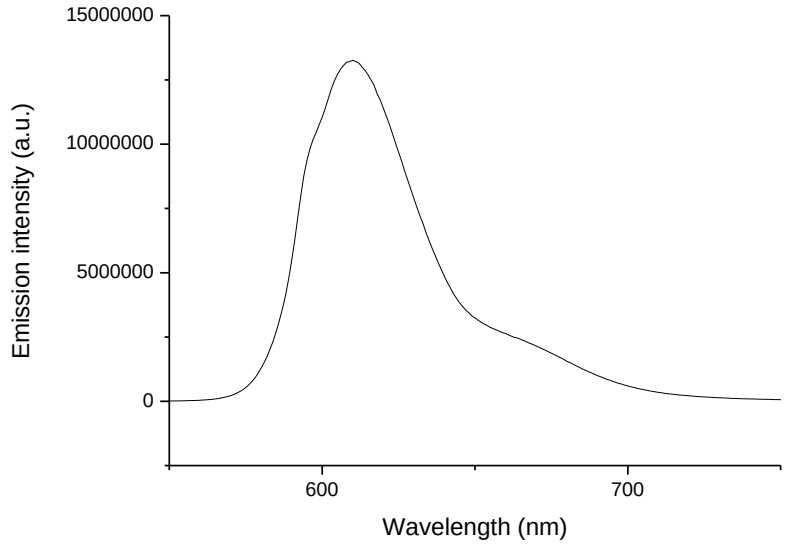

Figure 7.5- Emission spectrum of mGBP labelled with Texas Red.

Although the concentrations of sample are different, the emission profiles in figures 7.3 and 7.5 are nearly identical, indicating little change to the fluorescence properties of the dye when labelled, or indeed when the solvent is changed from DMF to water.

The emission spectra recorded when increasing the concentration of glucose in the sample are shown in figure 7.6.

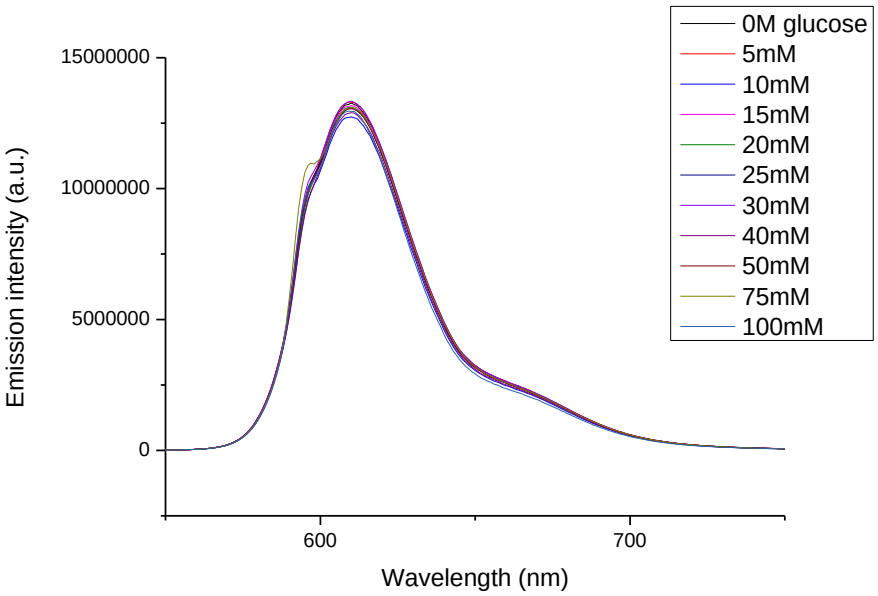

Figure 7.6- Emission spectra of mGBP labelled with Texas Red, with increasing glucose concentration.

It is clear that the differences between emission peaks are minimal. Plotting the emission intensity against glucose concentration provides the plot seen in figure 7.7.

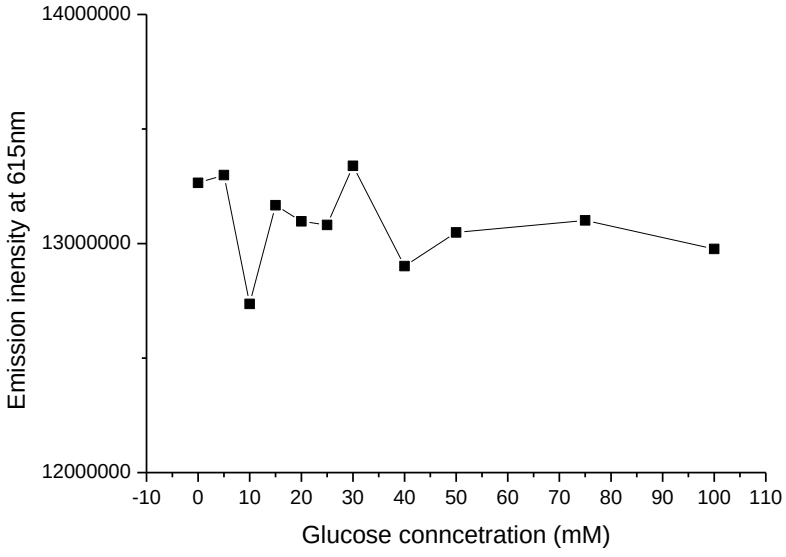

Figure 7.7- Emission intensities at 615nm of mGBP labelled with Texas red when glucose concentration is increased

As would be expected with the solvent-exposure theory of protein-dye response, no change in emission intensity is observed over the glucose concentration range 0-100 mM.

7.1.4 mGBP-Texas Red lifetimes

The fluorescence lifetime decays for each sample of the labelled protein were recorded, using a 590 nm excitation source. The fluorescence lifetime decay curve without glucose present is plotted in figure 7.8, showing a 2-exponential fit to the data.

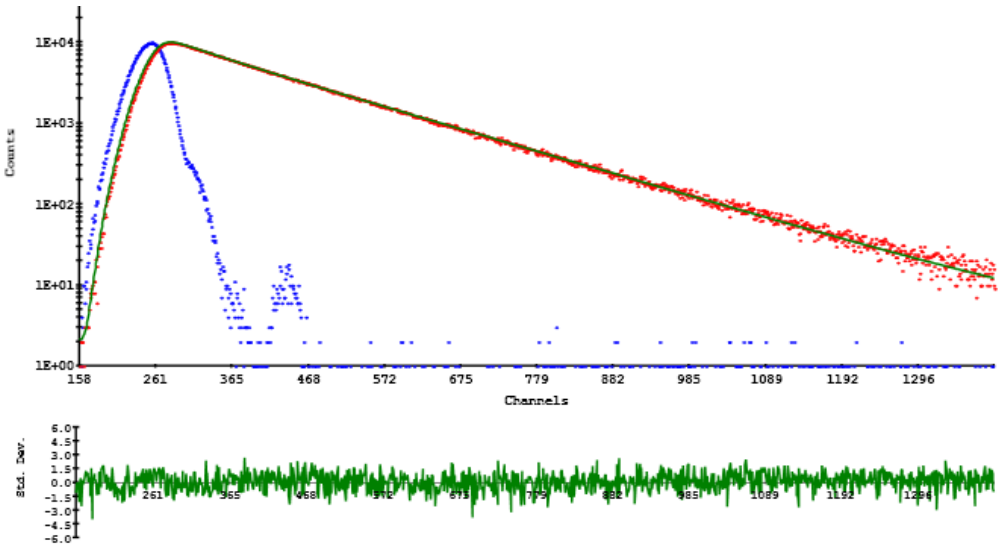

Figure 7.8- TCSPC data for mGBP-Texas Red at 0mM glucose concentration

Table 7.1 displays the single exponential fitting parameters.

mGBP-Texas Red in PBS buffer- Fluorescence lifetimes			
Glucose conc./mM	**T/ns**	**σ/ns**	**χ2**
0	4.63	0.01	2.01
5	4.61	0.01	1.95
10	4.63	0.01	1.97
15	4.64	0.01	1.89
20	4.61	0.01	2.02
25	4.63	0.01	1.59
30	4.61	0.01	1.33
40	4.65	0.01	1.44
50	4.66	0.01	1.29
75	4.66	0.01	1.32
100	4.65	0.01	1.25

Table 7.1- Single-exponential lifetime decay parameters of mGBP labelled with Texas Red with increasing glucose concentration

The lifetimes clearly do not change over the course of the experiment. In DMF, the free dye was found to exhibit a mono-exponential fluorescence lifetime decay of 4.05 ns. After labelling, the bound dye is found to have a lifetime of 4.63 ns. Compared to the free dye in DMF, the assumption of a mono-exponential decay curve is less valid, as evidenced by the large χ^2 values. An extra fitting parameter was therefore considered for the labelled protein, and the 2-exponential results can be seen in table 7.2.

mGBP-Texas Red in PBS buffer- Fluorescence lifetimes									
Glucose conc./mM	T1/ns	σ/ns	T2/ns	σ/ns	B1	σ	B2	σ	χ2
0	1.86	0.28	4.80	0.02	8.14	3.60	91.86	0.39	1.21
5	1.88	0.28	4.79	0.02	8.06	3.60	91.94	0.39	1.39
10	2.02	0.28	4.81	0.02	8.60	3.60	91.40	0.39	1.21
15	1.45	0.28	4.81	0.02	8.18	3.60	91.82	0.39	1.18
20	1.82	0.28	4.79	0.02	7.61	3.60	92.39	0.39	1.33
25	1.75	0.28	4.79	0.02	7.23	3.60	92.77	0.39	1.12
30	1.73	0.28	4.81	0.02	8.07	3.60	91.93	0.39	1.03
40	1.63	0.28	4.81	0.02	7.03	3.60	92.97	0.39	1.09
50	1.80	0.28	4.82	0.02	7.29	3.60	92.71	0.39	1.04
75	1.89	0.28	4.83	0.02	7.64	3.60	92.36	0.39	1.08
100	1.93	0.28	4.83	0.02	7.73	3.60	92.27	0.39	1.09

Table 7.2- 2-exponential lifetime decay parameters of mGBP labelled with Texas Red with increasing glucose concentration

As table 7.2 shows, the curves obtained fit slightly better (mean χ^2 of 1.16 compared with 1.64 in table 7.1) with the extra parameter. In comparison with the single-exponential results, however, there is negligible change in any of the calculated parameters in table 7.2. Neither lifetime nor relative amplitude changes much over the progression of increases in glucose concentration.

The protein-dye complex is therefore seen to be functionally non-responsive when both the fluorescence intensities and fluorescence lifetimes are considered- much as was expected. That there is no response for a dye not known to exhibit solvent-dependent effects (Texas Red), but a useful and marked response for a dye which is known to be environmentally sensitive (BADAN) provides strong confirmation of importance of the effect of solvent-dye interactions.

7.1.5 mGBP-Texas Red anisotropy

Fluorescence anisotropy measurements were also made on the samples, and depolarisation times calculated using a single exponential fit. The anisotropy decay in the absence of glucose is shown in figure 7.9.

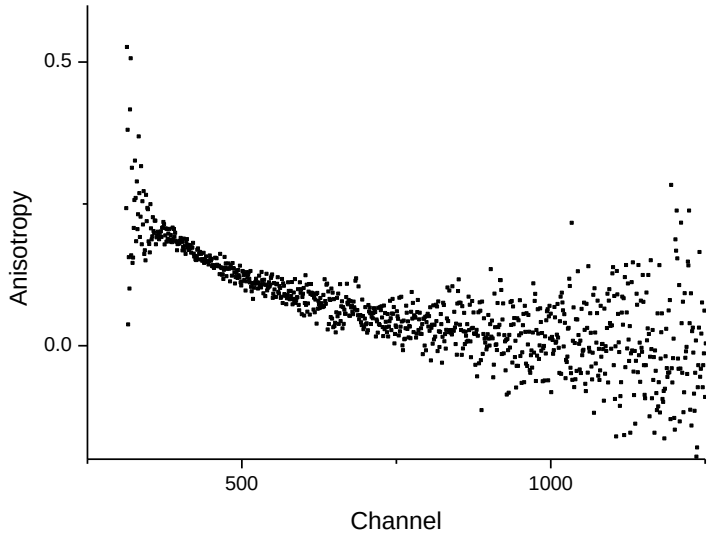

Figure 7.9- Anistropy decay of mGBP-Texas Red

The calculated fitting parameters are presented in table 7.3

mGBP-Texas Red Single exponential rotational times					
Glucose conc./mM	T/ns	σ/ns	χ2	Diameter/nm	σ/nm
0	8.78	0.18	1.30	4.07	0.08
5	8.91	0.18	1.30	4.09	0.08
10	8.69	0.23	1.21	4.52	0.12
15	8.74	0.20	1.27	4.07	0.09
25	9.84	0.18	0.84	4.23	0.08
30	9.20	0.20	1.33	4.14	0.09
40	9.81	0.20	1.24	4.23	0.09
50	8.03	0.23	1.25	3.95	0.11
75	8.70	0.27	1.29	4.06	0.13
100	10.26	0.28	1.19	4.29	0.12

Table 7.3- Anisotropy rotational times of mGBP labelled with Texas Red

In comparison with the results in table 5.6 for mGBP-BADAN, the rotational correlation time here is 9ns, compared to 33 ns with the shorter-wavelength fluorophore. It is known from the lattice parameters discussed previously that the results in table 5.6 are correct. The shorter correlation times obtained in table 7.4 therefore need to be addressed, as does the lack of trend in the calculated hydrodynamic diameter. The rotational correlation times are plotted against glucose concentration in figure 7.10, which graphically confirms the relatively unchanging nature of the correlation time.

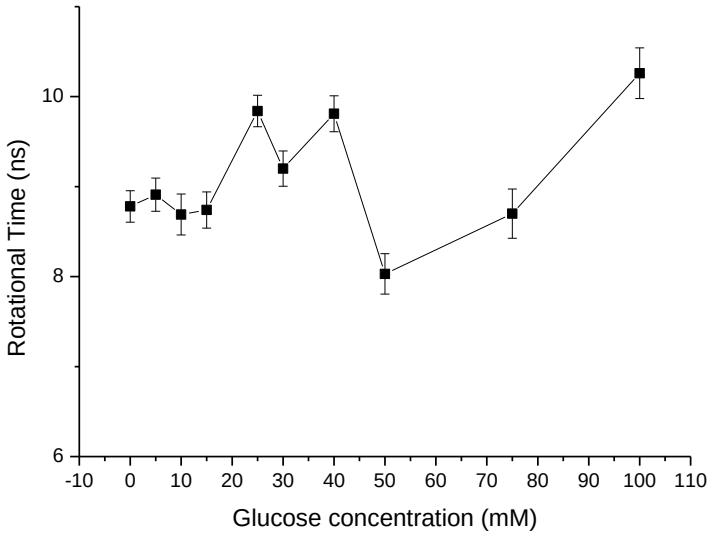

Figure 7.10- Single-exponential rotational time of mGBP labelled with Texas Red when increasing glucose concentration.

The fact that the calculated diameter does not decrease is surprising. The protein response to glucose is assumed even if the dye response is not apparent, yet the data do not show such a response. One reasonable explanation for both the lack of response and the shorter observed correlation time is that the Texas Red dye has bound to the protein in a non-rigid manner. Calculations of rotational correlation times are dependent on the assumption of a rigid rotor being the system studied: if the system is not a rigid rotor then the observed correlation time may correspond to movement of the dye itself (oscillations, for example), rather than the protein-dye complex. This would explain the recorded data.

Whatever the reason for the lack of response, it is clear that the environmentally-insensitive dye Texas Red confirms that solvent interactions are of great importance in the mGBP-BADAN system, and that Texas Red is an ineffective dye for glucose sensing applications.

7.2 IANR

Part of the utility of the environmentally sensitive dye BADAN as a glucose sensor is its thiol-reactive nature. This reactivity allows efficient binding with the cysteine group on the mutated mGBP-protein. The fluorescent dye known as Nile Red is known to be sensitive to environment polarity[75], and has been shown to be an effective probe in the investigation of protein surfaces[76],[77], while also remaining effective in gel matrices[78]. Nile Red itself, however, does not possess the thiol-reactivity

which would allow binding to the mutated cysteine group of mGBP. Thomas *et al.* have reported a nile red derivative known as IANR[79], which possesses the necessary reactivity for binding to a cysteine group. Although attachment to a glucose binding protein has been reported[57], the characterisation data are scant, and more data on the subject can only be viewed as useful.

IANR was prepared as described in section 3.9.

The starting material was extremely difficult to obtain, and only 47mg of the starting material could be procured from any major supplier, while exhausting the stocks at Sigma-Aldrich. As a result, no more IANR could be created within the timescale of the project. The chemical yield of the sample was found to be lower than that reported in literature, and so the dye derivative was treated as precious. It was judged by Mr Hutton that there was insufficient dye product to conduct tests to verify the dye identity. With the available dye derivative, experiments on solvent polarity and glucose sensing were carried out.

The IANR sample was investigated for its fluorescence properties in solvents of varying polarity. The labelling protocol followed for mGBP-BADAN was utilised here also- with IANR replacing BADAN but otherwise the steps kept the same. The mGBP-IANR complex was then investigated for its fluorescence response to glucose.

7.2.1 IANR fluorescence

A stock sample of IANR (a few grains dissolved in DMF) was prepared, in order to test the fluorescence and spectroscopic properties of the fluorophore itself, in particular with regards to solvent polarity. The stock solution was diluted 1000 times to a suitable concentration for absorption spectroscopy.

The absorbance spectrum in each solvent was recorded and these are presented in figure 7.11.

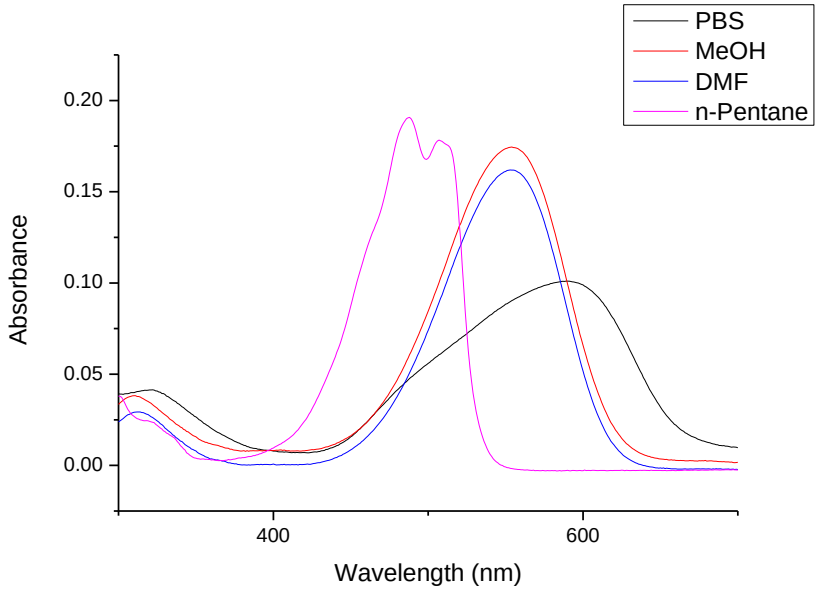

Figure 7.11- Absorbance spectrum of stock IANR solution, diluted in different solvents.

The absorbance wavelength shift is clear from the figure. With increasing solvent polarity, the absorption peak shifts to longer wavelength- similar to the property observed with the environmentally-sensitive dye BADAN.

Electronically exciting each sample at the absorbance peaks previously recorded, the emission spectra were measured. These emission spectra are shown in figure 7.12:

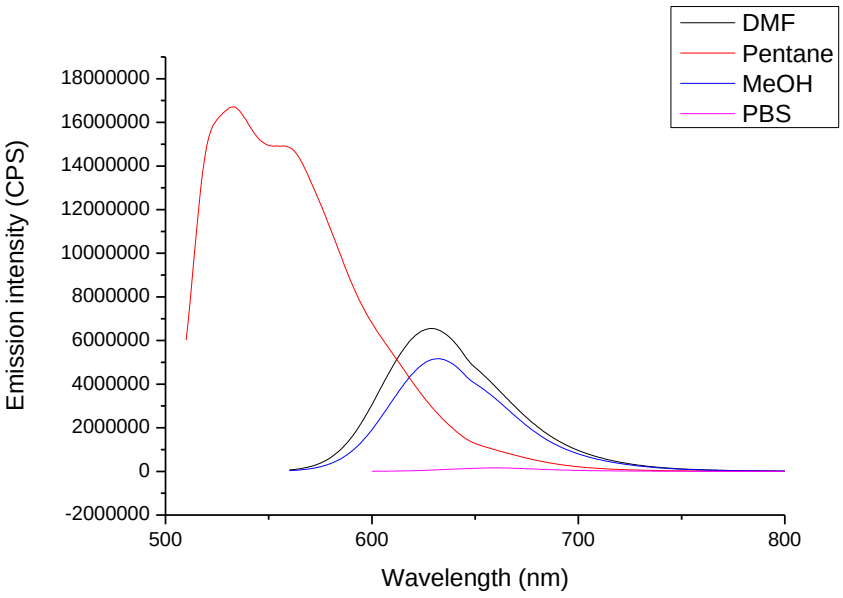

Figure 7.12- Emission spectra of IANR stock dissolved in various solvents

The differences in emission wavelength and emission intensity when varying solvent polarity are evident. The non-polar pentane provides the environment for the shortest wavelength, highest intensity emission profile, and the more polar saline solution allows the least intense and longest wavelength profile of the solvents examined. This is again similar to what was seen for the dye BADAN.

Given the confirmed polarity-dependent intensity variance, it was hypothesised that labelling the triple-mutant glucose binding protein with a Nile Red derivative would provide a similar change in florescence intensity with respect to glucose as was seen with the mGBP-BADAN complex, but at the potentially more useful long wavelength regime.

The fluorescence lifetime decays of the Nile Red derivative dye were recorded after dilution in the previously investigated solvents. The analysed parameters of the decay curves are presented in table 7.4, using an excitation source at 590 nm for PBS, MeOH, and DMF, and 500 nm for n-Pentane.

IANR fluorescence lifetimes in solvents of varying polarity												
Solvent	**1-exponential**			**2-exponential**								
	T1/ns	**σ/ns**	**χ2**	**T1/ns**	**σ/ns**	**T2/ns**	**σ/ns**	**B1**	**σ**	**B2**	**σ**	**χ2**
PBS	0.55	0.00	16.54	0.27	0.01	0.84	0.01	64.41	0.93	35.59	1.00	1.41
MeOH	2.84	0.00	1.02	1.48	0.03	2.85	0.01	1.10	23.52	98.90	0.30	1.08
DMF	3.75	0.00	1.07	2.05	0.10	3.75	0.03	1.06	28.73	98.94	0.36	1.05
n-Pentane	2.73	0.00	1.08	1.77	0.47	2.83	0.02	9.08	4.38	90.92	0.47	1.03

Table 7.4- Fluorescence lifetime decay of IANR stock when diluted in different solvents

There appear to be two distinct classes of decay here- the lifetime decay when in water, and the lifetime decay when in other, less polar solvents. The decay curve appears to fit a mono-exponential pattern when in the three other solvents, whereas in water the χ^2 value shows a far better fit to a two-exponential decay. The lifetime observed in DMF is around one nano-second longer than in the methanol or in pentane- this perhaps relates to the original stock solution for dissolution itself being DMF- or perhaps some other factor. Regardless, it is clear that the lifetime lengthens and becomes more mono-exponential as the polarity of the solvent is decreased.

These results were promising as regards a labelled bio-sensor for glucose. The emission intensity and the fluorescence decay lifetime both show significant changes when the solvent polarity is decreased- providing a sound basis for testing the 'water-extrusion' hypothesis of the GBP folding response to glucose.

7.2.2 mGBP-IANR labelling

On the first attempt at attaching the dye, using the same protocol as for the mGBP-BADAN labelling experiment, a sample was produced which contained a tiny fraction of labelled protein, but the signal was very weak, taking a prohibitively long time to measure.

In order to obtain results on a more reasonable timescale, the remaining stocks of dye and protein were used- left to reduce and bind; then filtered and centrifuged as before.

The absorbance spectrum of mGBP-IANR in PBS was recorded at a ten times dilution of the labelled stock solution. The spectrum is shown in figure 7.13:

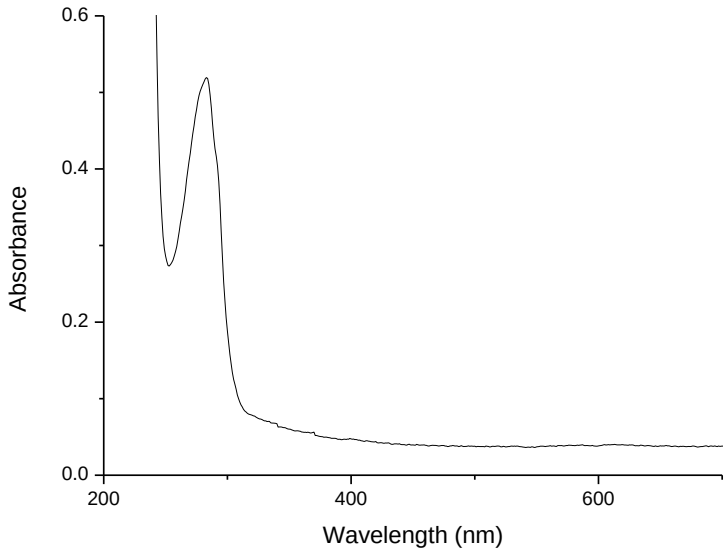

Figure 7.13- Absorbance spectrum of IANR-labelled mGBP stock solution

Although it is of very low intensity, there is a small peak observable at 600nm.

Based on careful examination of the absorbance spectrum, the relative concentrations of mGPB and IANR can be calculated (for IANR $\varepsilon = 2.9*10^4\ M^{-1}cm^{-1}$). The absorbance values at 280nm and 600nm are 0.48 and 0.004 above baseline respectively. The calculated ratio of concentrations is found to be

0.0133 corresponding to 1.3% of the protein molecules being labelled with IANR. This is obviously far fewer binding events than the 43% binding observed for mGBP-BADAN.

7.2.3 mGBP-IANR emission

Exciting this partially-labelled sample at 600nm, the emission spectrum was obtained. It is shown in figure 7.14:

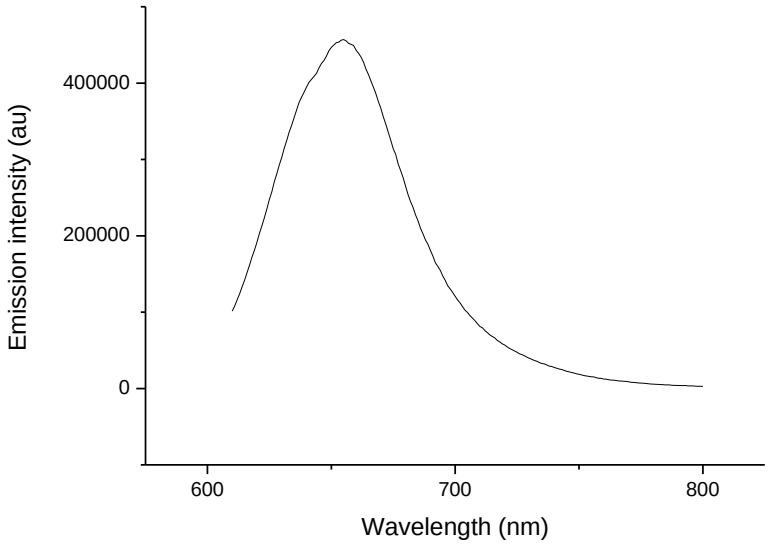

Figure 7.14- Emission spectrum of IANR-labelled mGBP, excited at 600 nm.

The peak emission wavelength is 655 nm for the labelled protein in PBS. This corresponds closely to the emission wavelength of the free dye in PBS (which is 660 nm) but not exactly. Figure 7.13 shows the wavelength of maximum emission intensity for IANR in DMF to be 620 nm, and 530 nm in pentane. The peak emission intensity wavelength shifts to shorter wavelengths with decreasing polarity. It is assumed, therefore, that being held on the binding site provides a small amount of protection and environmental shielding for the dye.

Aliquots of glucose solution were added to the sample to investigate the potential for glucose sensing. After each step of glucose addition to the cuvette, the sample was incubated for 10 minutes to allow full response to take place.

The sample investigated was prepared to concentration half that of the stock solution- that is, dye concentration of 0.17 µM, bound to proteins of concentration 13.0 µM. Glucose solution aliquots were added to the cuvette, and measurements taken. A plot of all of the spectra obtained is shown in figure 7.15.

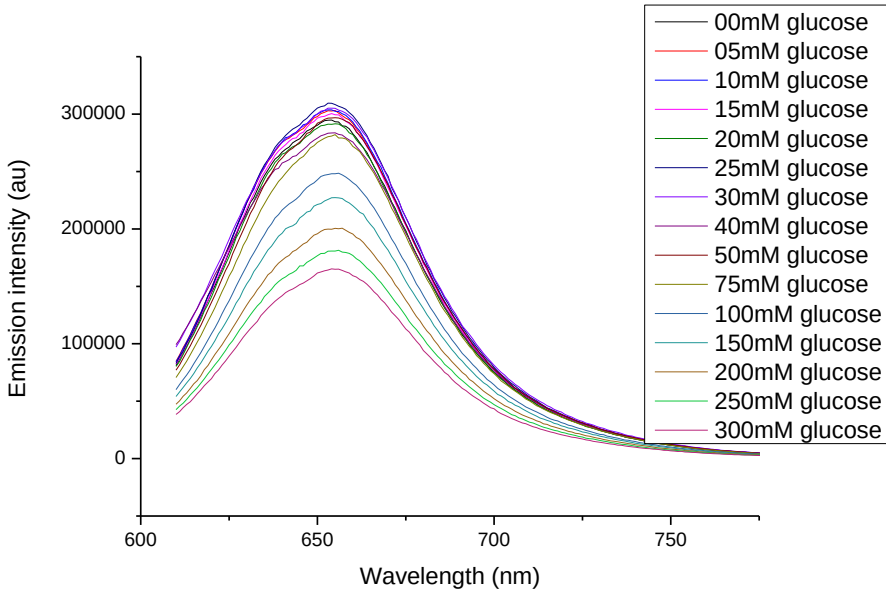

Figure 7.15- Emission spectra of IANR-labelled mGBP with glucose addition

It appears that there is a trend in the data. Plotting emission maxima against glucose concentration provides a clearer picture. Such a plot is shown in figure 7.16.

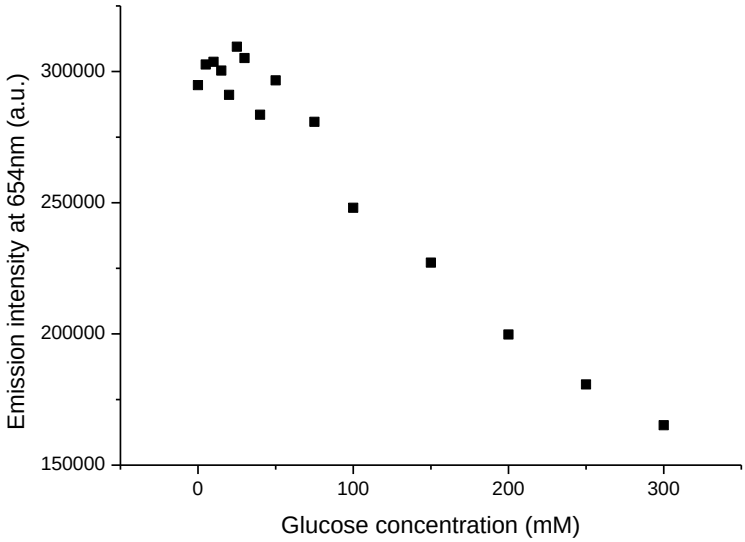

Figure 7.16: Emission maxima of IANR labelled mGBP with glucose concentration.

Figure 7.16 shows a clear negative correlation between glucose concentration and emission intensity at 654 nm. This is unexpected. GBP-BADAN shows a clear positive correlation between glucose concentration and emission intensity, and the Nile Red derivative was hypothesised to produce a complex with a similar glucose response. There is a 50 % reduction in fluorescence intensity with glucose concentration- this contrasts with the 500 % increase in intensity displayed by mGBP-BADAN in figure 5.10. However, the trend is clear, and a repeat experiment confirmed this trend. Using the data from figure 7.16, a linear fit to the points provides an adjusted R^2 value of 0.97. This shows an imperfect fit, but a very close correlation.

It was seen earlier that emission intensity of Nile Red decreases when the solvent polarity increases, so it can be inferred that upon protein folding (in the presence of glucose), the dye molecules become more exposed to the solvent environment. If this is the case, this is in direct contrast to the assumed mechanism of the mGBP-BADAN complex, and the inference is therefore that the binding site occupied by the IANR is potentially not the desired cysteine group.

What can be concluded from the data is that there is a definite trend with glucose addition, and that trend is a negative one. The plot provides very nearly a straight line over a large range of glucose concentrations, which if repeatable is a potentially useful result. However, the greatest deviation

from linearity in the results is found in the key 0-30 mM glucose concentration range, rendering the result less useful for a functioning biosensor based on mGBP-IANR emission.

7.2.4 mGBP-IANR lifetimes

The TCSPC fluorescence lifetime decays of IANR labelled mGBP were recorded, after excitation at 590 nm, and using a filter to remove light below 610 nm. The observed fluorescence lifetime decay in the absence of glucose is displayed in figure 7.17.

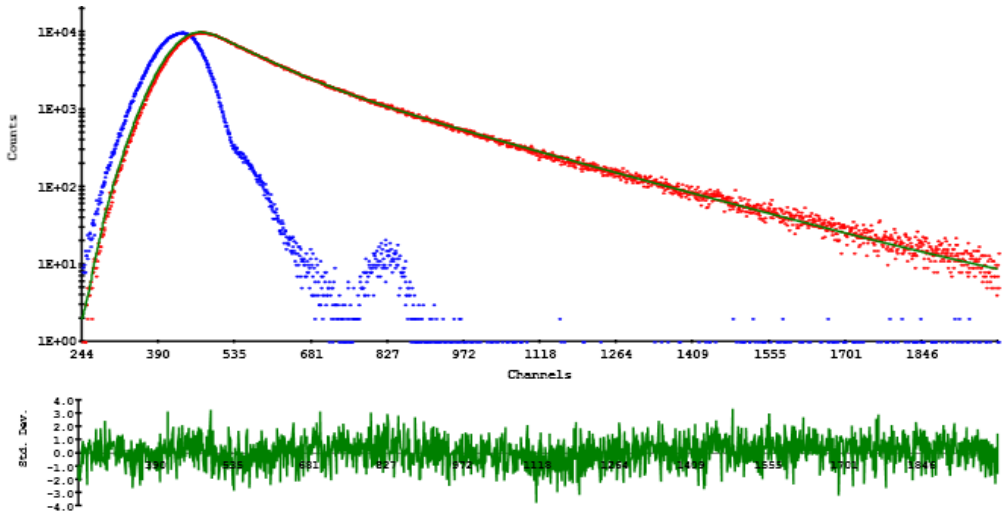

Figure 7.17- TCSPC data for mGBP-IANR in the absence of glucose

The decay profiles obtained at 0mM glucose, and with 300mM glucose present, are shown in figure 7.18.

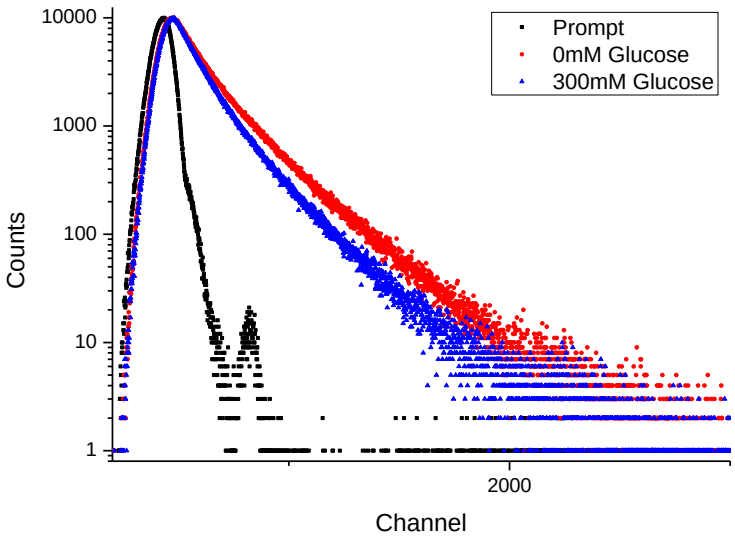

Figure 7.18- TCSPC decay curves for mGBP-IANR, with both 0mM and 300mM glucose concentration

The data were then analysed. The decay curves had mono-, and bi-exponential plots fitted to them. The mono-exponential plots were poor fits (χ^2>20), and so the 2 exponential fits with χ^2~1.05 were deemed appropriate and these are shown in table 7.5.

mGBP-IANR fluorescence lifetimes									
Glucose conc./mM	**T1/ns**	**σ/ns**	**T2/ns**	**σ/ns**	**B1**	**σ**	**B2**	**σ**	**χ2**
0	1.21	0.04	3.31	0.03	47.12	0.63	52.88	0.56	1.11
5	1.21	0.04	3.27	0.03	47.01	0.63	52.99	0.55	1.06
10	1.20	0.03	3.27	0.03	47.64	0.63	52.36	0.56	1.10
15	1.21	0.04	3.27	0.03	48.62	0.61	51.38	0.57	1.09
20	1.21	0.03	3.28	0.03	49.42	0.60	50.58	0.57	1.06
25	1.21	0.03	3.26	0.03	49.72	0.60	50.28	0.58	1.10
30	1.13	0.03	3.32	0.03	47.15	0.63	52.85	0.53	1.10
40	1.12	0.03	3.19	0.03	48.39	0.64	51.61	0.57	1.06
50	1.19	0.03	3.18	0.03	51.09	0.58	48.91	0.60	1.11
75	1.22	3.21	3.19	0.00	53.68	0.57	46.32	0.63	1.05
100	1.22	0.03	3.17	0.00	54.25	0.57	45.75	0.64	1.06
150	1.20	0.03	3.09	0.00	54.91	0.57	45.09	0.68	1.09
200	1.14	0.03	2.90	0.00	55.74	0.59	44.26	0.70	1.05
250	1.11	0.03	2.83	0.00	54.58	0.60	45.42	0.69	1.05
300	1.13	0.03	2.84	0.00	55.86	0.58	44.14	0.71	1.04

Table 7.5- 2-exponential fits to decay lifetimes of mGBP-IANR with glucose variation

As can be seen from table 7.5, the plots fit well (χ^2<1.10) to a 2-exponential decay. The two calculated lifetimes observed both show a decrease with increasing glucose intensity, and the

relative amplitudes of the pre-exponential factors change in a progressive manner. Figure 7.19 shows the changes in relative amplitude for the best-fitting 2-exponential plot.

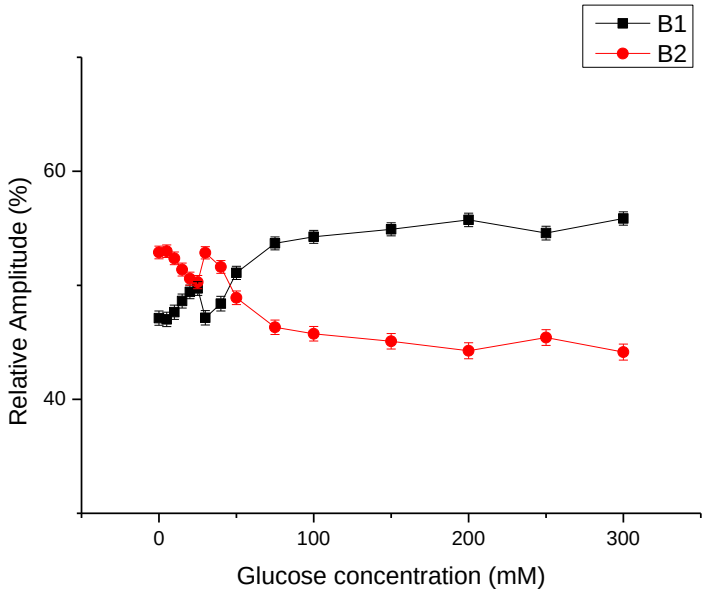

Figure 7.19- Relative amplitude changes of pre-exponential factors, fitting a two-exponential plot to the lifetime decay of IANR-labelled mGBP.

Once again, there is a trend on display. As with the intensity measurements, the trend is in the unexpected direction. In contrast with mGBP-BADAN, the short-lifetime component of this complex becomes more dominant with glucose addition.

The TCSPC lifetime fits were re-calculated while keeping the lifetimes themselves as constants. The 2-exponential plots with constant lifetimes are given in table 7.6.

mGBP-IANR fluorescence lifetime decay parameters							
Glucose conc./mM	**T1/ns**	**T2/ns**	**B1**	**σ**	**B2**	**σ**	**χ^2**
0	1.20	3.25	45.72	0.78	54.28	0.56	1.12
5	1.20	3.25	46.43	0.75	53.57	0.56	1.06
10	1.20	3.25	47.17	0.74	52.83	0.57	1.08
15	1.20	3.25	47.94	0.73	52.06	0.58	1.06
20	1.20	3.25	48.69	0.72	51.31	0.58	1.09
25	1.20	3.25	49.25	0.72	50.75	0.59	1.09
30	1.20	3.25	50.38	0.93	49.62	0.59	1.22
40	1.20	3.25	51.05	0.76	48.95	0.62	1.13
50	1.20	3.25	52.53	0.70	47.47	0.63	1.12
75	1.20	3.25	54.13	0.67	45.87	0.65	1.10
100	1.20	3.25	55.24	0.66	44.76	0.66	1.14
150	1.20	3.25	57.62	0.63	42.38	0.68	1.26
200	1.20	3.25	63.17	0.58	36.83	0.76	1.32
250	1.20	3.25	64.02	0.57	35.98	0.77	1.42
300	1.20	3.25	64.72	0.58	35.28	0.81	1.39

Table 7.6- mGBP-IANR lifetimes with glucose addition: variation in pre-exponential factors when lifetimes are kept constant

These results are graphically displayed in figure 7.21.

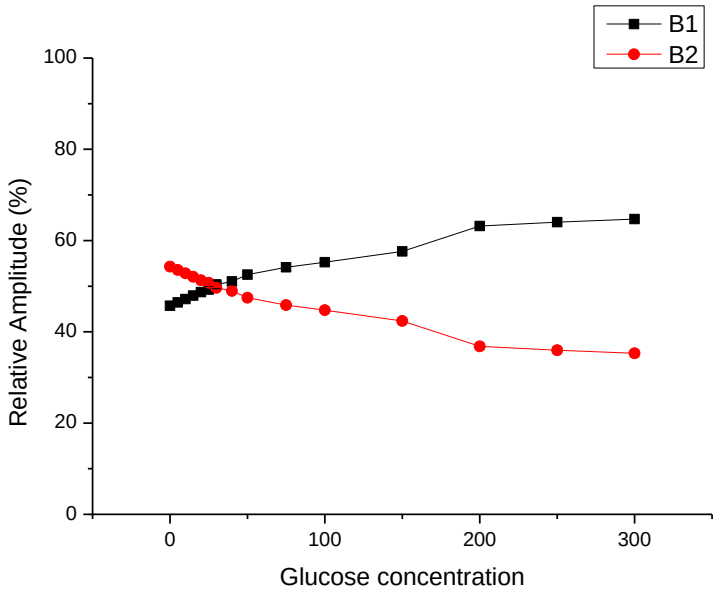

Figure 7.21- mGBP-IANR lifetimes with glucose addition: variation in pre-exponential factors when lifetimes are kept constant

There is a clear trend here, one which is especially well-defined over the useful 0-30 mM range. The 1.2 ns lifetime component contributes to 45.7 % of the decay lifetime with no glucose present- this

rises in a linear fashion (R^2=1.00 for a linear fit over the range 0-30mM) with glucose addition, contributing 50.4 % to the decay at a glucose concentration of 30mM. The increasing dominance of the 1.2 ns component continues as the glucose concentration is itself increased, but in a non-linear manner.

7.2.5 mGBP-IANR anisotropy

Anisotropy measurements were made on a selection of the same samples used for the lifetime decay readings. Figure 7.22 shows the anisotropy decay recorded at 0mM glucose concentration.

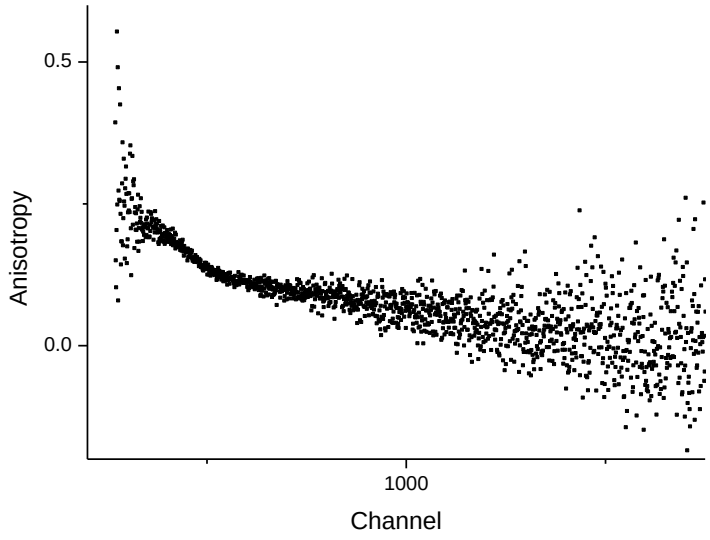

Figure 7.22- Anisotropy decay for mGBP-IANR with 0mM glucose

After data analysis, it was seen that a mono-exponential decay was the most appropriate model for understanding the depolarisation. This nanosecond regime measurement is of the correct timescale to correspond to the rotational time of the mGBP-IANR complex. Table 7.8 shows the rotational times at varying concentrations of glucose.

mGBP-IANR Rotational correlation times					
Glucose conc./mM	T1/ns	σ/ns	χ2	Diameter/nm	σ/nm
0	4.67	0.18	1.08	3.30	0.13
50	3.85	0.10	1.12	3.10	0.08
150	3.32	0.10	1.17	2.95	0.09
300	2.44	0.09	1.18	2.66	0.10

Table 7.8- Anisotropy measurements of mGBP-IANR with increasing glucose concentration

The apparent rotational time and the apparent diameter are both shorter than that seen for mGBP-BADAN, but the figures are of the same order of magnitude. The red dye has a quicker depolarisation time than the shorter-wavelength BADAN, and so when labelled with IANR the apparent diameter is seen to vary from 3.3 nm to 2.7 nm for the hydroscopic diameter of the protein.

7.3 Conclusions

The complex mGBP-Texas Red showed very little change in any fluorescence characteristic with increasing glucose concentration. This was expected, and confirms the importance of dye-solvent interactions for a sensor constructed in this manner.

The mGBP-IANR has been previously reported to show promise as a viable biosensor[57], and using the triple mutant with the Nile Red derivative IANR bound to the C152 mutant site has in this instance produced a system which responds to changes in glucose concentration. Although the emission intensity data indicate the attachment may potentially be elsewhere on the protein than the desired cysteine group, the lifetime data show a very promising response. The pre-exponential factors were found to vary in a linear way over the physiological glucose range, a finding which lends itself well to application of the system as a viable sensor. The anisotropy data provided a calculated hydrodynamic diameter which decreased in response to glucose, indicating adequate performance of the protein function when labelled with this dye.

The binding protocol, which as mentioned may not have succeeded as planned when it comes to location, left something to be desired in the realm of efficiency also. The nature and purity of the dye were questioned by the scientist who prepared the stock, and this may be what led to such

inefficient binding. If it was possible to get every protein molecule labelled with an IANR molecule, then the results would be that much stronger for it.

The results show promise, especially when the fluorescence lifetimes are considered. Fluorescence lifetime data are independent of concentration, and so the inefficiency of the labelling protocol would not be expected to impact on the lifetime decays. However, more efficient labelling would allow for faster collection of data, and be more applicable for use as a biosensor. Repeating this experiment, starting from synthesis of IANR, would provide insight into whether mGBP-IANR is inherently inefficient when it comes to labelling, or if this was just a flawed synthesis in this experiment.

8 Gel encapsulation

In order for any sensor molecule to be a viable clinical sensor, there must be an encapsulation or immobilisation procedure which takes place. The hypothesised and predicted models of smart tattoos and implanted sensors necessitate an immobilisation of some description, lest the sensor molecules diffuse throughout the cardiovascular system of the patient. Keeping the sensor molecules in one defined position allows for targeted interrogation of the system, as well as attachment to probe tips[69]. Sol gels[44] and hydrogels[39] have been successfully used for protein immobilisation with respect to glucose sensing- as have alternatives such as agarose substrates[60] and eggshell membranes[10].

8.1 Sol gels

Silica sol gels provide a method for low temperature fabrication of glasses. Sol gel technology has been around for more than a century[80,81] , and has in recent decades taken on new importance, especially with regards to fabrication of optical components and uses in biotechnology[82].

Silica sol gels are formed from the polymerisation of silicilic acid, and the end result of the formative reactions is a complex, branched silica polymer gel. The transition from sol- a fluid colloidal dispersion- to gel- a rigid network of channels and pores- is the defining characteristic of the sol gel process. This transition is judged to have happened at the point in time (known as the gel point) when the rigid network spans the containing vessel- whereby the gel network can support an elastic stress.

These silica gels can be used to efficiently and safely encapsulate proteins[83]; methods and protocols are well established which can do so while preserving their structure and function[84].

The initial protocol used in this project was taken from work by Macmillan, *e. al*., which utilised TMOS as a precursor to successfully encapsulate a functioning fluorophore for up to 20 days[63]. Another alkoxide precursor which was used in the project was TEOS. TEOS has also been shown to successfully immobilise proteins while preserving their function over a period of 16 days [64]. In each case, the silicate precursor is hydrolysed with acid catalyst to form silicilic acid. The silicilic acid then condenses over a period of days to form a rigid, porous silicate network.

Using TMOS, the chemical pathway is acid catalysed hydrolysis of the tetra-functional TMOS solution into silicilic acid (equation 30), followed by condensation of the silicilic acid into a porous network comprised of $(SiO_2)_n$ (equation 31).

The chemical equations for these processes are shown:

$$Si(OCH_3)_4 + 4H_2O \rightarrow Si(OH)_4 + 4CH_3OH \quad (30)$$

$$nSi(OH)_4 \rightarrow (SiO_2)n + H_2O \quad (31)$$

The by-product of the hydrolysis is methanol, for which account must be taken if sensitive biomolecules are being studied.

Using TEOS as a precursor, the chemistry is in principle the same, and can be summarised thus:

$$Si(OC_2H_5)_4 + 4H_2O \rightarrow Si(OH)_4 + 4C_2H_5OH \quad (32)$$

$$nSi(OH)_4 \rightarrow (SiO_2)n + H_2O \quad (33)$$

Where ethanol is the by-product of hydrolysis, and as with TMOS, allowance must be made for this alcohol if solvent effects are being studied.

Both TMOS and TEOS initiated sol gels were investigated in the project. Before using them to immobilise the BADAN-labelled mGBP however, protocols to remove the resultant alcohol (from the steps described in equations 30 and 32) from the gel environment were tested.

Confirming the safety of the silica sol gel environment was the first priority. The main concern was the possible presence of alcohol, and the potential consequent solvent polarity variations. Solvent polarity variations are thought to be the mechanism by which the mGBP-BADAN complex is effective, and therefore foreign solvents would hinder the use of such a complex as a sensor. Figure 5.4 shows the variation in fluorescence emission when the solvent is methanol, compared with PBS

buffer. Any alcohol present in the gel system could potentially alter the solvent polarity around the dye molecules, and it has been observed that decreasing polarity has a similar effect to increasing glucose concentration (contrast lifetime changes in tables 5.1 and 5.3) on the mGBP-BADAN complex. In short, alcohol in the system would obscure the results, and therefore its removal was deemed a priority.

The protein allophycocyanin (APC) can exist in two forms- monomeric and trimeric APC. Each form has a different fluorescence emission wavelength, and the native trimeric form dissociates into monomers in the presence of alcohol[63]. It is therefore an effective test for alcohol in a system, and the test which was used for the gels in question.

8.2 TMOS sol-gel

8.2.1 Allophycocyanin

A silica sol was prepared, starting from the precursor TMOS, and the fluorescent protein allophycocyanin (APC) was encapsulated in the resulting gel. The trimeric APC has a fluorescence emission peak at 660 nm, which is wavelength-shifted to 640 nm in the presence of alcohol. The presence or absence of each of these emission peaks therefore indicates how efficient was the alcohol removal procedure[63].

The fluorescence emission was measured on the Horiba Scientific Fluoromax 2 spectrometer after excitation at 600nm, and is shown in figure 8.1.

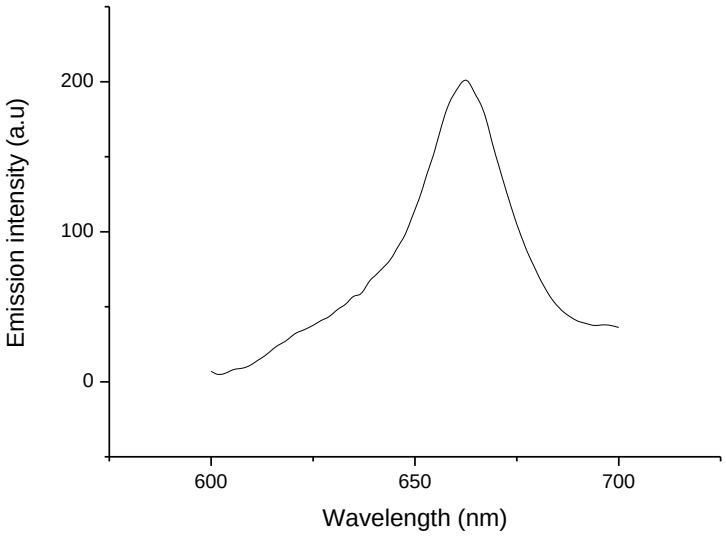

Figure 8.1- Emission spectrum of APC in TMOS sol gel

The figure clearly shows an emission peak centred at 660 nm, indicating that the sol gel preparation was appropriate in the available laboratory conditions.

8.2.2 mGBP-BADAN in TMOS sol gel: emission

A TMOS sol gel was prepared which encapsulated a sample of mGBP-BADAN. Initial experiments showed little response to glucose when adding the glucose solution in the same manner as in buffer. There was no measurable immediate response to glucose concentration in the sub-100 mM range. Time, therefore- rather than concentration- was used as the varying parameter for all subsequent experiments with TMOS.

A 70 µL aliquot of (1 M) glucose solution was placed in the cuvette, which sat on top of the sol gel, providing a total sample volume of 140 µL, with averaged glucose concentration of 500 mM. This moment of addition was taken to be time '0 hours'. Measurements were made at various time intervals, investigating the changes in fluorescence with time. Fluorescence intensity measurements were recorded with 400 nm excitation, and these spectra are shown in figure 8.2.

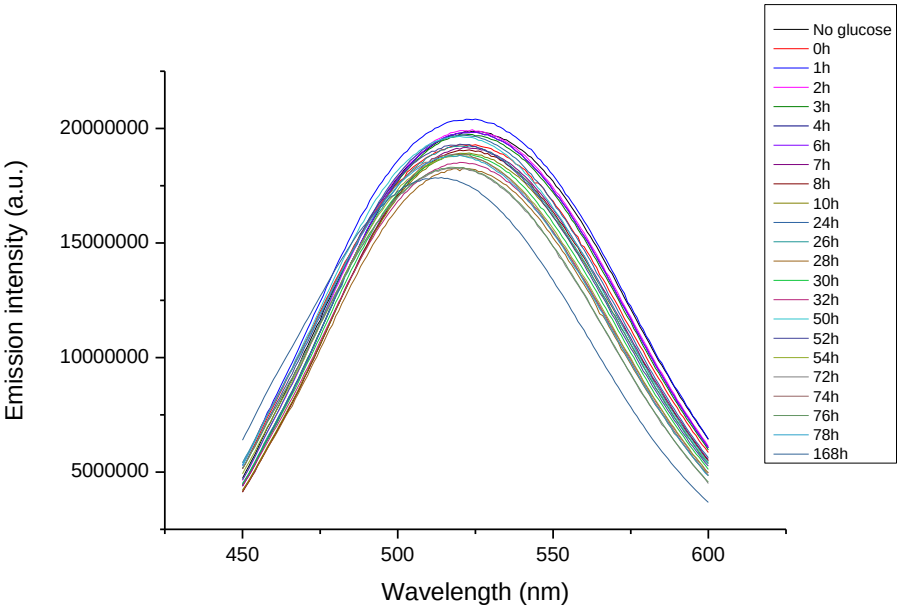

Figure 8.2- Fluorescence emission spectra of mGBP-BADAN in TMOS sol gel in the presence of glucose

There are slight variations in emission intensity as the experiment progresses. Plotting the changes in maxima against time elapsed results in figure 8.3.

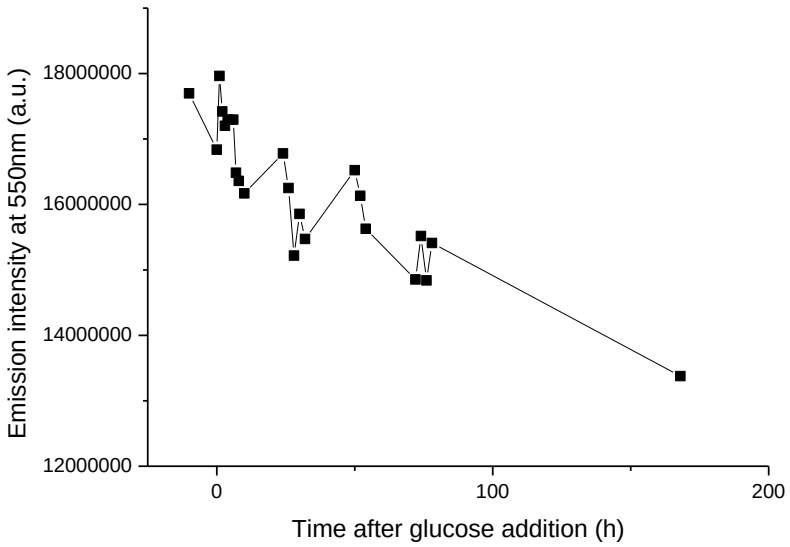

Figure 8.3- Emission intensity at 550 nm of mGBP-BADAN in TMOS sol gel with time after glucose addition.

The trend- in direct contrast to that seen in buffer- is a clear negative correlation. Evidently the TMOS gel is interfering in some way with the normal functioning of the labelled protein, and it is possible that the gel environment itself is causing this uncharacteristic drop-off in intensity. What Is

equally clear is that a response which takes 168 hours to complete is far too slow for any practical glucose sensing, where responses are desired in seconds, not hours.

8.2.3 mGBP-BADAN in TMOS sol gel: lifetimes

The TCSPC fluorescence lifetime decays of mGBP-BADAN in the TMOS sol gel were recorded, using a 379nm excitation source. The data recorded before addition of the glucose solution are shown in figure 8.4.

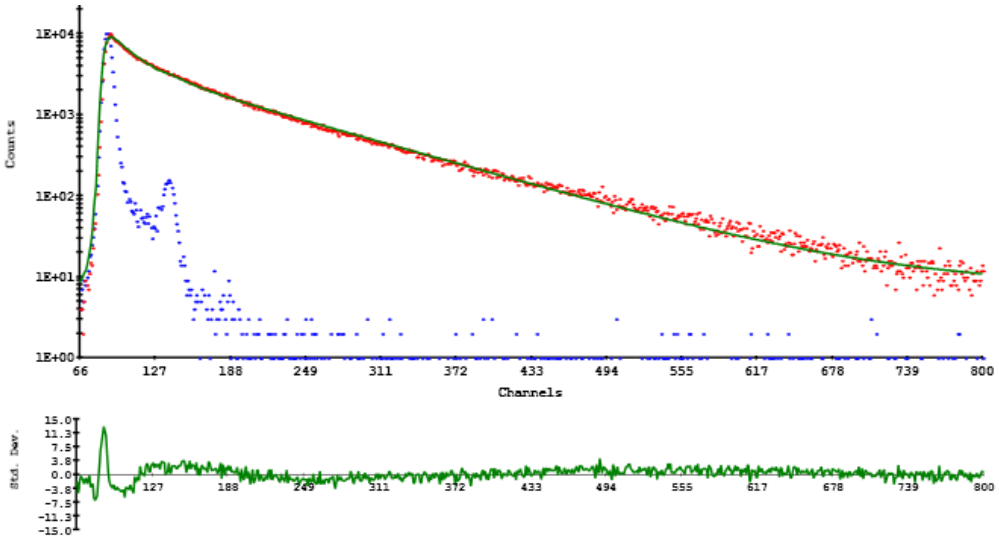

Figure 8.4- TCSPC data for mGBP-BADAN in TMOS sol gel

For each of the samples measured above, the fluorescence lifetime decays were also measured. The best-fitting calculated two exponential decay parameters are shown in table 8.1.

mGBPBADAN in TMOS sol gel; Fluorescent lifetimes									
Time elapsed/h	**T1/ns**	**σ/ns**	**T2**	**σ/ns**	**B1**	**σ**	**B2**	**σ**	**χ2**
No glucose	0.90	0.05	3.18	0.04	33.30	1.77	66.70	0.81	1.25
0	0.92	0.06	3.25	0.04	33.77	1.81	66.23	0.80	1.14
1	1.12	0.06	3.28	0.04	64.08	1.86	35.92	0.80	1.08
2	0.97	0.06	3.25	0.04	27.02	1.91	72.98	0.79	1.06
3	1.17	0.06	3.37	0.04	63.02	1.96	36.98	0.78	1.10
4	0.94	0.06	3.24	0.04	24.44	2.01	75.56	0.77	1.15
6	0.98	0.06	3.27	0.04	26.26	2.06	73.74	0.77	1.04
7	1.05	0.06	3.30	0.04	26.88	2.11	73.12	0.76	1.07
8	1.00	0.07	3.29	0.04	25.18	2.16	74.82	0.75	1.17
10	1.14	0.07	3.31	0.04	40.62	2.22	59.38	0.74	1.06
24	0.96	0.07	3.26	0.04	21.62	2.28	78.38	0.74	1.02
26	0.92	0.07	3.23	0.04	22.02	2.33	77.98	0.73	1.13
28	0.94	0.07	3.27	0.04	22.15	2.39	77.85	0.72	1.13
30	0.95	0.07	3.27	0.04	22.92	2.46	77.08	0.71	1.12
32	0.97	0.08	3.26	0.04	22.93	2.52	77.07	0.71	1.14
48	0.91	0.08	3.28	0.04	20.07	2.58	79.93	0.70	1.05
50	1.24	0.08	3.40	0.04	37.52	2.65	62.48	0.69	1.04
52	0.91	0.08	3.28	0.04	21.23	2.72	78.77	0.69	1.11
54	0.98	0.08	3.33	0.04	22.18	2.79	77.82	0.68	1.10
72	1.24	0.09	3.44	0.04	38.14	2.86	61.86	0.67	1.05
74	1.03	0.09	3.39	0.04	21.65	2.93	78.35	0.67	1.05
76	0.96	0.09	3.28	0.04	21.04	3.01	78.96	0.66	1.05
78	1.09	0.09	3.39	0.04	23.64	3.08	76.36	0.65	1.00
168	0.94	0.10	3.39	0.04	21.96	3.16	78.04	0.65	1.11

Table 8.1- Two-exponential lifetime decays of mGBP-BADAN in TMOS sol gel with time after addition of saturation glucose concentration

The lifetimes show no noticeable trend, but variations can be seen between consecutive measurements which are larger than the uncertainty in the measurement. New parameters were calculated, keeping the lifetimes constant at 0.9 ns and 3.2 ns, as in previous experiments. The results of these forced fits are presented in table 8.2.

mGBPBADAN in TMOS sol gel; Fluorescent lifetime parameters							
Time elapsed/h	**T1/ns**	**T2**	**B1**	**σ**	**B2**	**σ**	**χ2**
No glucose	0.90	3.20	33.64	1.77	98.23	0.85	1.25
0	0.90	3.20	33.04	1.81	98.19	0.86	1.14
1	0.90	3.20	26.24	1.86	98.14	0.88	1.08
2	0.90	3.20	25.78	1.90	98.09	0.85	1.07
3	0.90	3.20	25.69	1.95	98.04	0.85	1.13
4	0.90	3.20	23.47	2.00	97.99	0.85	1.15
6	0.90	3.20	24.67	2.05	97.94	0.86	1.06
7	0.90	3.20	24.12	2.10	97.89	0.87	1.11
8	0.90	3.20	22.99	2.16	97.84	0.91	1.19
10	0.90	3.20	23.20	2.21	97.78	0.88	1.06
24	0.90	3.20	20.19	2.27	97.72	0.99	1.04
26	0.90	3.20	21.35	2.32	97.67	0.82	1.13
28	0.90	3.20	20.81	2.38	97.61	0.81	1.15
30	0.90	3.20	21.62	2.44	97.54	0.95	1.14
32	0.90	3.20	21.31	2.51	97.48	0.88	1.15
48	0.90	3.20	18.51	2.57	97.42	0.88	1.11
50	0.90	3.20	18.22	2.63	97.35	0.87	1.15
52	0.90	3.20	19.79	2.70	97.28	0.85	1.16
54	0.90	3.20	19.27	2.77	97.21	0.85	1.17
72	0.90	3.20	17.00	2.84	97.14	0.85	1.24
74	0.90	3.20	17.55	2.91	97.07	0.86	1.20
76	0.90	3.20	19.26	2.98	96.99	0.85	1.07
78	0.90	3.20	18.80	3.06	96.92	0.90	1.09
168	0.90	3.20	18.44	3.14	96.84	0.85	1.33

Table 8.2- Two-exponential lifetime decays of m-GBPBADAN in TMOS sol gel with time after addition of saturation glucose concentration

Forcing the fits allows a trend to be realised. The change in relative amplitudes over the course of the experiment follows the same pattern as observed in buffer- although the magnitude is smaller. Over the course of one week, there is an observed change of 15%, compared to the change of 18% in buffer- on a much shorter timescale.

The greatest difference in size of amplitude takes place between the readings at 0 h and 1 h. The 6.80 % difference between these measurements is almost as great as the 7.80 % change between 1 h and 168 h. Most of the glucose response in the sol gel takes place in the first hour, although the fact that the changes continue with no further glucose addition suggests that there is still a response unfolding in this time. There are occasional increases in B1 against the trend- at 76 h for example- but overall the change is consistent.

The changes are shown graphically in figure 8.5.

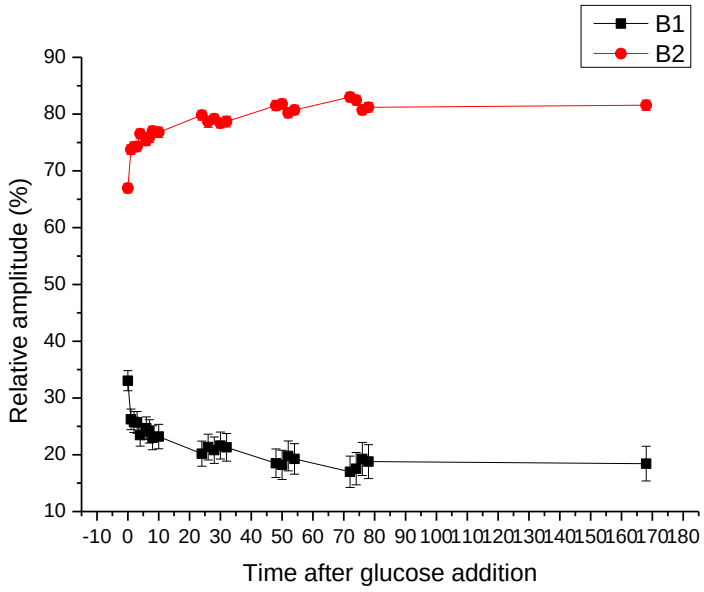

Figure 8.5- Relative lifetime contributions in mGBP-BADAN immobilised in TMOS sol gel

Figure 8.5 illustrates the fact that the response increases over the first three days (72 h), but that the next four days after that show no noticeable increase in the size of the B2 factor.

The expected direction of relative amplitude variance is at odds with the unexpected direction of fluorescence emission. Once again, the intensity and lifetime data appear to behave independently.

8.2.4 Glucose diffusion

Given the apparent protein-safety of the silica sol gel, and the reduced response to glucose with time, the gel permeability to glucose was investigated. Silica sol gels derived from TMOS have been shown to possess large enough permeability to allow diffusion of a small molecule like glucose[44], but confirmation of this fact was sought for the current protocol.

To this end, hexokinase was immobilised in a sol gel prepared by the above methods, and glucose solution added to the cuvette containing the gel. Hexokinase has previously shown a response to glucose while encapsulated in a sol gel[44], showing a reduction of 25 % in fluorescence emission intensity at 330nm with saturation levels of glucose. The fluorescence of hexokinase results from the tryptophan residues in the enzyme, which show a reduction in fluorescence intensity in the presence of glucose. The prepared sol gel was excited at 295 nm and the emission spectra recorded on the

Horiba Scientific Fluoromax 2 at a few different times after glucose addition. The emission maxima are plotted against time in figure 8.6.

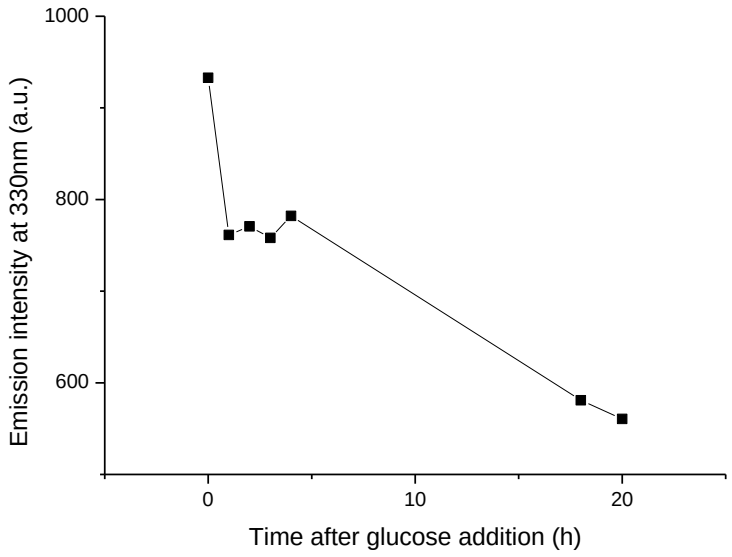

Figure 8.6- Emission intensity of TMOS sol gel immobilised hexokinase with time after glucose addition

There is a distinct drop in emission intensity in the first hour after glucose addition, indicating immediate diffusion of a portion of the glucose through the sample. After 1 hour a reduction in intensity of 20 % is observed. It is observed that after 20 h, the full hexokinase response of 41 % intensity reduction has taken place.

This result compares with the changes in mGBP-BADAN pre-exponential factor relative amplitudes- where the first hour saw the greatest change in amplitude values, and changes after that point came more slowly and gradually.

It is notable from this experiment that after 1 h the diffusion of the glucose solution is halfway complete, and fully complete after 20 h, yet changes continue to occur in the gel-immobilised mGBP-BADAN for many hours after this. The possibility should be considered that there are other factors in the silica matrix which hinder the response of the mGBPBADAN complex, even after glucose diffusion has certainly completed.

8.3 TEOS sol-gel

8.3.1 Allophycocyanin

Although the literature protocol described by Hungerford *et al.*, was unconcerned with ethanol in the finished gel[64], alcohol removal was desirable for a BADAN-based sensor. The same rotary evaporation procedure was used as for the TMOS gels- after some initial testing. APC was again used as an indicator of alcohol presence, and the rotary evaporator employed for varying lengths of time. It was quickly found that 6 minutes at 50 ^{o}C was too long a time- the sample gelled before it could be removed from the evaporator. TEOS gel samples with APC were therefore prepared with 0 minutes, 3 minutes, 4 minutes, and 5 minutes of evaporation time at 50 ^{o}C: the fluorescence emission spectra for these samples with excitation at 600 nm were recorded and are shown in figure 8.7. As was the case with the TMOS protocol, the desired outcome here was a peak at 660 nm (trimeric form), with no noticeable fluorescence at 640 nm (monomeric form).

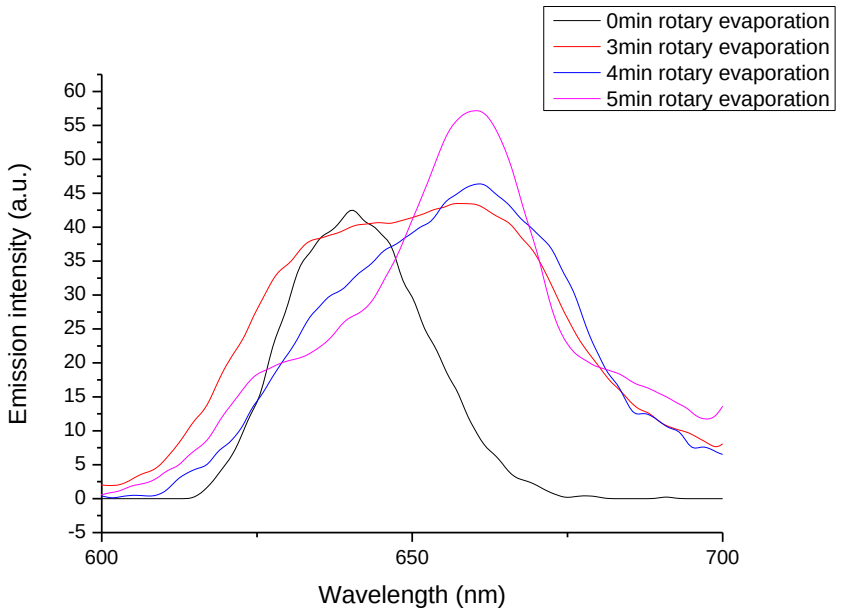

Figure 8.7- Emission intensity of APC in TEOS sol gels

From figure 8.6, the 640 nm peak which is clearly evident in the gel with 0 minutes of evaporation gradually gives way to a near-single peak at 660 nm, which is found with 5 minutes of evaporation time at 50 ^{o}C. The emission at 640nm from the APC monomers still provides a slight contribution with 5 minutes of evaporation time (see the shoulder on the peak in figure 8.7), but the majority of the fluorescence- and therefore the majority of the sol gel environment- is seen to be free of

alcohol. This evaporation procedure was the experimental protocol used for mGBP-BADAN encapsulation.

8.3.2 mGBP-BADAN in TEOS sol gel: emission

A 10 µM sample of mGBP-BADAN was encapsulated in the TEOS sol-gel, and experiments were conducted with glucose solution. 70 µL of 1 M glucose solution was placed on top of the gel matrix in the cuvette, and the fluorescence spectra were recorded as time progressed, with 400nm excitation. These spectra are presented in figure 8.8.

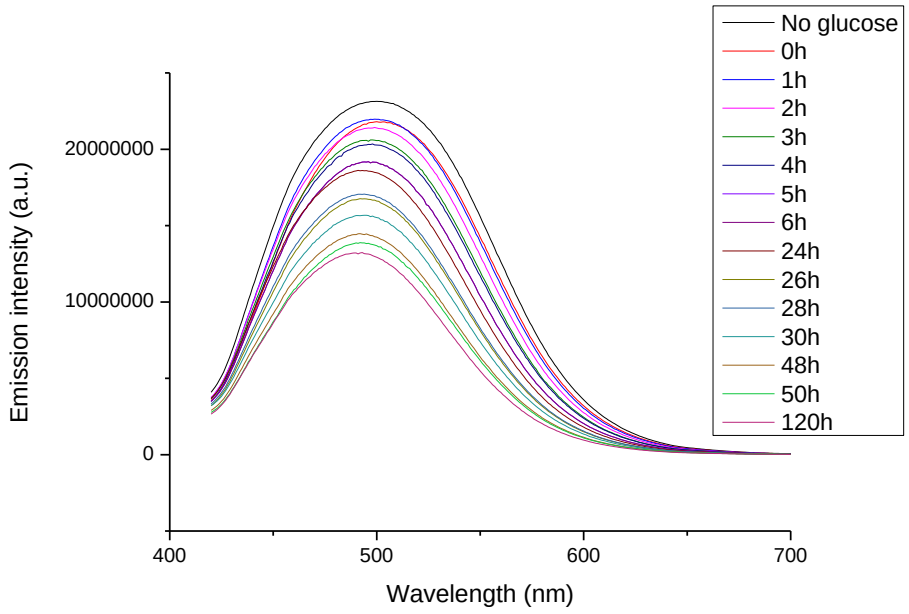

Figure 8.8- Fluorescence emission spectra of mGBP-BADAN in TEOS sol gel with increasing time after glucose addition.

The fluorescence emission maximum was recorded for each value of time following glucose addition, and the maxima are plotted against time in figure 8.9.

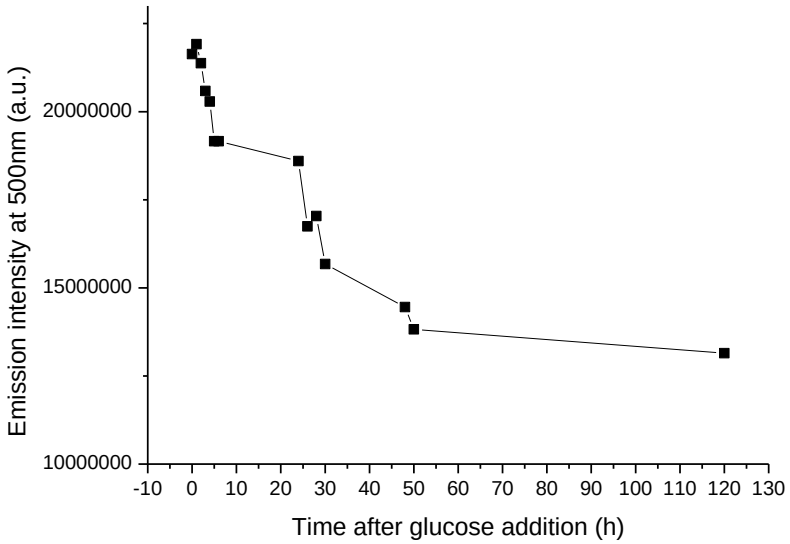

Figure 8.9- Emission intensities at 500nm of mGBP-BADAN in TEOS sol gel, with respect to time elapsed after glucose addition.

In a similar pattern to that observed for the TMOS sol gel, the emission intensity decreases- rather than increases- with time after addition of glucose.

8.3.3 mGBP-BADAN in TEOS sol gel: lifetimes

For each sample investigated for emission intensity, fluorescence lifetime measurements were also recorded with 379 nm excitation. The data recorded before addition of the glucose solution are shown in figure 8.9.

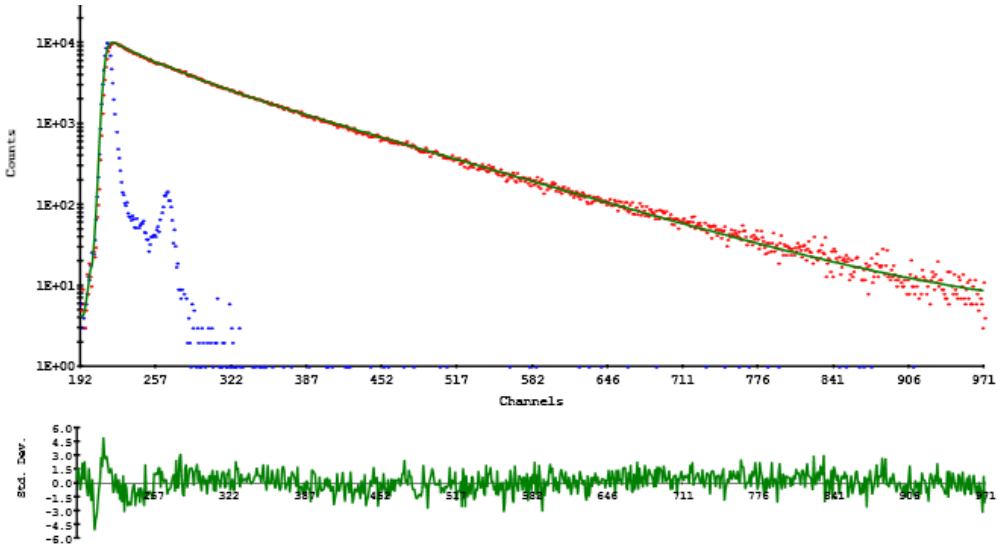

Figure 8.10- TCSPC data for mGBP-BADAN in TEOS sol gel in the absence of glucose

The two-exponential fits to the analysed data are presented in table 8.3.

mGBP-BADAN in TEOS sol gel; Fluorescence lifetimes									
Time elapsed/h	T1/ns	σ/ns	T2/ns	σ/ns	B1	σ	B2	σ	χ2
No Glucose	1.35	0.03	3.18	0.04	44.78	2.06	55.22	0.82	1.16
0	1.12	0.09	3.06	0.04	25.68	2.18	74.32	0.76	1.07
1	1.07	0.08	3.09	0.03	24.27	2.14	75.73	0.69	1.09
2	1.08	0.08	3.14	0.03	23.02	2.31	76.98	0.69	1.00
3	1.16	0.10	3.18	0.03	24.24	2.31	75.76	0.73	1.04
4	1.08	0.08	3.16	0.03	23.75	2.19	76.25	0.68	1.08
5	1.02	0.08	3.10	0.03	22.29	2.26	77.71	0.66	0.98
6	1.04	0.08	3.11	0.03	23.06	2.25	76.94	0.68	1.11
24	1.04	0.07	3.19	0.04	22.59	2.13	77.41	0.64	1.06
26	1.15	0.09	3.25	0.04	24.55	2.28	75.45	0.71	1.12
28	1.38	0.11	3.31	0.03	46.41	2.19	53.59	0.83	1.08
30	1.11	0.09	3.22	0.04	23.70	2.33	76.30	0.70	1.08
48	1.34	0.10	3.33	0.03	50.11	2.06	49.89	0.82	0.99
50	1.05	0.07	3.18	0.03	25.24	2.04	74.76	0.69	1.14
120	1.28	0.11	3.28	0.04	43.35	2.17	56.65	0.80	1.15

Table 8.3- Two-exponential lifetime decays of mGBP-BADAN in TEOS sol gel with time after addition of saturation glucose concentration

There is no particular trend in the values of the lifetimes recorded. Calculations were performed using the same data, and constraining the lifetime values to be 0.9 ns and 3.2 ns respectively provided the parameters shown in table 8.4.

mGBP-BADAN in TEOS sol gel; Fluorescence lifetimes parameters							
Time elapsed/h	T1/ns	T2/ns	B1	σ	B2	σ	χ2
No Glucose	0.90	3.20	23.65	2.06	76.35	0.82	2.21
0	0.90	3.20	21.18	2.18	78.82	0.76	1.35
1	0.90	3.20	22.28	2.14	77.72	0.69	1.99
2	0.90	3.20	20.30	2.31	79.70	0.69	1.51
3	0.90	3.20	21.75	2.31	78.25	0.73	1.65
4	0.90	3.20	20.79	2.19	79.21	0.68	1.56
5	0.90	3.20	21.17	2.26	78.83	0.66	1.53
6	0.90	3.20	21.50	2.25	78.50	0.68	1.72
24	0.90	3.20	20.15	2.13	79.85	0.64	1.26
26	0.90	3.20	21.43	2.28	78.57	0.71	1.38
28	0.90	3.20	19.27	2.19	80.73	0.83	1.42
30	0.90	3.20	21.25	2.33	78.75	0.70	1.33
48	0.90	3.20	22.78	2.06	77.22	0.82	1.23
50	0.90	3.20	22.41	2.04	77.59	0.69	1.45
120	0.90	3.20	21.76	2.17	78.24	0.80	1.42

Table 8.4- Two-exponential lifetime decays of mGBP-BADAN in TEOS sol gel with time after addition of saturation glucose concentration

In contrast with the results for the TMOS gel observed in table 8.2, there is no large change in the relative amplitudes shown in table 8.4. Over 120 h there is an overall increase in the B2 value of 1.91%, rather less than the 14.6% in the TMOS gel, and much less than the 18% recorded in buffer.

The B1 and B2 pre-exponential values are plotted against time in figure 8.11.

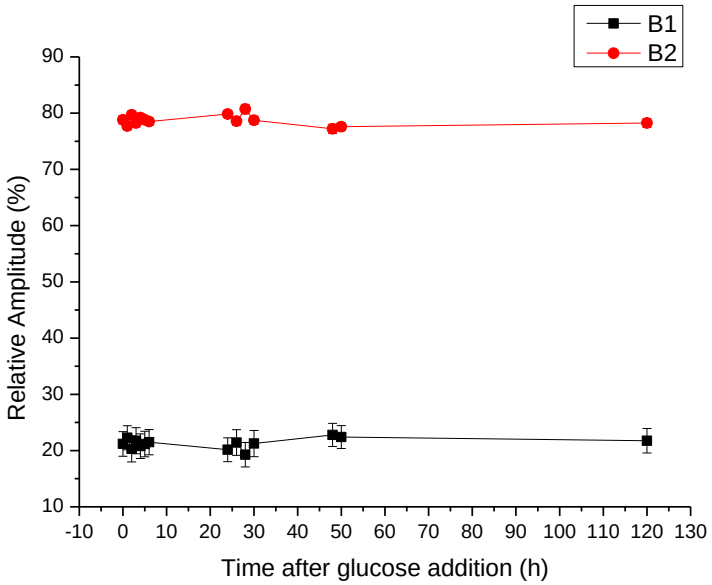

Figure 8.11- Relative lifetime contributions in mGBP-BADAN immobilised in TMOS sol gel

This figure merely confirms the points made previously.

The TEOS sol gel shows little response in the lifetime changes, and shows the opposite response to that expected when considering emission. One possible conclusion from this is that the TEOS gel does not allow for proper functioning of the labelled protein, and in fact degrades the fluorescence efficiency over time.

Neither silica gel proved itself to be effective. It was noted by Hungerford *et al.* that sol gel monoliths undergo a progressive shrinking as part of the gel aging process. It is possible that this naturally occurring physical restriction in the size of the pores and channels over a period of days was responsible for restricting the efficiency of the binding protein. The mGBP molecule depends on protein conformational change for its function; if the gel aging increasingly constrained the physical space available for movement of the protein lobes then the lack of glucose response would be explained.

8.4 Hydrogels

Hydrogels are hydrophilic polymer networks, comprised mostly of structured water molecules, which make them a useful tool for biological applications. Physical hydrogels consist of 99% water molecules, ordered into a gel structure by the integration of protein molecules in the matrix[85]. The physical properties of hydrogels are programmable and variable through selection of the properties of the protein molecules chosen. The aqueous nature of hydrogels, coupled with their tuneable characteristics, makes them useful for biological encapsulation[86]. In recent years there has been increasing interest in these hydrogels for their use in a variety of medical applications[87,88,89] including sensors[85,90,91], and in related clinical settings such as drug delivery[92].

Hydrogels are already known to safely encapsulate variants of glucose binding protein[39]. When it became clear in this project that the silica sol gels were inadequate for efficient immobilisation, a hydrogel system was investigated. FMOC-YL was the basis for the hydrogel used in this experiment, as described in section 3.10 of this report[93].

It was evident that the IANR- labelled mGBP complex showed a response to glucose in buffer. Given the scarcity of labelled protein available, and the unpromising response the mGBP-BADAN complex exhibited in a silica sol-gel, only the hydrogel method of immobilisation was investigated for this dye.

Initially mGBP-BADAN was encapsulated in the hydrogel and investigated, then in a successive experiment mGBP-IANR was immobilised for interrogation.

8.4.1 mGBP-BADAN in FMOC-YL hydrogel: emission

Aliquots of glucose solution were added to the hydrogel matrix containing mGBP-BADAN, and measurements were taken. With the limited supplies of labelled protein available, the experiments in hydrogel were conducted initially as in buffer solution- changing the concentration of glucose over the whole sample. Fluorescence emission spectra were recorded after excitation at 380 nm and are presented in figure 8.12.

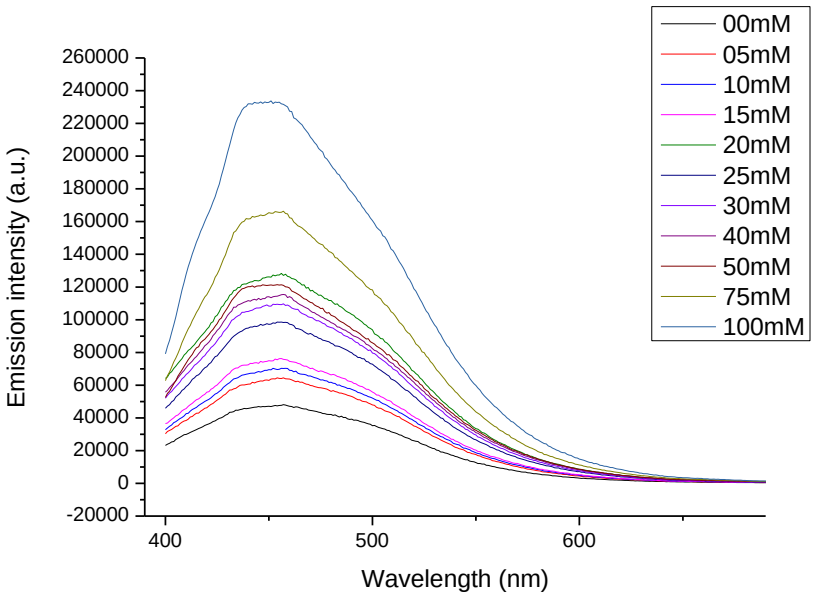

Figure 8.12- Fluorescence emission spectra of mGBP-BADAN immobilised in FMOC-YL hydrogel

It is interesting that the peak emission wavelength is found at 460 nm in the hydrogel, compared with 530 nm in buffer. Hydrogels are in essence an ordered array of water molecules. Imposed order in the hydrogel environment must be assumed to inhibit the movement and re-orientation of the water molecules. Such an inhibition would mitigate the solvent-dye interactions, leaving the excited state dipole moment at higher energy, and therefore exhibiting shorter wavelength emission. As observed in PBS, there is a slight blue shift with increasing glucose concentration. There are evidently increases in emission intensity with increasing glucose concentration, and the intensity values are plotted against concentration in figure 8.13.

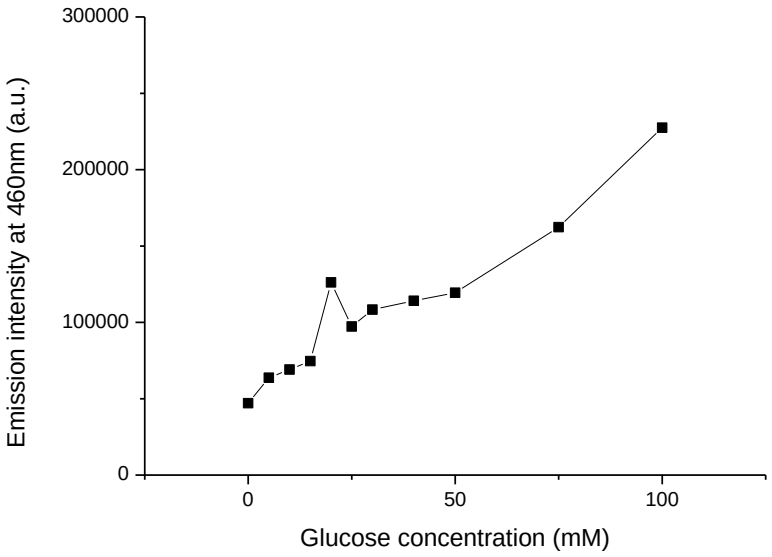

Figure 8.13- Emission intensities at 460nm of mGBP-BADAN in FMOC-YL hydrogel with glucose concentration

Over the range 0-100 mM, the positive correlation between emission intensity and glucose concentration is clear. There is an increase in emission intensity of 500% over the range- a comparable increase to the 500% increase observed in figure 5.10. It would appear that the emission intensity variations of mGBP-BADAN are not disrupted in the FMOC-YL environment, even though the wavelength shift is large.

8.4.2 mGBP-BADAN in FMOC-YL hydrogel: lifetimes

The fluorescence lifetime decays were recorded, and the lifetimes calculated after excitation at 379nm. The TCSPC decay data in the absence of glucose are shown in figure 8.14.

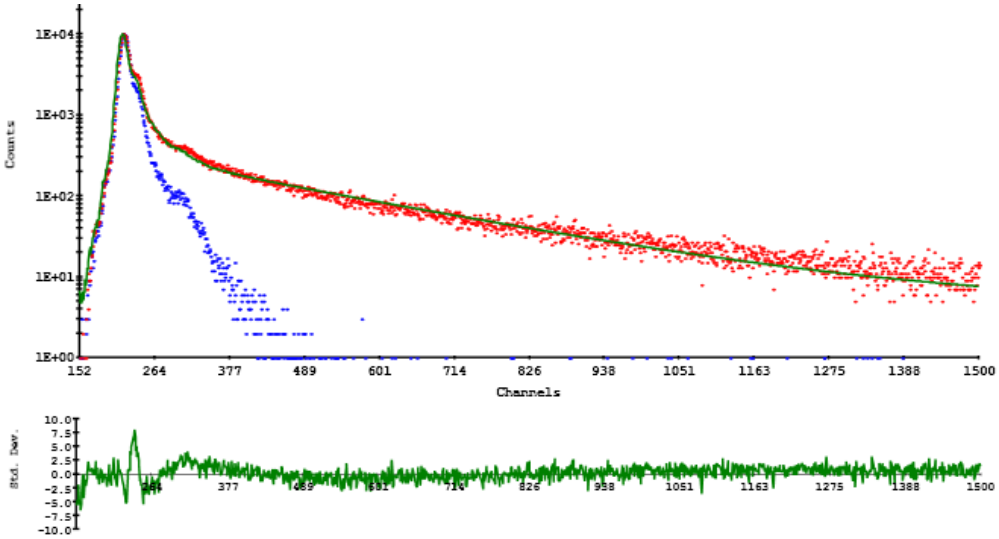

Figure 8.14- TCSPC data for mGBP-BADAN in FMOC-YL

The calculated parameters from these data are presented in table 8.5.

mGBP-BADAN in FMOC-YL hydrogel: Fluorescence lifetimes									
Glucose conc./mM	**T1/ns**	**σ/ns**	**T2/ns**	**σ/ns**	**B1**	**σ**	**B2**	**σ**	**χ2**
0	0.80	0.01	4.36	0.10	80.11	1.31	19.89	1.16	1.12
5	0.83	0.01	4.46	0.10	80.12	1.32	19.88	1.26	1.03
10	0.79	0.01	4.55	0.11	83.17	1.30	16.83	1.37	1.25
15	0.82	0.01	4.48	0.10	80.14	1.26	19.86	1.23	1.22
20	0.84	0.01	4.57	0.10	80.19	1.33	19.81	1.30	1.19
25	0.81	0.01	4.50	0.11	80.65	1.25	19.35	1.20	1.13
30	0.77	0.01	4.39	0.10	82.21	1.22	17.79	1.23	1.11
40	0.78	0.01	4.36	0.10	79.83	1.32	20.17	1.18	1.13
50	0.92	0.01	4.61	0.09	72.00	1.37	28.00	0.95	1.10
75	0.94	0.01	4.74	0.10	72.15	1.31	27.85	0.93	1.10
100	0.94	0.02	4.79	0.09	72.80	1.34	27.15	0.85	1.01

Table 8.5- 2-exponential analysis of mGBP-BADAN in FMOC-YL hydrogel

The T2 lifetime appears to be varying around 4.5 ns, in comparison to the results seen in PBS of T2 being roughly 3.5 ns. Fixing the lifetimes to the same values as used in PBS, the relative amplitudes were calculated. These are presented in table 8.6.

mGBP-BADAN in FMOC-YL hydrogel: Fluorescence lifetime parameters							
Glucose conc./mM	T1/ns	T2/ns	B1	σ	B2	σ	χ^2
0	0.90	3.20	56.25	11.14	43.75	2.67	1.48
5	0.90	3.20	60.44	10.87	39.56	3.04	1.34
10	0.90	3.20	61.16	11.32	38.84	2.11	1.50
15	0.90	3.20	57.82	11.27	42.18	2.75	1.51
20	0.90	3.20	60.17	11.12	39.83	2.01	1.41
25	0.90	3.20	57.69	11.05	42.31	2.46	1.51
30	0.90	3.20	51.03	14.41	48.97	2.18	1.41
40	0.90	3.20	53.52	12.57	46.48	1.41	1.42
50	0.90	3.20	48.31	17.62	51.69	1.39	1.63
75	0.90	3.20	48.17	11.65	51.83	1.80	1.77
100	0.90	3.20	50.66	10.98	49.34	1.17	1.71

Table 8.6- Fixed lifetime 2-exponential analysis of mGBP-BADAN in FMOC-YL hydrogel

Table 8.6 shows that there is a limited overall lifetime response to glucose concentration in this experiment. The B2 relative amplitude increased from 39.56 % to 51.8 3% over the range 5-75 mM; an increase of 12.27 %. However, viewing the entire range of concentration shows the increases to be erratic, and indeed from 0-100 mM the increase in B2 value is merely 5.59 %. The relative amplitude variance with glucose concentration is plotted in figure 8.15.

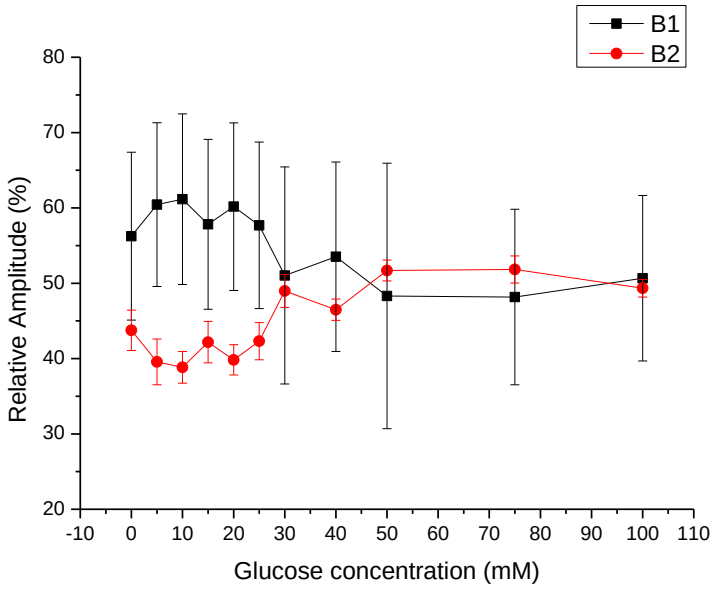

Figure 8.15- Relative lifetime contributions in mGBP-BADAN immobilised in FMOC-YL hydrogel

The lifetime changes are roughly as would be expected. The long-lifetime component does increase in relative amplitude with increasing glucose concentration, but the shape of the curve does not

follow the smooth line observed in buffer. However, the very large standard deviations for these results suggest that we should not put too much stock in small deviations at high or low concentrations.

8.4.3 mGBP-IANR in FMOC-YL hydrogel: emission

The fluorescence emission spectra of the mGBP-IANR complex in FMOC-YL hydrogel were recorded after excitation at 590 nm. Glucose concentration was varied from 0 to 300mM. The spectra are shown in figure 8.16.

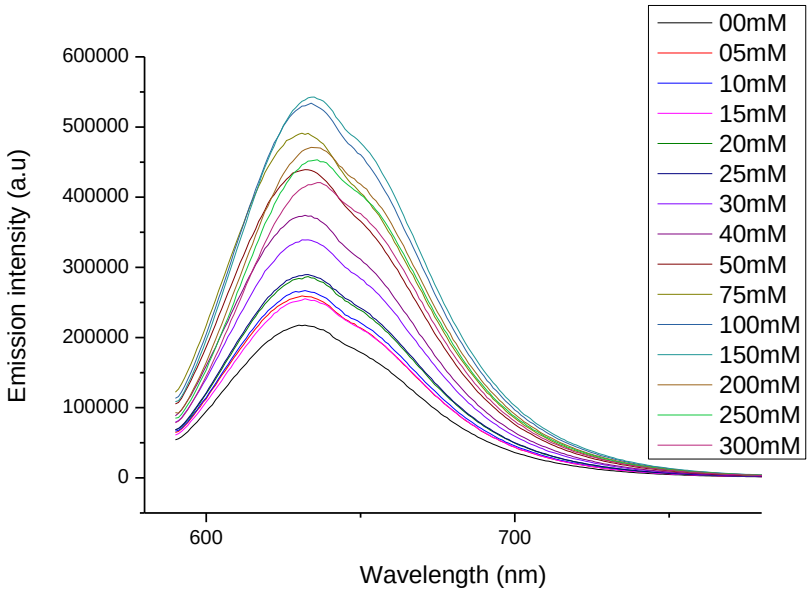

Figure 8.16- Emission spectra of mGBP-IANR in hydrogel with increasing glucose concentration

In a similar manner to the blue-shift experienced by the mGBP-BADAN complex in the FMOC-YL gel, the peak emission intensity has here shifted from 650nm in solution to 630nm in gel, in a similar manner to the mGBP-BADAN wavelength shift seen in figure 8.12. The variation in maximal emission intensity at 630 nm is shown in figure 8.17.

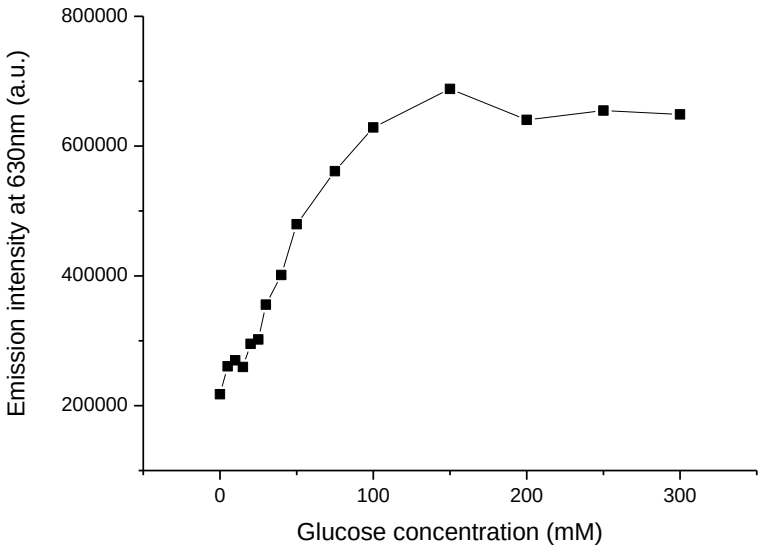

Figure 8.17- Emission intensity at 630nm of mGBP-IANR in FMOC-YL hydrogel with varying glucose concentration

The system appears to saturate at 100mM, which is what is expected for this concentration of mGBP. Saturation glucose concentration for mGBP-BADAN was reported to be 100mM: this is also the concentration in figure 8.17 after which no further increases in emission intensity are observed. Plotting the increase in fluorescence intensity against the logarithm of the glucose concentration (in the same manner as reported by Khan *et al.* for GBP-BADAN mutant variants)[58] provides the sigmoidal dose-response curve shown in figure 8.18.

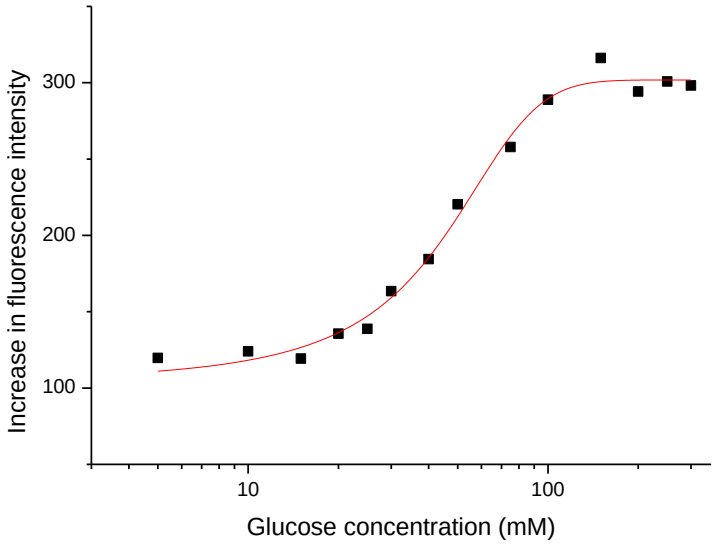

Figure 8.18- Dose Response curve of mGBP-IANR in FMOC-YL

Using the dose-response curve-fitting software in the Origin program, a Kd value of 41.99 (±3.78) mM was obtained.

The emission intensity results observed in the hydrogel are very similar to those hypothesised, but not observed, in buffer. The reason for this is not clear from the data, but it could potentially be the case that the degree of protection provided by the ordered structure of the hydrogel (and indicated by the wavelength shift in figure 8.16) allows the fluorophore to operate at higher energies (the emission experiences less quenching of intensity): and at these higher energies the more sueful operational response is realised.

8.4.4 mGBP-IANR in FMOC-YL hydrogel: lifetimes

The fluorescence lifetimes of the labelled protein in the gel were measured on the same equipment as previously used for TCSPC readings. Figure 8.19 shows the fluorescence decay curve in the absence of glucose, with a 2-exponential fit to the data.

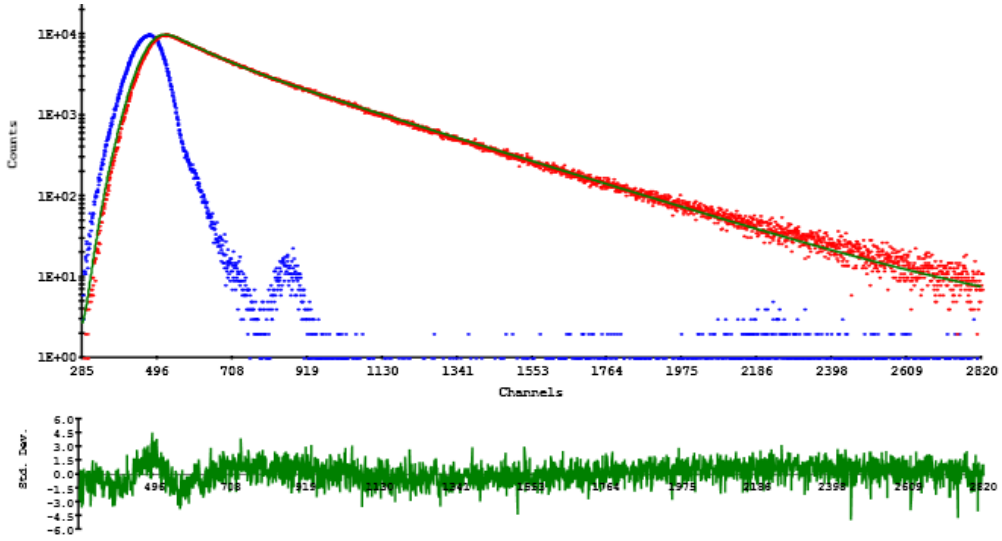

Figure 8.19- TCSPC data for mGBP-IANR in FMOC-YL in the absence of glucose

The lifetime decays with increasing concentration were found to be well represented by a 2-exponential decay and the results of these fits are shown in table 8.7.

mGBP-IANR in FMOC-YL hydrogel: Fluorescence lifetimes									
Glucose conc./mM	**T1/ns**	**σ/ns**	**T2/ns**	**σ/ns**	**B1**	**σ**	**B2**	**σ**	**χ2**
0	1.62	0.09	4.54	0.02	23.74	1.16	76.26	0.35	1.14
5	1.55	0.08	4.51	0.02	22.84	1.20	77.16	0.34	1.10
10	1.60	0.09	4.54	0.02	24.04	1.20	75.96	0.35	1.10
15	1.58	0.09	4.51	0.02	23.59	1.21	76.41	0.35	1.10
20	1.56	0.08	4.53	0.02	23.90	1.16	76.10	0.34	1.12
25	1.57	0.08	4.54	0.02	24.03	1.17	75.97	0.35	1.13
30	1.58	0.07	4.52	0.02	24.63	1.13	75.37	0.35	1.09
40	1.58	0.08	4.53	0.02	24.44	1.11	75.56	0.35	1.14
50	1.58	0.08	4.53	0.02	24.44	1.12	75.56	0.35	1.08
75	1.51	0.07	4.51	0.02	23.88	1.06	76.12	0.34	1.08
100	1.54	0.07	4.48	0.02	25.50	1.10	74.50	0.35	1.13
150	1.54	0.07	4.43	0.02	25.94	1.10	74.06	0.36	1.02
200	1.51	0.07	4.37	0.02	21.16	1.10	78.84	0.35	1.07
250	1.49	0.07	4.34	0.02	25.16	1.17	74.84	0.36	1.05
300	1.55	0.08	4.36	0.02	26.75	1.12	73.25	0.37	1.14

Table 8.7- 2-exponential plots to lifetime decay of glucose response of mGBP-IANR in FMOC hydrogel

There is apparently the same trend of shortening lifetimes and increasing relevance of the shorter lifetime component as observed in buffer, but the sample in gel starts off as more dominantly longer-lifetime, and indeed the longer lifetime component is a full nanosecond longer than the one which presents in the buffer sample. The variation with glucose concentration, however, is consistent but slight.

Holding the lifetimes constant, and calculating the amplitude of the pre-exponential factors based on the lifetimes of 1.5 ns and 4.5 ns provides a series of results which are displayed in table 8.8.

mGBP-IANR in FMOC-YL hydrogel: Fluorescence lifetime parameters							
Glucose conc./mM	**T1/ns**	**T2/ns**	**B1**	**σ**	**B2**	**σ**	**χ^2**
0	1.50	4.50	22.69	1.16	77.31	0.33	1.14
5	1.50	4.50	22.80	1.18	77.20	0.33	1.10
10	1.50	4.50	23.17	1.28	76.83	0.34	1.10
15	1.50	4.50	23.38	1.27	76.62	0.34	1.10
20	1.50	4.50	23.76	1.24	76.24	0.34	1.09
25	1.50	4.50	23.49	1.23	76.51	0.34	1.10
30	1.50	4.50	24.24	1.19	75.76	0.34	1.09
40	1.50	4.50	24.17	1.31	75.83	0.35	1.12
50	1.50	4.50	24.03	1.29	75.97	0.35	1.07
75	1.50	4.50	24.09	1.19	75.91	0.34	1.14
100	1.50	4.50	25.70	1.07	74.30	0.35	1.11
150	1.50	4.50	26.99	1.07	73.01	0.36	1.10
200	1.50	4.50	27.59	1.08	72.41	0.36	1.25
250	1.50	4.50	28.27	1.06	71.73	0.37	1.29
300	1.50	4.50	28.77	1.03	71.23	0.37	1.38

Table 8.8- 2-exponential plots to lifetime decays of glucose response of mGBP-IANR in FMOC hydrogel when lifetimes are fixed

These results are graphically displayed in figure 8.20.

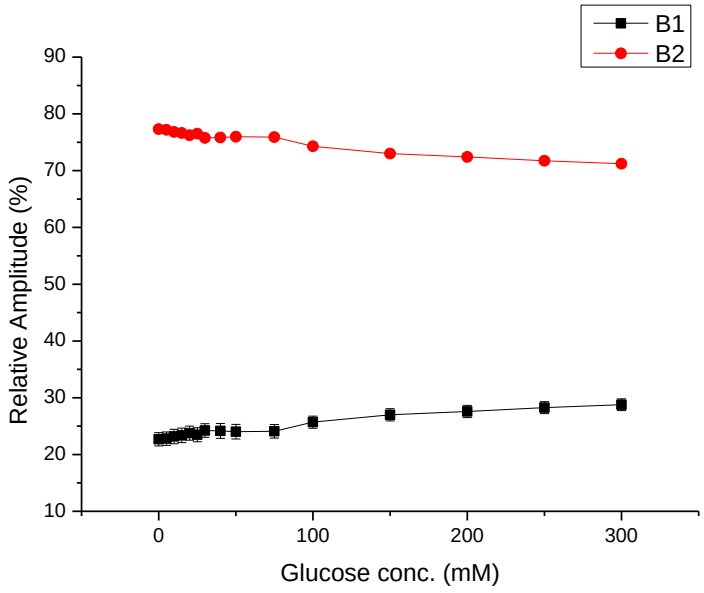

Figure 8.20- Relative amplitude of pre-exponential factors fitted to mGBP-IANR when lifetimes are fixed

There is certainly a response over the concentration range 0-300 mM, a trend of increasing contribution from the 1.5 ns lifetime component. Comparing this trend to a straight line of best fit,

the linear R^2 value is found to be 0.96, showing a positive correlation between B1 relative amplitude and glucose concentration- as was observed for mGBP-IANR in buffer.

8.5 Conclusions

Silica sol gels and an FMOC-YL hydrogel were investigated for their safety and efficiency in mGBP-BADAN encapsulation, and the hydrogel was then used to encapsulate mGBP-IANR. Both silica gel systems showed a decrease in the fluorescence emission intensity of mGBP-BADAN with increasing glucose concentration: the reverse trend to that observed in buffer. The fluorescence lifetime changes for mGBP-BADAN in the gel environment were seen to be minimal. These results indicate that silica gels are not a reliable method of immobilisation for mGBP systems.

FMOC-YL hydrogels were utilised for the encapsulation of both mGBP-BADAN and mGBP-IANR. Both protein-dye complexes showed an increase in fluorescence emission intensity with increasing glucose concentration, and both showed the same qualitative response in fluorescence lifetime changes in the hydrogel compared with those observed in buffer. The hydrogel environment utilised in this project would therefore appear to be one which allows for the functioning of mGBP systems.

This experiment, and thesis, therefore shows a proof of concept confirmation for use of a mGBP-IANR labelled protein encapsulated in an FMOC-YL hydrogel as a viable glucose sensor. With more efficient dye production and labelling, and fine-tuning of the hydrogel concentrations and parameters, it is conceivable that this arrangement could be taken further for more realistic clinical testing.

9 Conclusions and future work

Glucose biosensor molecules consisting of a triple mutant GBP labelled with an extrinsic fluorophore were the main topic of investigation in this project, with the purpose being construction of a viable basis for a clinical glucose sensor.

The intrinsic fluorescence of mGBP was examined with excitation at 280 nm and 295 nm. Fluorescence emission intensity data and lifetime decay curves in response to glucose certainly contain useful data, but were seen to be too complex for resolution as a result of the large number of fluorophores (12 amino acids in different microenvironments) in the molecule. Anisotropy studies showed that the characteristic protein folding could be observed with intrinsic fluorescence.

Labelling this mutant protein with the fluorescent dye BADAN produced a complex which showed a change in fluorescence emission intensity of 500% in the presence of saturating glucose. A response to glucose concentration was observed in the recorded fluorescent lifetimes, with the long lifetime component of a 2-exponential decay becoming increasingly dominant as concentration was increased. Anisotropy analysis provided hydrodynamic diameter values with good correspondence to crystal lattice parameters obtained from x-ray diffraction. The calculated diameter decreased with

The fluorescent dye BADAN is known to be environmentally sensitive- especially to the effects of solvent polarity. What we have shown is that the dye is sensitive to the level of exposure to a solvent environment when the solvent polarity does not change. Labelling mGBP with the dye produced a complex which showed a change in fluorescence emission intensity of 500% in the presence of saturating glucose. The fluorescence lifetimes similarly showed a response to glucose concentration, with the long lifetime component of a 2-exponential decay becoming increasingly dominant as concentration was increased. Anisotropy studies of the labelled protein revealed a calculated hydrodynamic diameter comparable to the lattice parameters observed in x-ray diffraction. This calculated diameter decreased with increasing glucose concentration, confirming the action of protein folding by which the mGBP is understood to function.

The robustness of the mGBP-BADAN sensor was investigated. No fluorescence response was seen in response to increasing concentrations of either fructose or lactose, yet with saturating concentrations of either sugar the sensor still responded positively to glucose, with K_d values obtained which compare favourably with literature values. The mGBP-BADAN sensor was therefore seen to be selective for glucose. Fluorescence responses to glucose concentration were retained at

37 °C and at pH 9.2, but the more hostile environments of 50 °C and pH 4.0 both degraded the system function, rendering it ineffective in these environments. It became clear that large deviations of the system from physiological conditions render the sensor ineffective.

The complex mGBP-Texas Red was created, but experiments revealed it to display very little change in any fluorescence characteristic with increasing glucose concentration. This was expected, and confirms the importance of dye-solvent interactions for a sensor constructed in this manner.

Labelling the mGBP with IANR produced a protein-dye complex which responded to changes in glucose concentration. The recorded lifetime data showed a promising response. The pre-exponential factors were found to vary in a linear way over the physiological glucose range, a finding which lends itself well to application of the system as a viable sensor. The anisotropy data provided a calculated hydrodynamic diameter which decreased in response to glucose, indicating that the protein retains its functional ability when labelled with this dye

It was, however, observed that only ~1% of the mGBP molecules were labelled with IANR, as determined by absorbance measurements. Any development of the mGBP-IANR system must address this issue, and it can be assumed that improving the labelling efficiency will improve results in this field. More efficient labelling would allow for greater confidence in the results, and in faster collection of data, making it more applicable for use as a biosensor

Silica sol gels and an FMOC-YL hydrogel were investigated for their safety and efficiency in mGBP-BADAN encapsulation, and the hydrogel was then used to encapsulate mGBP-IANR. Both silica gel systems showed a decrease in the fluorescence emission intensity of mGBP-BADAN with increasing glucose concentration: the reverse trend to that observed in buffer. The fluorescence lifetime changes for mGBP-BADAN in the gel environment were seen to be minimal. These results indicate that silica gels are not a reliable method of immobilisation for mGBP systems.

FMOC-YL hydrogels were utilised for the encapsulation of both mGBP-BADAN and mGBP-IANR. Both protein-dye complexes showed an increase in fluorescence emission intensity with increasing glucose concentration, and both showed the same qualitative response in fluorescence lifetime changes in the hydrogel compared with those observed in buffer. The hydrogel environment utilised in this project would therefore appear to be one which allows for the functioning of mGBP systems.

This experiment, and thesis, therefore shows a proof of concept confirmation for use of a mGBP-IANR labelled protein encapsulated in an FMOC-YL hydrogel as a viable glucose sensor. With more efficient dye production and labelling, and fine-tuning of the hydrogel concentrations and parameters, it is conceivable that this arrangement could be taken further for more realistic clinical testing.

With the sensor apparently functioning in a physics laboratory, future work should involve increasingly clinical settings. Animal studies have been performed for various biosensors prior to human trials, and this would seem the logical progression for advancement of this project. If animal trials were successful, then human clinical trials should take place to determine the viability of mGBP-IANR as part of a functioning glucose sensor.

Development of a useful and practical sensor system would, however, require a further degree of equipment miniaturisation than is currently available. Miniaturised lifetime analysis equipment is within the realm of possibility- the progression over the years from flash-lamps to LEDs is an apt example of the continual progress in the field, and further steps are to be both desired and expected.

The accelerating scientific (and industrial) interest in sensors for continuous glucose monitoring means that promising avenues must be fully explored. Each month sees new papers published in this area of research: hopefully some of these can be successfully employed for effective glucose monitoring in diabetes patients. Time will tell whether or not mGBP-IANR has any future as a biosensor, but this thesis has shown that it certainly has potential.

References

1. Shaw, J. E., Sicree, R. A & Zimmet, P. Z. Global estimates of the prevalence of diabetes for 2010 and 2030. *Diabetes research and clinical practice* **87**, 4–14 (2010).

2. Zhang, P. *et al.* Global healthcare expenditure on diabetes for 2010 and 2030. *Diabetes research and clinical practice* **87**, 293–301 (2010).

3. Diabetes, D. O. F. Diagnosis and classification of diabetes mellitus. *Diabetes care* **33 Suppl 1**, S62–9 (2010).

4. The Massachusetts Medical Society The effect of intensive treatment of diabetes on the development and progression of long-term complications in insulin-dependent diabetes mellitus. *The New England Journal of Medicine* **329**, 977–986 (1993).

5. O'Kane, M. & Pickup, J. Self-monitoring of blood glucose in diabetes: is it worth it? *Ann Clin Biochem.* **46**, 273–82 (2009).

6. Klonoff, D. C. Continuous Glucose Monitoring Roadmap for 21st century diabetes therapy. *Diabetes care* **28**, 1231–1239 (2005).

7. Burge, M. R., Mitchell, S., Sawyer, A. & Schade, D. S. Continuous Glucose Monitoring: The Future of Diabetes Management. *Diabetes Spectrum* **21**, 112–119 (2008).

8. Heller, A. & Feldman, B. Electrochemistry in diabetes management. *Accounts of chemical research* **43**, 963–73 (2010).

9. Maran, A. Continuous subcutaneous glucose monitoring in diabetic patients. *Diabetes care* **25**, 347–352 (2002).

10. Zheng, B. *et al.* Gold nanoparticles-coated eggshell membrane with immobilized glucose oxidase for fabrication of glucose biosensor. *Sensors and Actuators B: Chemical* **152**, 49–55 (2011).

11. Singh, N. K., Jain, B. & Annapoorni, S. ZnO modified gold disc: A new route to efficient glucose sensing. *Sensors and Actuators B: Chemical* **156**, 383–387 (2011).

12. Campbell, H. B., Elzanowska, H. & Birss, V. I. Towards a reliable and high sensitivity O_2-independent glucose sensor based on Ir oxide nanoparticles. *Biosensors & bioelectronics* **42**, 563–9 (2013).

13. Chen, X. *et al.* A novel bienzyme glucose biosensor based on three-layer Au–Fe_3O_4@SiO_2 magnetic nanocomposite. *Sensors and Actuators B: Chemical* **159**, 220–228 (2011).

14. Kotanen, C. N., Tlili, C. & Guiseppi-Elie, A. Amperometric glucose biosensor based on electroconductive hydrogels. *Talanta* **103**, 228–35 (2013).

15. Chou, J.-C., Yang, H.-Y. & Chen, C.-W. Glucose biosensor of ruthenium-doped TiO_2 sensing electrode by co-sputtering system. *Microelectronics Reliability* **50**, 753–756 (2010).

16. Park, B.-W. *et al.* A novel glucose biosensor using bi-enzyme incorporated with peptide nanotubes. *Biosensors & bioelectronics* **38**, 295–301 (2012).

17. Zhang, Y. *et al.* A new preparation of Au nanoplates and their application for glucose sensing. *Biosensors & bioelectronics* **28**, 344–8 (2011).

18. Che, X. *et al.* A glucose biosensor based on chitosan-Prussian blue-multiwall carbon nanotubes-hollow PtCo nanochains formed by one-step electrodeposition. *Colloids and surfaces. B, Biointerfaces* **84**, 454–61 (2011).

19. Yang, X., Bai, J., Wang, Y., Jiang, X. & He, X. Hydrogen peroxide and glucose biosensor based on silver nanowires synthesized by polyol process. *The Analyst* **137**, 4362–7 (2012).

20. Jang, H. D. *et al.* A glucose biosensor based on TiO_2-Graphene composite. *Biosensors & bioelectronics* **38**, 184–8 (2012).

21. Claussen, J. C. *et al.* Electrochemical glucose biosensor of platinum nanospheres connected by carbon nanotubes. *Journal of diabetes science and technology* **4**, 312–9 (2010).

22. Lee, D. & Cui, T. Low-cost, transparent, and flexible single-walled carbon nanotube nanocomposite based ion-sensitive field-effect transistors for pH/glucose sensing. *Biosensors & bioelectronics* **25**, 2259–64 (2010).

23. Maghsoodi, S., Gholami, Z., Chourchian, H., Mortazavi, Y. & Khodadadi, A. A. A novel biosensor using entangled carbon nanotubes layer grown on an alumina substrate by CCVD of methane on FeOx–MgO. *Sensors and Actuators B: Chemical* **141**, 526–531 (2009).

24. Ahmadalinezhad, A., Wu, G. & Chen, A. Mediator-free electrochemical biosensor based on buckypaper with enhanced stability and sensitivity for glucose detection. *Biosensors & bioelectronics* **30**, 287–93 (2011).

25. Wang, J., Thomas, D. F. & Chen, A. Nonenzymatic electrochemical glucose sensor based on nanoporous PtPb networks. *Analytical chemistry* **80**, 997–1004 (2008).

26. Cao, F. *et al.* Highly sensitive nonenzymatic glucose sensor based on electrospun copper oxide-doped nickel oxide composite microfibers. *Talanta* **86**, 214–20 (2011).

27. Wang, Y., Zhang, D., Zhang, W., Gao, F. & Wang, L. A facile strategy for nonenzymatic glucose detection. *Analytical biochemistry* **385**, 184–6 (2009).

28. Zhu, Z. G. *et al.* Enzyme-free glucose biosensor based on low density CNT forest grown directly on a Si/SiO_2 substrate. *Sensors and Actuators B: Chemical* **178**, 586–592 (2013).

29. Luo, L., Zhu, L. & Wang, Z. Nonenzymatic amperometric determination of glucose by CuO nanocubes-graphene nanocomposite modified electrode. *Bioelectrochemistr* **88**, 156–63 (2012).

30. Quoc Dung, N., Patil, D., Jung, H. & Kim, D. A high-performance nonenzymatic glucose sensor made of CuO-SWCNT nanocomposites. *Biosensors & bioelectronics* **42**, 280–6 (2013).

31. Huang, J., Zhang, L., Liang, R.-P. & Qiu, J.-D. “On-off” switchable electrochemical affinity nanobiosensor based on graphene oxide for ultrasensitive glucose sensing. *Biosensors & bioelectronics* **41**, 430–5 (2013).

32. Guo, D., Zhang, D., Zhang, L. & Lu, G. Non-invasive blood glucose monitoring for diabetics by means of breath signal analysis. *Sensors and Actuators B: Chemical* **173**, 106–113 (2012).

33. Bequette, B. A critical assessment of algorithms and challenges in the development of an artificial pancreas. *Diabetes Technology and Therapeutics* **7**, 28–47 (2005).

34. Bequette, B. W. Continuous glucose monitoring: real-time algorithms for calibration, filtering, and alarms. *Journal of diabetes science and technology* **4**, 404–18 (2010).

35. Nathan, D. M. & Russell, S. The future of care for type 1 diabetes. *CMAJ : Canadian Medical Association journal* **185**, 285–6 (2013).

36. Zhi, Z., Liu, B., Jones, P. M. & Pickup, J. C. Polysaccharide multilayer nanoencapsulation of insulin-producing beta-cells grown as pseudoislets for potential cellular delivery of insulin. *Biomacromolecules* **11**, 610–6 (2010).

37. Ricotti, L., Assaf, T., Dario, P. & Menciassi, A. Wearable and implantable pancreas substitutes. *Journal of artificial organs* **16**, 9–22 (2013).

38. Liao, K.-C. *et al.* Percutaneous fiber-optic sensor for chronic glucose monitoring in vivo. *Biosensors & bioelectronics* **23**, 1458–65 (2008).

39. Weidemaier, K. *et al.* Multi-day pre-clinical demonstration of glucose/galactose binding protein-based fiber optic sensor. *Biosensors & bioelectronics* **26**, 4117–23 (2011).

40. Moschou, E. A, Sharma, B. V, Deo, S. K. & Daunert, S. Fluorescence glucose detection: advances toward the ideal in vivo biosensor. *Journal of fluorescence* **14**, 535–47 (2004).

41. Lakowicz, J. R. *Principles of Fluorescence Spectroscopy*. (2009).

42. Burns, D. M. & Johnson, N. L. Metrology of fluorescent retroreflective materials and its relationship to their daytime visibility. *Analytica Chimica Acta* **380**, 211–226 (1999).

43. Barone, P. W., Parker, R. S. & Strano, M. S. In vivo fluorescence detection of glucose using a single-walled carbon nanotube optical sensor: design, fluorophore properties, advantages, and disadvantages. *Analytical chemistry* **77**, 7556–62 (2005).

44. Hussain, F., Birch, D. J. S. & Pickup, J. C. Glucose sensing based on the intrinsic fluorescence of sol-gel immobilized yeast hexokinase. *Analytical biochemistry* **339**, 137–43 (2005).

45. Auria, S. D., Herman, P. & Lakowicz, J. R. The fluorescence emission of the apo-glucose oxidase from Aspergillus niger as probe to estimate glucose concentrations. *Biochemical and biophysical research communications* **553**, 550–553 (1999).

46. Feng, L., Liang, F., Wang, Y., Xu, M. & Wang, X. A highly sensitive water-soluble system to sense glucose in aqueous solution. *Organic & biomolecular chemistry* **9**, 2938–42 (2011).

47. Pickup, J. C., Hussain, F., Evans, N. D., Rolinski, O. J. & Birch, D. J. S. Fluorescence-based glucose sensors. *Biosensors & bioelectronics* **20**, 2555–65 (2005).

48. Huang, Y.-J. *et al.* Glucose sensing via aggregation and the use of "knock-out" binding to improve selectivity. *Journal of the American Chemical Society* **135**, 1700–3 (2013).

49. McCartney, L. J., Pickup, J. C., Rolinski, O. J. & Birch, D. J. Near-infrared fluorescence lifetime assay for serum glucose based on allophycocyanin-labeled concanavalin A. *Analytical biochemistry* **292**, 216–21 (2001).

50. Tolosa, L., Szmacinski, H., Rao, G. & Lakowicz, J. R. Lifetime-based sensing of glucose using energy transfer with a long lifetime donor. *Analytical biochemistry* **250**, 102–8 (1997).

51. Tolosa, L., Malak, H., Raob, G. & Lakowicz, J. R. Optical assay for glucose based on the luminescnence decay time of the long wavelength dye Cy5™. *Sensors and Actuators B: Chemical* **45**, 93–99 (1997).

52. Veetil, J. V, Jin, S. & Ye, K. A glucose sensor protein for continuous glucose monitoring. *Biosensors & bioelectronics* **26**, 1650–5 (2010).

53. Jin, S., Veetil, J. V, Garrett, J. R. & Ye, K. Construction of a panel of glucose indicator proteins for continuous glucose monitoring. *Biosensors & bioelectronics* **26**, 3427–31 (2011).

54. Khan, F., Gnudi, L. & Pickup, J. C. Fluorescence-based sensing of glucose using engineered glucose/galactose-binding protein: a comparison of fluorescence resonance energy transfer and environmentally sensitive dye labelling strategies. *Biochemical and biophysical research communications* **365**, 102–6 (2008).

55. Tolosa, L. *et al.* Glucose sensor for low-cost lifetime-based sensing using a genetically engineered protein. *Analytical biochemistry* **267**, 114–20 (1999).

56. Ge, X., Tolosa, L. & Rao, G. Dual-labeled glucose binding protein for ratiometric measurements of glucose. *Analytical chemistry* **76**, 1403–10 (2004).

57. Thomas, K. J., Sherman, D. B. & Amiss, T. J. A long-wavelength fluorescent glucose biosensor based on bioconjugates of galactose/glucose binding protein and nile red derivatives. *Diabetes technology & therapeutics* **8**, 261–268 (2006).

58. Khan, F., Saxl, T. E. & Pickup, J. C. Fluorescence intensity- and lifetime-based glucose sensing using an engineered high-Kd mutant of glucose/galactose-binding protein. *Analytical biochemistry* **399**, 39–43 (2010).

59. Sakaguchi-Mikami, A., Taneoka, A., Yamoto, R., Ferri, S. & Sode, K. Engineering of ligand specificity of periplasmic binding protein for glucose sensing. *Biotechnology letters* **30**, 1453–60 (2008).

60. Saxl, T., Khan, F., Ferla, M., Birch, D. & Pickup, J. A fluorescence lifetime-based fibre-optic glucose sensor using glucose/galactose-binding protein. *The Analyst* **136**, 968–72 (2011).

61. Paek, S.-H. *et al.* Label-free, needle-type biosensor for continuous glucose monitoring based on competitive binding. *Biosensors & bioelectronics* **40**, 38–44 (2013).

62. The Prashant Kamat Laboratory Spectroscopic Characterization. *http://www3.nd.edu/~kamatlab/facilities_spectroscopy.html*

63. Macmillan, A. M. *et al.* Improved biocompatibility of protein encapsulation in sol–gel materials. *Journal of Sol-Gel Science and Technology* **49**, 380–384 (2008).

64. Hungerford, G., Rei, A. & Ferreira, M. I. C. Use of fluorescence to monitor the incorporation of horseradish peroxidase into a sol-gel derived medium. *Biophysical chemistry* **120**, 81–6 (2006).

65. Stepanenko, O. V *et al.* New insight into protein-ligand interactions. The case of the D-galactose/D-glucose-binding protein from Escherichia coli. *The journal of physical chemistry. B* **115**, 2765–73 (2011).

66. Koehorst, R. B. M. *et al.* Profiling of dynamics in protein-lipid-water systems: a time-resolved fluorescence study of a model membrane protein with the label BADAN at specific membrane depths. *European biophysics journal : EBJ* **39**, 647–56 (2010).

67. Koehorst, R. B. M., Spruijt, R. B. & Hemminga, M. A Site-directed fluorescence labeling of a membrane protein with BADAN: probing protein topology and local environment. *Biophysical journal* **94**, 3945–55 (2008).

68. Hansen, J. S. *et al.* Formation of giant protein vesicles by a lipid cosolvent method. *Chembiochem : a European journal of chemical biology* **12**, 2856–62 (2011).

69. Pickup, J. C., Zhi, Z., Khan, F., Saxl, T. & Birch, D. J. S. Nanomedicine and its potential in diabetes research and practice. *Diabetes/metabolism research and reviews* **24**, 604–10 (2008).

70. Bin Mat Yunus, W. M. Refractive index of solutions at high concentrations: erratum. *Applied optics* **28**, 2465 (1989).

71. Topsakal, E., Karacolak, T. & Moreland, E. C. Glucose-dependent dielectric properties of blood plasma. *2011 XXXth URSI General Assembly and Scientific Symposium* 1–4 (2011).

72. Gill, S. & Vonhippel, P. Calculation of protein extinction coefficients from amino acid sequence data. *Analytical biochemistry* **182**, 319–326 (1989).

73. Titus, J. & Haugland, R. Texas Red, a hydrophilic, red-emitting fluorophore for use with fluorescein in dual parameter flow microfluorometric and fluorescence microscopic studies. *Journal of Immunological Methods.* **50**, 193–204 (1982).

74. Fluorophores.org. Texas Red. *http://www.fluorophores.tugraz.at/substance/740*

75. Greenspan, P., Mayer, F. P. & Fuller, S. D. Nile red: a selective fluorescent stain for intracellular lipid droplets. *Journal of Cell Biology* **100**, 965-973 (1985).

76. Sackett, D. L. & Wolff, J. Nile red as a polarity-sensitive fluorescent probe of hydrophobic protein surfaces. *Analytical biochemistry* **167**, 228–234 (1987).

77. Davis, D. & Birch, D. J. S. Extrinsic Fluorescence Probe Study of Human Serum Albumin Using Nile Red. *Journal of fluorescence* **6**, (1996).

78. Hungerford, G. The effect of the nature of retained solvent on the fluorescence of Nile Red incorporated in sol–gel-derived matrices. *Journal of Luminescence* **93**, 155–165 (2001).

79. Thomas, J., Sherman, D. B., Amiss, T. J., Andaluz, S. A. & Pitner, J. B. Synthesis and biosensor performance of a near-IR thiol-reactive fluorophore based on benzothiazolium squaraine. *Bioconjugate chemistry* **18**, 1841–6 (2007).

80. Ebelmen, M. Recherches sur les combinaisons des acides borique et silicique avec les ethers. *Annales de Chimie et de Physique* **116**, (1846).

81. Graham, T. On the Properties of Silicic Acid and Other Analogous Colloidal Substances. *Journal of the Chemical Society of London,* **17**, (1864).

82. Zarzycki, J. Past and present of sol-gel science and technology. *Journal of Sol-Gel Science and Technology* **8**, 17–22 (1997).

83. Reisfeld, R. Spectroscopy and applications of molecules in glasses. *Journal of Non-Crystalline Solids* **121**, (1990).

84. Jin, W. & Brennan, J. D. Properties and applications of proteins encapsulated within sol–gel derived materials. *Analytica Chimica Acta* **461**, 1–36 (2002).

85. Buenger, D., Topuz, F. & Groll, J. Hydrogels in sensing applications. *Progress in Polymer Science* **37**, 1678–1719 (2012).

86. Chen, J., Park, H. & Park, K. Synthesis of superporous hydrogels: hydrogels with fast swelling and superabsorbent properties. *Journal of biomedical materials research* **44**, 53–62 (1999).

87. Deligkaris, K., Tadele, T. S., Olthuis, W. & van den Berg, A. Hydrogel- based devices for biomedical applications. *Sensors and Actuators B: Chemical* **147**, 765–74 (2010).

88. Peppas, N. A., Hilt, J. Z., Khademhosseini, a. & Langer, R. Hydrogels in Biology and Medicine: From Molecular Principles to Bionanotechnology. *Advanced Materials* **18**, 1345–1360 (2006).

89. Ulijn, R. V. *et al.* Bioresponsive hydrogels. *Materials today* **10**, 40–48 (2007).

90. Pedrosa , V. A., Yan, J., Simonian, A. L. & Revzin, A. Micropatterned Nanocomposite Hydrogels for Biosensing Applications. *Electroanalysis* **23**, 1142–1149 (2011).

91. Justin, G., Finley, S., Abdur Rahman, A. R. & Guiseppi-Elie, A. Biomimetic hydrogels for biosensor implant biocompatibility: electrochemical characterization using micro-disc electrode arrays (MDEAs). *Biomedical microdevices* **11**, 103–15 (2009).

92. Qiu, Y. & Park, K. Environment-sensitive hydrogels for drug delivery. *Advanced drug delivery reviews* **53**, 321–39 (2001).

93. Roy, S. *et al.* Dramatic specific-ion effect in supramolecular hydrogels. *Chemistry- A European Journal* **18**, 11723–31 (2012).